

Multi-Proxy Reconstruction of South Asian Monsoon Variability in Sri Lanka

Dissertation

zur Erlangung des akademischen Grades doctor rerum naturalium

(Dr. rer. nat.)

vorgelegt dem Rat der Chemisch-Geowissenschaftlichen Fakultät der

Friedrich-Schiller-Universität Jena

von MPhil. Kasun Gayantha Henadheera Arachchige

geboren am 23.05.1989 in Wathupitiwala, Sri Lanka

Gutachter:

1. apl. Prof. Dr. Gerd Gleixner

Max-Planck-Institut für Biogeochemie; FSU Jena

2. Prof. Dr. Roland Mäusbacher

Institut für Geographie, FSU Jena

Tag der Verteidigung: 14.07.2021

Dissertation, Friedrich-Schiller-Universität Jena, [2021]

Acknowledgements

First and foremost, I wish to extend my gratitude to my supervisors **apl. Prof. Dr. Gerd Gleixner** at the Max Planck Institute for Biogeochemistry (MPI-BGC), Jena, **Prof. Dr. Achim Brauer** at the German Research Centre for Geosciences (GFZ), Potsdam, **Dr. Patrick Roberts** at the Max Planck Institute for the Science of Human History (MPI-SHH), Jena, **Prof. Joyanto Routh** at Linköping University, Sweden, and **Prof. Dr. Roland Mäusbacher** at Friedrich-Schiller University, Jena. Without them, this thesis would not be possible, and I will always be immensely grateful for their guidance and advice throughout the process.

I would also like to express my gratitude to **Prof. Rohana Chandrajith**, University of Peradeniya, Sri Lanka, **apl. Prof. Dr. Peter Frenzel**, IGW, Friedrich-Schiller University, Jena, and **Dr. Anupama Krishnamurthy**, French Institute of Pondicherry, India for their collaborations and support that have enabled me to enrich my datasets and expertise through training in novel methods. I thank them for taking the time out to teach me and allow me to develop my toolkit further.

I would like to offer my special thanks to **Dr. Oshan Wedage**, University of Sri Jayawardenepura, Sri Lanka for his support on logistic matters and organizing the field campaign on which the cores were obtained. I would also like to acknowledge **Dr. Florian Ott**, GFZ, Potsdam and **Dr. Jana Ilgner**, MPI-SHH, Jena for their guidance and support during the field work.

I am grateful to **Dr. Markus Lange**-MPI-BGC, Jena for his support and guidance for statistical analyses. I also greatly appreciate the technical support provided by **Steffen Rühlow**, **Maria Foerster**, **Axel Steinhof** (¹⁴C Lab), and the **Iso Lab** and **ROMA** staff at MPI-BGC, Jena. In addition, I also thank **Dr. Oliver Rach** and **Dr. Rik Tjallingii** at GFZ-Potsdam, and **Susanne Karlsson** at Linköping University, Sweden, for their guidance and help during laboratory analyses.

Away from the academic work more specifically, I would also like to thank **Dr. Steffi Rothhardt**, **John Kula** and **Stefanie Burkert** at the IMPRS-gBGC coordination office for their kind support through my PhD process. In addition, I also want to thank all fellow PhD students in Gleixner group, as well as all of my colleagues and friends within the MPI-BGC, for their support, motivation, and for making me feel welcome during my time in Germany.

This research would not have been possible without the **Government of Sri Lanka** and the relevant authorities (**Department of Wildlife Conservation**, **Irrigation Department**, **Department of Coastal Conservation**, **Geological Survey and Mines Bureau** and **Sri Lanka Customs**) who granted permissions for the field work and **Sri Lanka Navy** for their great support during the field campaign. Finally, I owe my gratitude to **Max Planck Society (MPG)** for providing funding for this research project and for my doctoral work.

Table of Content

Acknowledgements	I
Table of Content.....	II
List of Figures	IV
List of Tables.....	VI
List of Abbreviations.....	VII
1. Introduction	1
1.1 Motivation	1
1.2 Reconstruction of the South Asian Monsoon in Sri Lanka.....	3
1.3 Objectives.....	7
2. Mechanism, Reconstruction and Cultural Impacts of South Asian Monsoon – Literature Review.....	9
2.1 Driving Mechanism and Factors Influencing South Asian Monsoon System	9
2.1.1 Forcing Factors.....	12
2.1.2 Modes of Climate Variables.....	14
2.1.3 Mean Latitudinal Migration of ITCZ	22
2.2 Proxies Used in Palaeo-monsoonal Reconstructions	24
2.2.1 Controls of δD and $\delta^{18}O$ in Monsoon Rainfall in Sri Lanka.....	25
2.2.2 Controls of Sediment Leaf Wax Hydrogen and Carbon Isotopes Composition	26
2.3 Indian Ocean Monsoon Variability and Cultural Impacts during Holocene.....	29
3. Study Areas and Methods	32
3.1 Study Areas	32
3.1.1 Climate, Geology, and Vegetation of Sri Lanka	32
3.1.2 The Study Sites.....	38
3.1.2.1 Bolgoda South Lake	38
3.1.2.2 Panama Lagoon	40
3.1.2.3 Horton Plains.....	41
3.2 Materials and Methods.....	44
3.2.1 Sampling/ Sediment Core Collection	44
3.2.2 ^{14}C dating and Construction of Age-depth Models.....	45
3.2.3 Grain Size Analysis.....	46
3.2.4 X-Ray Fluorescence Core Scanning	46
3.2.5 Biomarker Extraction and Analysis	47
3.2.6 Bulk Organic Stable Carbon Isotope Analysis and Total Organic Carbon (TOC) Analysis.....	49
3.2.7 Compound Specific Isotope Analysis of <i>n</i> -alkanes.....	50
3.2.8 Statistical Analysis	51
4. Results	52
4.1 Present Status of the Study Sites	52
4.2 Stratigraphy	52
4.3 Chronology.....	54

4.4. Grain Size Distribution.....	57
4.5. Elemental Composition	58
4.6 Biomarker Variation.....	62
4.6.1 <i>n</i> -Alkane	62
4.6.2 Sterols	66
4.7 Bulk Organic Carbon and $\delta^{13}\text{C}_{\text{org}}$ Variation	67
4.8 Compound Specific Carbon and Hydrogen Isotope Variation in <i>n</i> -Alkanes	70
5. Discussion	76
5.1 ^{14}C Chronology and Depositional Conditions/Events	76
5.2 Implications about Catchment and in Lake Processes by Physical and Inorganic Geochemical Parameters	78
5.3 Sources of Organic Matter	81
5.4 Climate and Environmental Implications Inferred by ^{13}C and D Isotopes in Leaf Wax <i>n</i> - Alkane	85
5.5 Marine Influence Inferred by ^{13}C and D Isotopes in bacterial lipids (<i>n</i> -alkane)	89
5.6 Behaviour of Monsoon Rainfall and Environmental Impacts in Sri Lanka	90
5.7 Regional Comparison of Palaeo-monsoonal Records	97
5.8 The Influence of Climate Forcing Factors on Monsoon Variability in Sri Lanka	102
5.9 Mid-Late Holocene Climate-Cultural Impacts in Sri Lanka	107
6. Conclusions	109
Summary	113
Zusammenfassung	117
Bibliography	121
Appendix	134
Selbständigkeitserklärung	143

List of Figures

Fig. 1.1	Global monsoon system and boreal summer and winter rainy seasons in the globe.....	2
Fig. 1.2	Seasonal migration of ITCZ and behaviour of Monsoons.....	4
Fig. 2.1	Schematic picture of Hadley Cell.....	11
Fig. 2.2	Variation of external forcing factors during the Holocene.....	14
Fig. 2.3	Historical maxima and minima of the 1000-year Eddy solar activity cycle.....	14
Fig. 2.4	Modes of climate variables influencing Asian monsoon system during the Holocene.....	15
Fig. 2.5	El Niño Southern Oscillation (ENSO) and Walker Circulation.....	18
Fig. 2.6	Indian Ocean Dipole (IOD).....	20
Fig. 2.7	North Atlantic Oscillation (NAO)	22
Fig. 3.1	Seasonal rainfall distribution in Sri Lanka	34
Fig. 3.2	Topography and climate zonation in Sri Lanka.....	37
Fig. 3.3	Bolgoda Lake system and surrounding area.....	39
Fig. 3.4	Panama Lagoon and surrounding vegetation.....	41
Fig. 3.5	Horton Plains national park area and main vegetation types.....	43
Fig. 4.1	Age model and stratigraphy of Bolgoda South Lake sediment core.	56
Fig. 4.2	Age model and stratigraphy of Panama Lagoon sediment core.....	56
Fig. 4.3	Age model and stratigraphy of Horton Plains peat core.....	57
Fig. 4.4	Grain size distribution in Bolgoda South Lake and Panama Lagoon	58
Fig. 4.5	XRF element trends in Bolgoda South Lake	61
Fig. 4.6	XRF element trends in Panama Lagoon.....	61

Fig. 4.7	Trends of relative abundance of <i>n</i> -alkane.....	63
Fig. 4.8	PCA biplots and cluster distributions of <i>n</i> -alkane.....	65
Fig. 4.9	Biomarker and bulk geochemical proxy trends in Bolgoda South Lake	68
Fig. 4.10	Biomarker and bulk geochemical proxy trends in Panama Lagoon core.....	69
Fig. 4.11	Biomarker and bulk geochemical proxy trends in Horton Plains peat core.....	69
Fig. 4.12	<i>n</i> -alkane carbon and hydrogen stable isotope variation in Bolgoda South Lake.....	73
Fig. 4.13	<i>n</i> -alkane carbon and hydrogen stable isotope variation in Panama Lagoon.....	74
Fig. 4.14	<i>n</i> -alkane carbon and hydrogen stable isotope variation in Horton Plains.....	75
Fig. 5.1	Climate and environmental implications inferred by selected proxy trends in Bolgoda South Lake.....	94
Fig. 5.2	Climate and environmental implications inferred by selected proxy trends in Horton Plains.....	95
Fig. 5.3	Climate and environmental implications inferred by selected proxy trends in Panama Lagoon.....	96
Fig. 5.4	Comparison of regional palaeoclimate records.....	100-101
Fig. 5.5	Location map of selected palaeoclimate records in the region.....	101
Fig. 5.6	Comparison of the monsoon rainfall trends in Sri Lanka with external forcing factors and modes of climate variables.....	106
Fig. 5.7	Schematic illustration of southward migration of the mean position of ITCZ during middle and late Holocene.....	107
	Graphical Summary.....	116

List of Tables

Table. 3.1 Site information and coring techniques used in the study.....	44
Table 4.1: Average water quality parameters in each site.....	52
Table 4.2: Varimax Rotated components and their variance.....	58
Table 4.3: PCA loadings for Bolgoda South Lake.....	59
Table 4.4: PCA loadings for Panama Lagoon.....	59
Table 4.5: Range of $\delta^{13}\text{C}$ and δD values of dominant <i>n</i> -alkanes in each core.....	72

List of Abbreviations

AD/CE	Anno Domini / Common Era
BC	Before Christ
BGSL	Bolgoda South Lake
BL	Bacterial Lipids
BOB	Bay of Bengal
cal yr BP	Calendar years Before Present
CLR	Centralized Log Ration
CPI	Carbon Preferential Index
CTCZ	Continental Tropical Convergence Zone
CWP	Current Warm Period
DCM	Dichloromethane
e.g.	exempli gratia (for example)
ENSO	El Niño Southern Oscillation
FIM	First Inter-monsoon
GC-IRMS	Gas Chromatography- Isotope Ratio Mass Spectrometer
GC-MS	Gas Chromatography- Mass Spectrometer
HP	Horton Plains
i.e.	id est (that is)
IOD	Indian Ocean Dipole
IPWP	Indo Pacific Warm Pool
ISM	Indian Summer Monsoon
ITCZ	Inter-Tropical Convergence Zone
IWM	Indian Winter Monsoon
ka BP	kilo annum (thousand years) Before Present
LIA	Little Ice Age
MWP	Medieval Warm Period
LW	Leaf Wax
NAO	North Atlantic Oscillation
NEM	North East Monsoon
NH	Northern Hemisphere
OM	Organic Matter

OTCZ	Oceanic Tropical Convergence Zone
PC	Principal Component
PCA	Principal Component Analysis
PN	Panama Lagoon
RWP	Roman Warm Period
RC	Rotated Component
SAM	South Asian Monsoon
SIM	Second Inter-monsoon
SST	Sea Surface Temperature
SWM	South West Monsoon
TOC	Total Organic Carbon
TLE	Total Lipid Extract
XRF	X-Ray Fluorescence

1. Introduction

1.1 Motivation

Global climate change due to anthropogenic activities is perhaps *the* major challenge facing humanity in the 21st century. According to the Global Climate Risk Index (2019), Sri Lanka is placed second among the most affected countries in the world, with human-induced climate change leading to increasingly frequent and extreme weather events such as floods, storms and droughts. Sri Lanka is not alone in its vulnerability to these impacts that are being brought about by an increasingly unpredictable monsoon systems. Nepal, Bangladesh, Vietnam and Thailand are also among the top 10 positions in this list and are all located in the tropical monsoon domain. Any changes in the monsoon intensity or fluctuations representing extreme events can severely influence the socio-economic conditions of the more than 70% of the world's population living in this monsoonal domain (Chiang, 2009) (Fig. 1.1). In addition, monsoon circulations also play a critical role in planetary atmospheric energy and water vapour transportation with ramifications for global systems and climates more widely (An et al., 2015).

Together, these points emphasise the climatic, humanitarian, and socio-economic importance of studying and understanding the changing behaviour of the tropical monsoon system over time in order to predict and mitigate future disasters related to monsoon anomalies. However, the instrumental climate records that cover the last few decades are not sufficient to understand the long-term behaviour of the monsoon system and its key components (Anderson, 2002). Therefore, palaeoclimate records from different regions of the global monsoon domain are essential in order to better understand the key driving forces controlling the monsoon system, to predict future trends and anomalies in monsoonal precipitation through global and regional climate models, and to better plan mitigation strategies for human populations living in different areas.

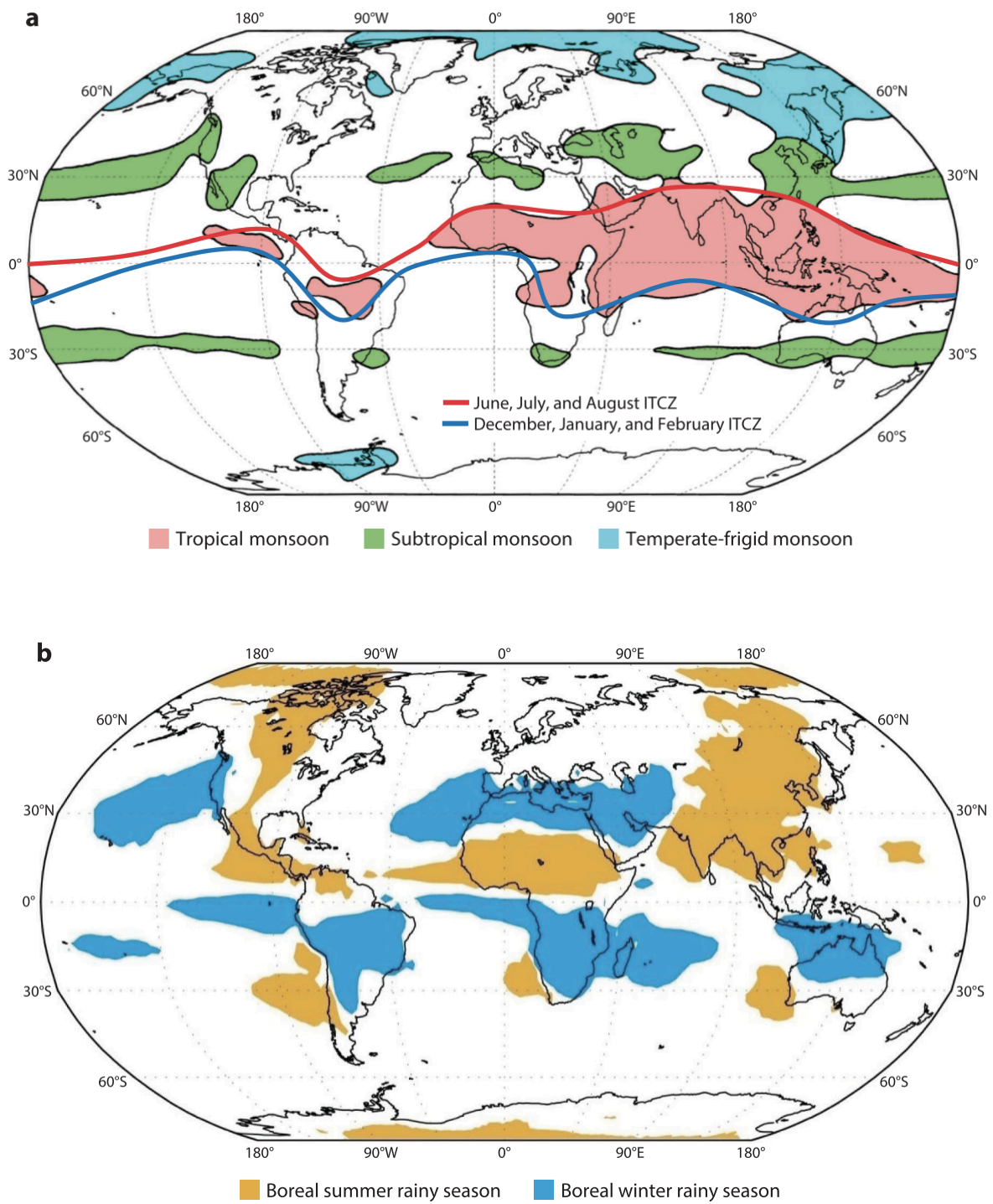


Fig.1.1 (a) Tropical and subtropical monsoon regions in the globe, and (b) Regions dominated by boreal summer and winter rainy seasons (Source: An et al., 2015)

1.2 Reconstruction of the South Asian Monsoon in Sri Lanka

The word monsoon derives from the Arabic word ‘Mausam’ that means ‘season’. The most important characteristic of the monsoon is large-scale seasonal variation in wind direction accompanied by large precipitation changes. The Asian Monsoon System is one of the major atmospheric circulation systems that plays a critical role in the global climate and the socio-economic conditions of nearly two thirds of the world’s population. The Asian Monsoon system consists of two main components, the South Asian or Indian Ocean Monsoon System and the East Asian Monsoon system (Banerji et al., 2020). The South Asian Monsoon (SAM) brings rainfall to the Indian subcontinent that is crucial for the agriculture practiced by dense human populations across the region. Even a slight shift in the intensity and/or duration of the monsoon can cause severe extreme events such as droughts, floods and mud slides (Mirza, 2011). These severe and unpredictable changes are increasingly regular phenomena affecting different parts of the region.

Seasonal migration of Inter Tropical Convergence Zone (ITCZ), controlled by the annual solar cycle determines the timing, intensity, and direction of tropical monsoon winds and accompanied rainfall caused by a cross-equatorial pressure gradient (An et al., 2015; Mohtadi et al., 2016). However, significant changes to the monsoonal rainfall pattern can be observed when moving from equator to the higher latitudes over the Indian sub-continent due to the varying insolation and teleconnections that exist with other climate systems including the El Niño southern oscillation (ENSO), the Indian Ocean Dipole (IOD) and the North Atlantic Oscillation (NAO). Holocene palaeoclimate records from the Indian sub-continent are unsurprisingly somewhat heterogenous, making it difficult to understand the key driving forces and impacts of the changing SAM in different parts of this diverse area (Achyuthan et al., 2016; Misra et al., 2019).

The Indian Ocean Monsoon consists of two main rainfall seasons. During the boreal summer, the ITCZ migrates to the Northern hemisphere and reaches its northern-most position around July-August, bringing summer monsoon rainfall (Southwest monsoon; SWM) to the Indian sub-continent, including Sri Lanka. Based on the distribution of the moisture, intensity, and timing two branches of the Indian Summer Monsoon (ISM) can be identified, namely, the Arabian Sea Branch (ASB) and the Bay of Bengal Branch (BBB) (Fig. 1.2) (Dixit and Tandon, 2016). The ASB brings rainfall initially to the windward side of Western Ghats in southwest India while the BBB brings rainfall to the southwestern parts of Sri Lanka and most of northeastern India. Later, during the boreal winter, the ITCZ retreats southward and reaches its southernmost position around January, resulting in a complete reversal of wind direction that brings winter monsoon rainfall (Northeast monsoon; NEM) to the southern tip of India and the northern and eastern parts of Sri Lanka (Fig. 1.2.; Banerji et al., 2020; Gupta et al., 2020).

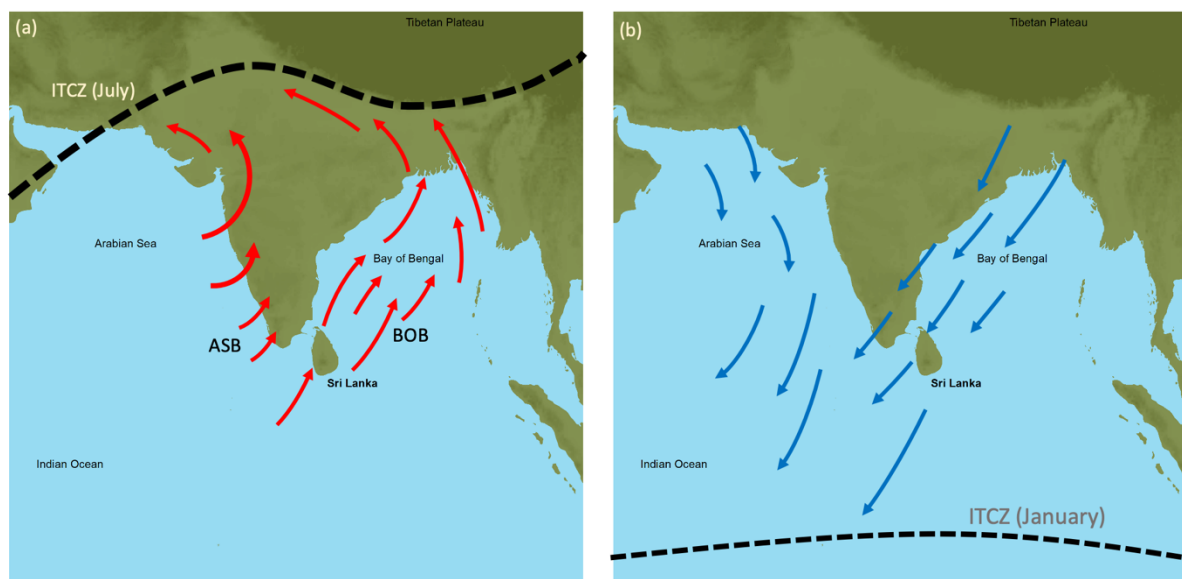


Fig.1.2. Seasonal migration of ITCZ and behaviour of (a) summer monsoon (SWM; red arrows) and winter monsoon (NEM; blue arrows) winds over the Indian subcontinent. (Source of shape file: <https://www.naturalearthdata.com/>)

The vast majority of existing palaeoclimate studies in India have primarily focused on studying ISM variability, with some studies noting the potential additional significant influence of the Indian Winter Monsoon (IWM) especially in the South Indian peninsular (eg; Rajmanickam et al., 2017; Sandeep et al., 2017; Veena et al., 2014). Very few records are available focused on IWM variability (eg; Böll et al., 2014; Misra et al., 2019; Ranasinghe et al., 2013), due to the lack of areas solely fed by winter monsoon rainfall in India. In addition, due to the large spatial (latitudinal) differences between the available summer and winter monsoon records, it is difficult to compare and understand the relationship between these two major components of the SAM system. Moreover, the teleconnection between the IWM and other climatic systems, such as ENSO and NAO, at different points in the past, remain poorly understood.

Many of the existing records from the ISM domain in India suggest gradual or stepwise decreasing trends in rainfall during the middle and Late Holocene (Ankit et al., 2017; Basavaiah et al., 2015; Leipe et al., 2014; Ponton et al., 2012) that are likely related to the southward migration of mean latitudinal position of ITCZ triggered by decreasing Northern hemisphere solar insolation (Fleitmann et al., 2007; Haug, 2001). However, palaeoclimate evidence that clearly and consistently support this hypothesis for the Indian sub-continent is limited due to the heterogeneity of the palaeoclimate records. Furthermore, it is not investigated how the IWM varied relative to the ISM during the migration of the mean position of ITCZ. Therefore, there remains a significant knowledge gap in the understanding of the past operation of the South Asian monsoon system, despite the existing large number of palaeoclimate records in the region.

This is particularly problematic given suggestions that SAM dynamics may have had a role in the appearance and collapse of several, often large, human societies in South Asia over the course of the Holocene (e.g.; Harappan civilization) (Kathayat et al., 2017; Sinha et al.,

2019; Staubwasser and Weiss, 2006). Factors such as the changing number of rainy seasons, amount and intensity of rainfall, frequency of extreme events such as floods, geographical and geomorphological conditions, and water management techniques determine the stability of an agricultural human society (Lucero et al., 2015). Therefore, understanding the impact of Holocene monsoonal changes on past human populations is also important for highlighting the effectiveness of different responses and mitigation strategies of relevance to 21st century societies in the same region.

As an island located close to the equator and in a central position within the seasonal ITCZ migration path, Sri Lanka is influenced by both summer (Southwest monsoon; SWM) and winter (Northeast monsoon; NEM) monsoon rainfall during different parts of the year. The central highlands of Sri Lanka (maximum altitude ~ 2500 m) act as an orographic barrier to these summer and winter monsoon winds, restricting summer monsoon rainfall/ SWM primarily to the southwestern part of the island and winter monsoon rainfall/ NEM to the northern and eastern parts. From a palaeoclimatic perspective, these unique geographical conditions facilitate the tracking of both of these seasonal rainfalls (SWM and NEM), separately, from records with a minimal spatial (latitudinal) difference. As a result, well-dated palaeo-monsoonal records from Sri Lanka can provide important information to fill knowledge gaps about the South Asian Monsoon system more widely.

Nevertheless, the geomorphological settings (eg; steep geomorphology) in Sri Lanka have led to a relative dearth of long-term climate archives such as natural lakes, peat bogs, and speleothems. Researchers have thus turned to the plentiful brackish water coastal lakes and lagoons along the coastal belt of the island (e.g.; Gayantha et al., 2020; Ranasinghe et al., 2013; Ratnayake et al., 2017). However, these coastal water bodies reflect signals from both terrestrial and marine environments that demand more specific environmental proxies for identifying OM sources and biogeochemical processes. Alternatively, isolated records from the

peat deposits of the central Highlands have been used to look at broader changes in rainfall across the island given their key geographical position (Premathilake and Risberg, 2003). Yet, these records have arguably yet to reach their full potential in terms of chronological resolution and multi-proxy analysis.

In this thesis I apply multi-proxy techniques combining organic geochemical proxies (diagnostic biomarkers and compound specific stable isotopes) with inorganic and sedimentological proxies (metals analysis and grain size distribution) to three different sites in Sri Lanka, that represent the major climatic (wet and dry zones) and geomorphological (lowland and highland) zones of the island. The analysed proxy results reveal a broad range of palaeoclimate and palaeoenvironmental information in the study areas, such as major organic matter sources, palaeohydrological information (rainfall, aridity, moisture source), vegetational changes, catchment processes (erosion, stream discharge) and marine influence, that can be used to test hypotheses relating to the operation of the SAM over the island in the past.

1.3 Objectives

I hypothesize that the southward migration of the mean position of the ITCZ during last 6000 years decreased the length of SWM season while increasing the length of NEM season, resulting in a long-term inverse relationship between *summer* and *winter* monsoon (SWM and NEM) rainfalls in Sri Lanka. To test this hypothesis, this thesis aims to track the sub-millennial scale variation of SWM and NEM rainfall in Sri Lanka during the Middle and Late Holocene (from ca. 6000 cal yr BP to present) by comparative reconstruction of monsoonal rainfall variation at three different sites in the island along a transect from the west coast to the east coast via the central highlands.

In addition, this study seeks to understand the influence of external forcing factors (e.g., solar insolation) and also other climate variables (e.g., ENSO, NAO) towards the general long-

term trend and abrupt changes of SWM and NEM rainfall in Sri Lanka during the last 6000 years. Finally, the reconstructed monsoonal trends will be compared with other regional palaeoclimate records to understand the regional behaviour of the South Asian Monsoon system and the impact of monsoonal rainfall trends on prehistoric and historic human societies in Sri Lanka.

2. Mechanism, Reconstruction and Cultural Impacts of South Asian Monsoon – Literature Review

2.1 Driving Mechanism and Factors Influencing South Asian Monsoon System

The mechanism driving the monsoon is still not fully resolved in tropical climate science. Several hypotheses have been proposed to explain the Asian monsoon variability by different climatologists. The first hypothesis proposed is that the monsoon is a gigantic land-sea breeze resulting from the differential heating of land and sea associated with solar insolation (Halley, 1687). This hypothesis was popular for over 300 years and, even today, some atmospheric circulation models consider the differential heating between land and ocean as the primary driver of the monsoon (eg; James, 1994; Meehl, 1992). However, there are significant spatial and temporal incompatibilities between the land sea thermal contrast and the precipitation over the Indian sub-continent (Gadgil, 2018). For example, the strongest Indian Summer Monsoon (ISM) winds are observed during July in India not the hottest month of June. Furthermore, the hottest region of northwest India has desert conditions and receives very little monsoonal precipitation (Gupta et al., 2020). Gadgil (2018) illustrated that the relationship between monsoon rainfall and the temperature difference between land and ocean is weaker than has often been argued.

As a result, several other alternative hypotheses have been proposed. Charney (1968) suggested that the monsoon is a manifestation of seasonal migration of the Inter-Tropical Convergence Zone (ITCZ), driven by the seasonal variation of maximum latitude solar insolation. The ITCZ acts as a dividing line between the southeast and northeast trade winds, collocated with the ascending branch of the Hadley cell (Chiang and Friedman, 2012) (the Hadley cell is the convection cell, with a rising motion near the equator and sinking motion near 30° latitude in the northern and southern hemispheres; Fig. 2.1). Several other definitions

are also available and according to all of them, ITCZ is characterised and tracked by the pressure minimum, surface wind convergence, rainfall maximum, the vorticity maximum, minimum in outgoing long wave radiation, or the cloudiness maximum (Nicholson, 2018). However, these features/assumptions about the ITCZ are not always true over the continents where the trade winds are weak in most cases. For example, a decoupling between pressure minima and maximum rainfall is prominent in West Africa. Therefore, using the term ITCZ over the Africa and South America is criticised by some scientists (Nicholson, 2018, 2009). However, when discussing the South Asian/Indian monsoon system the term ITCZ or equatorial trough is widely used in the literature despite its seasonal location over the southern Indian Ocean or Indian sub-continent. This is likely due to the fact that the Indian subcontinent is not as large as Africa and South America leading to a reduction in potential discrepancies. However, sometimes the terms Continental Tropical Convergence Zone (CTCZ) and Oceanic Tropical Convergence Zone (OTCZ) are used to illustrate the non-identical nature of ITCZ over the land and ocean (Gadgil, 2018). In this thesis I use the term ITCZ or the equatorial trough to refer the narrow low-pressure latitudinal zone that drive the monsoonal winds and accompanied rainfall over the Indian sub-continent.

The system responsible for the large-scale monsoon rainfall over the Indian region is shown to have all the important dynamical characteristics (eg; maximum cloudiness zone) of the ITCZ (Gadgil, 2018). Therefore, it can be considered seasonal migration of ITCZ is the main driving factor of the monsoon rainfall where land sea thermal contrast has a minor effect as also shown by modelling studies (Chao and Chen, 2001). This hypothesis is widely accepted today and supported by many scientists (Chao and Chen, 2001; Gadgil, 2003; Schneider et al., 2014; Sikka and Gadgil, 1980; Wang, 2009). The ITCZ seasonally migrates towards the warmer hemisphere and the ITCZ determines the onset, duration, and termination of monsoonal rainfall in the equatorial and sub-equatorial regions. It shifts between 9° N and 2°

N latitudes over the central Atlantic and Pacific Oceans during boreal summer and boreal winter respectively, but shows a more dramatic shift of between 20°N to 8°S latitudes over the Indian Ocean due to the presence of the Indian subcontinent (Schneider et al., 2014).

The studies leading to understand the mechanism of ITCZ and SAM is solely depend on tracking the behaviour of ISM that brings majority of rainfall to the Indian sub-continent. However, behaviour of IWM is mostly ignored due to lack of regions to track its long-term variation, despite it is a key component of SAM system. Contrast to ISM, IWM rainfall occur over the southern parts of Indian sub-continent due to moment of ITCZ over the Indian Ocean (Oceanic ITCZ) and therefore comparative study of ISM and IWM is important for complete understanding the ITCZ dynamics.

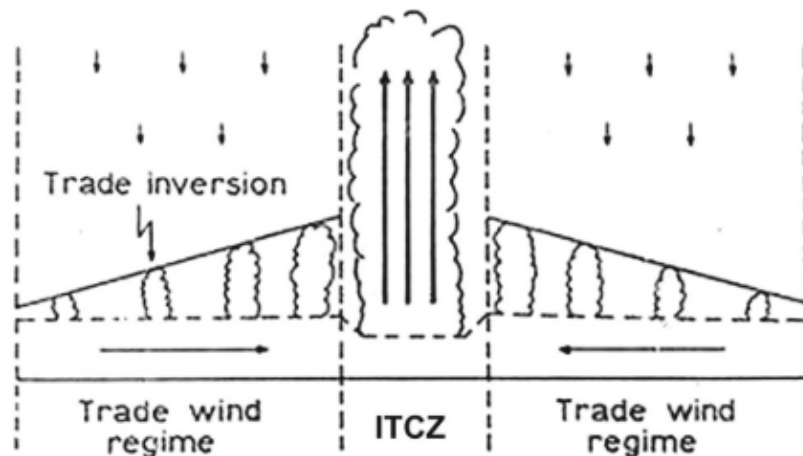


Fig.2.1 Schematic picture of Hadley cell (Source: Gadgil, 2018)

As noted by present-day instrumental and palaeoclimate records from the Indian sub-continent, the ISM is highly variable throughout the Indian sub-continent and demonstrates highly complex behaviour. This complexity is driven by the various forcing factors and teleconnection with different modes of climate variables that influence the intensity and timing of the Indian monsoon precipitation detailed below. Orbital forcing and solar forcing are the

(external) forcing factors that determine the energy input (solar variability) on Earth and thereby Earth's climate conditions including monsoon system. Modes of climate variables such as ENSO, NAO, IOD influence the Indian monsoon system by changing the energy balance and atmospheric circulations that have teleconnections with the South Asian monsoon system.

2.1.1 Forcing Factors

Changes in solar insolation reaching the Earth's surface or "solar variability" consists of two major variables: i) orbital forcing and ii) solar irradiance/forcing (Gupta et al., 2020). Changes in orbital forcing are a result of changes in the Earth's eccentricity (orbit shape), obliquity (axial tilt), and precession (axial wobble) and have, since the Pleistocene, been primarily reflected in the context of 'Milankovitch cycles' (Ruddiman, 2006) – orbital changes occurring with periodicities of ~100 kyr, ~41 ky and ~23 kyr respectively (Wanner et al., 2008). These orbital forcings result in periods of high or low solar insolation in the Northern hemisphere causing an expansion or melting of ice sheets in the polar and high-altitude regions that drive glacial/interglacial cycles on Earth, migration of the mean latitudinal position of ITCZ, variation in the land sea thermal contrast, and variation in evaporation and convection over the Indian Ocean (Banerji et al., 2020; Gupta et al., 2020; Wanner et al., 2008). These factors directly and indirectly influence the weakening or strengthening of the South Asian Monsoon. During the Holocene, Earth's precession cycle was the main controlling factor of solar insolation variability (Fig. 2.2) that caused the periodic southward migration of the mean position of ITCZ, weakening the ISM (Fleitmann, 2003; Haug, 2001).

Solar forcing is the changing of solar activity that is controlled by a series of quasi-periodical cycles that range from 11 to 2300 years. They are termed as Schwabe (11 years), Hale (22 years), Gleissberg (87 years), Suess (210 years), Eddy (1000 years) and Hallstatt cycles (2300 years). These solar cycles (solar maxima or minima) can cause warm and cold periods on the Earth. As an example, the 1000-year Eddy cycle shows clear correlation with

alternating warm and cold periods occurred during the last 2000 years (Fig. 2.3; Lüning and Vahrenholt, 2016). While, present-day advanced technology allows solar activity to be measured directly, cosmogenic isotopes (^{10}Be , ^{14}C and ^{36}Cl) generated by cosmic rays have been used to reconstruct past solar activity (Fig. 2.2; Banerji et al., 2020; Lüning and Vahrenholt, 2016). Using these techniques, several studies have speculated a link between solar activity cycles and centennial–millennial- scale tropical monsoon variability over the Indian Ocean and Indian sub-continent. Generally, high solar activity increases equatorial convection that brings higher rainfall to monsoonal domains. (Donges et al., 2015; Gupta et al., 2005; Thamban et al., 2007). It has also been shown that alternating cold and warm periods (Roman Warm Period, Dark Ages Cold Period, Medieval Warm Period, Little Ice Age; Fig. 2.3) occurred during last two millennia and that they correlate with a weak and strong ISM respectively (Banerji et al., 2020).

However, the boundaries of these cold and warm periods are not well defined, and their influence show significant differences based on the geographical regions. This is due to the influence of other climate variables such as ENSO, NAO can alter the direct impact of these external forcing factors. Therefore, a simple correlation between monsoon variation and variation of external forcing factors only helps for partial understanding of the SAM system.

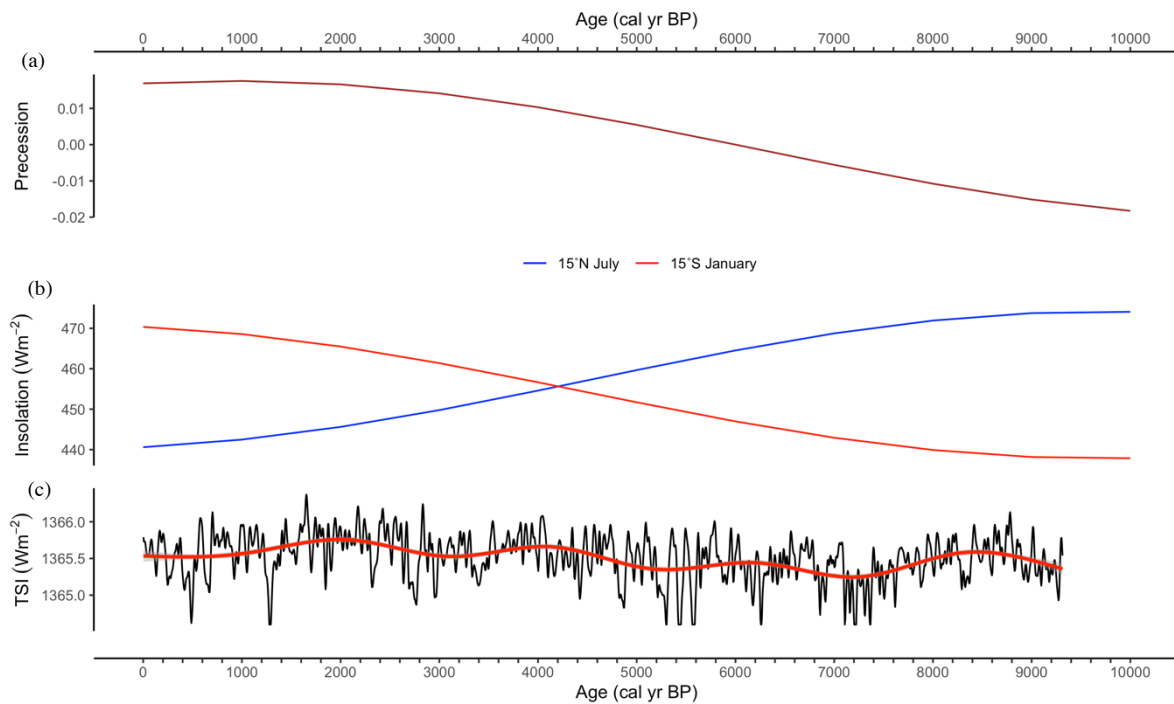


Fig.2.2 Variation of a) Earth’s precession b) solar insolation in tropical northern (blue) and southern hemisphere (red) (Berger and Loutre, 1994) and c) Total Solar Irradiance (Steinhilber et al., 2009) during the Holocene

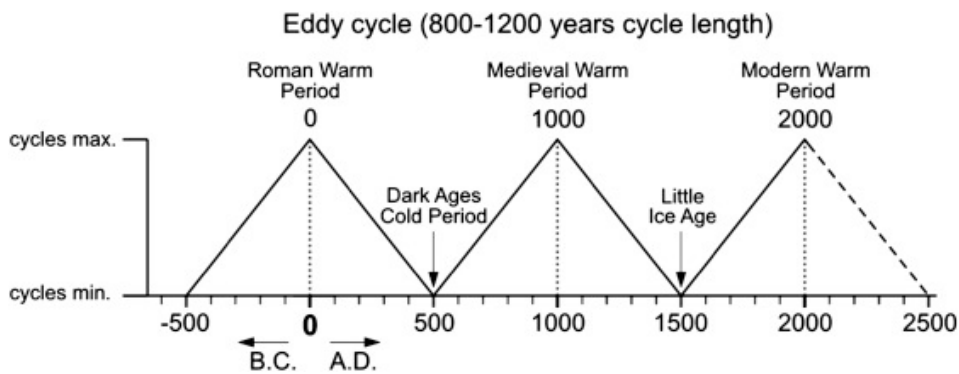


Fig.2.3 Schematic sketch of historical maxima and minima of the 1000-year Eddy solar activity cycle (Source: Lüning and Vahrenholt, 2016)

2.1.2 Modes of Climate Variables

Factors such as tectonic and orographic drivers can have million-year scale influences on ISM and not discuss here because our records only cover a portion of the Holocene. Other factors,

such as the Indian Ocean Dipole (IOD), El Niño Southern Oscillation (ENSO), North Atlantic Oscillation (NAO), mid-latitude Westerlies, and changes in snow cover (albedo effect) in the Eurasian and Himalayan regions can also impact on the Indian monsoon system on interannual, multi-decadal or centennial scales (Banerji et al., 2020; Gupta et al., 2020). Variation in these climate variables based on proxy indices are shown in Fig. 2.4 and are discussed below in terms of their relative teleconnections to the Indian summer monsoon variability.

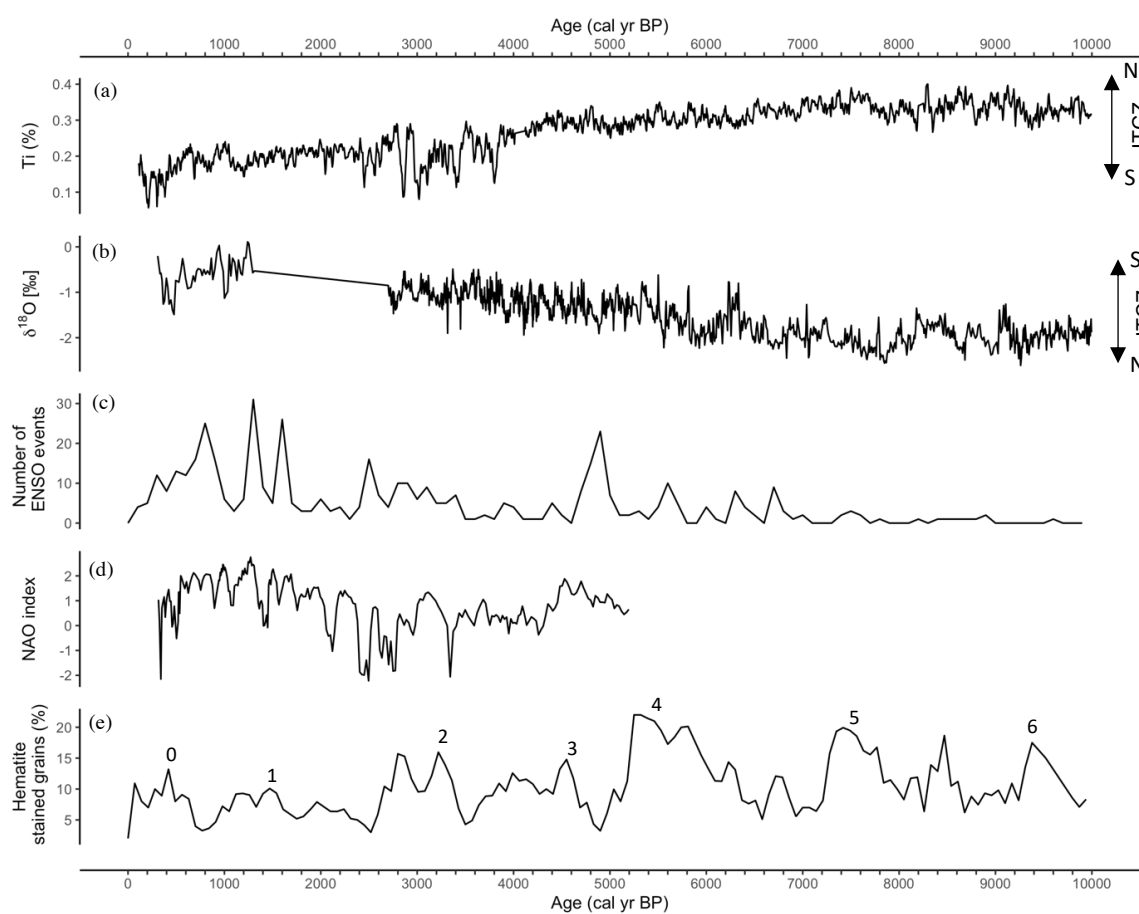


Fig.2.4 Different modes of climate variables influencing Asian monsoon system during the Holocene. a) ITCZ migration from Ti% in Cariaco Basin sediment (Haug, 2001) and b) ^{18}O isotope records from Qunf cave, Oman (Fleitmann, 2003). c) Number of ENSO events in 100 yrs non-overlapping window (Moy et al., 2002). d) Reconstructed NAO index (Olsen et al., 2012). e) Hematite-stained grains from North Atlantic and Bond events (Bond et al., 2001).

El Niño Southern Oscillation (ENSO)

The anomalous oscillation in surface ocean warming in the central and eastern Pacific region, with improved convection in the atmosphere (El Niño) and an unusual cooling of ocean surface waters with reduced convection in the atmosphere (La Niña), has been described as the El Niño Southern Oscillation (ENSO) (Gadgil et al., 2004). ENSO is one of the strongest internal factors that affect the global climate, particularly in the tropics, impacting rainfall in equatorial regions of Asia, Africa and South America via changes in the atmospheric circulation (Fig.2.5; Gupta et al., 2020; Kumar et al., 2006). The “normal” atmospheric circulation system in the equatorial Pacific Ocean, characterized by high surface pressure and a concurrent sinking motion in the east and relatively low surface pressure and a concurrent rising motion in the west, with easterly trade winds at the surface and westerlies aloft is called the Walker circulation (Rohli and Vega, 2017). Interaction between altered Walker circulation and Hadley circulation during ENSO events can influence the Indian monsoon system.

During El Niño, weakening of the strength and amount of ISM rainfall can usually be observed over the Indian subcontinent and commonly results in droughts in the region. (Kumar et al., 2006; Rasmusson and Carpenter, 1983; Sinha et al., 2011). In contrast, enhanced rainfall and floods in southern India occur during the winter monsoon rainfall season (October – December) associated with El Niño events. Intensified deep convection over the Indian Ocean during El Niño, increase storms and cyclones that hit the southern Indian region (Yadav, 2012). Generally, opposite effects can be observed during La Niña conditions.

Similar trends can be observed for the Southwest Monsoon (SWM) in Sri Lanka. During ENSO extremes (El Niño), reduction of SWM (summer monsoon) rainfall is observed in Sri Lanka. The NEM (winter monsoon) does not appear to show a significant correlation with ENSO extremes, however the Second Inter Monsoon rainfall (SIM; October-November) showed clear changes in sync with the El Niño events, leading to widespread enhanced rainfall

accompanied with catastrophic floods and landslides in the island (Hapuarachchi and Jayawardena, 2015; Kane, 1998; Malmgren et al., 2003). Some authors (eg; Zubair and Ropelewski, 2006) claim an increase of the winter monsoon in Sri Lanka during an El Niño events. However, this is a misinterpretation because they refer to the period October – December which, although it represents the winter monsoon in India, is actually the SIM in Sri Lanka.

In a palaeoclimatic context, a shift towards higher ENSO activity (high frequency of ENSO) during the Late Holocene, in contrast to the mid-Holocene, has been suggested by several studies conducted in the Peruvian region (eg; Keefer et al., 1998; Moy et al., 2002; Rein et al., 2005; Fig.2.4) and coupled ocean-atmospheric models (Clement et al., 2000). Lithic fluxes observed in Peruvian sediments revealed that enhanced ENSO activity during 5600 – 3500 cal yr BP was followed by a constant frequency during 3500 – 2000 cal yr BP (Rein et al., 2005). Increased ENSO frequency during the Late Holocene is suggested as a main reason for decreased ISM during the Late Holocene (Banerji et al., 2020). Number of IWM records are very low and most of them only cover the Late Holocene making it difficult to understand the influence of changing ENSO frequency towards IWM variation during Holocene.

However, for the last few decades with instrumental records it has been noted that the relationship of ISM rainfall with ENSO has weakened whilst the relationship between ENSO and NEM rainfall is strengthening or remains unchanged (Yadav, 2012; Zubair and Ropelewski, 2006). This is possibly due to the influence of other modes of climate variability that have been suggested such as the Indian Ocean Dipole (IOD), increasing SST in the central and western Indian Ocean, and the Indo-Pacific Warm Pool (IPWP) (Gupta et al., 2020; Zubair and Ropelewski, 2006). This implies that the relationship between ENSO and Asian Monsoon system was not constant over time due to the influence of varying geographical, climatic, and environmental factors that are not well understood.

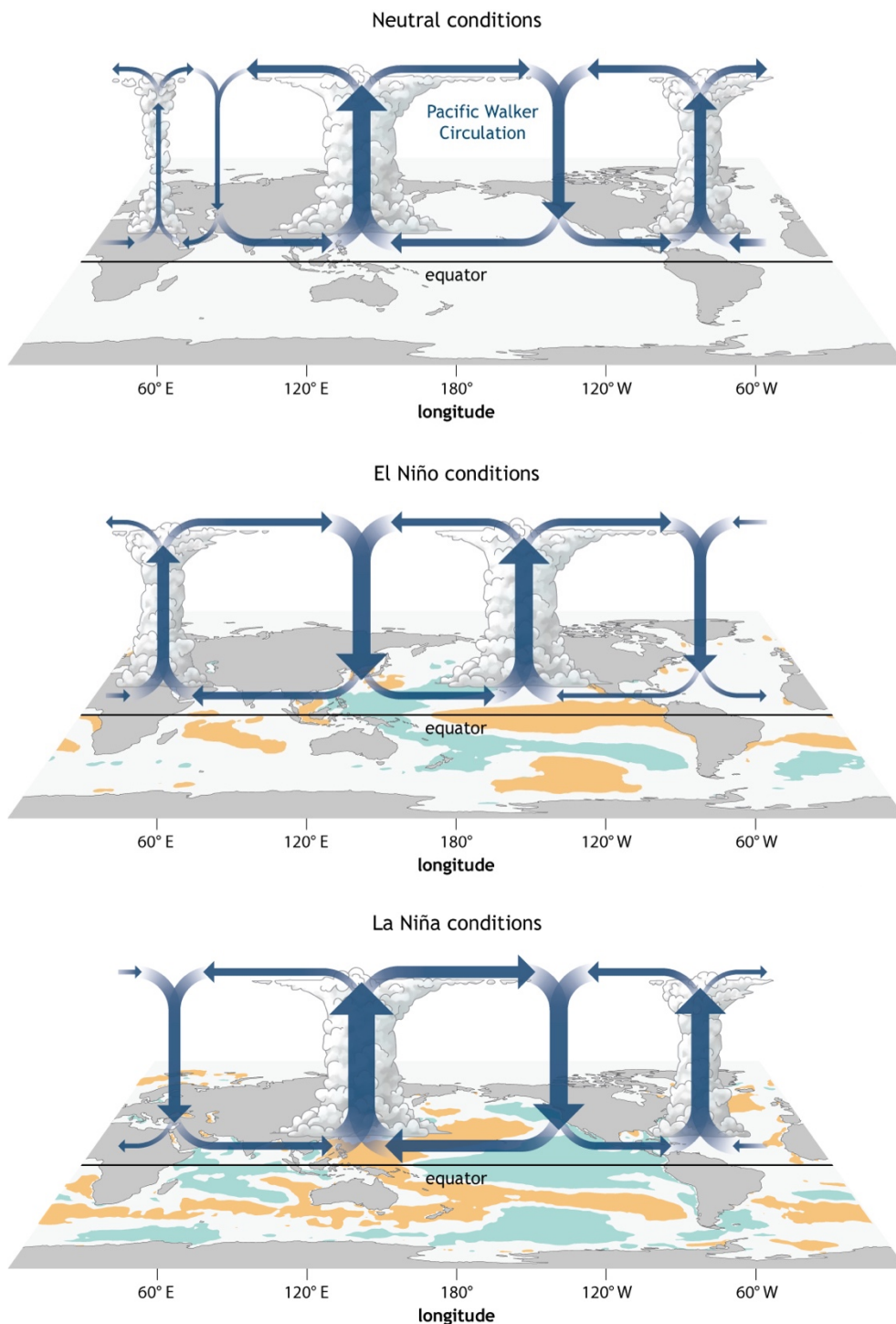


Fig.2.5. Generalized Walker Circulation (December-February) anomaly during ENSO neutral, El Niño and La Niña events, overlaid on map of average sea surface temperature anomalies. Anomalous ocean warming (orange); Anomalous ocean cooling (blue-green). (Source: <https://www.climate.gov/news-features/blogs/enso/walker-circulation-ensos-atmospheric-buddy>)

Indian Ocean Dipole (IOD)

The relationship between ENSO and reduced ISM has not always been maintained and 'normal' monsoon rainfall has also been observed during intense El Niño years. This is possibly due to the impact of Indian Ocean Dipole (IOD) (Abram et al., 2020; Ashok et al., 2001). The IOD is an irregular oscillation of sea surface temperature (SST) in the western and eastern Indian Ocean accompanying wind and precipitation anomalies (Fig.2.6; Saji et al., 1999). A positive IOD (higher SST in the western Indian Ocean) is associated with higher rainfall, while negative IOD (higher SST in the eastern Indian Ocean) is correlated with lower rainfall over the Indian sub-continent and the Arabian Sea (Fig.2.6; Ashok et al., 2001). The IOD can individually, or together with ENSO, significantly impact the operation of the Indian monsoon (Ashok et al., 2004; Jayakody, 2015; Kripalani and Kumar, 2004).

Generally, co-occurrence of IOD (positive) with ENSO (extreme) reduces the impacts of ENSO on ISM rainfall. However, sometimes the IOD (negative) and ENSO can have complementary effects towards the ISM. Hence, the IOD acts as a modulator to the ENSO impact on ISM rainfall (Hrudya et al., 2020). It is likely that the frequent occurrence of the IOD during the last few decades has weakened the link between ENSO and ISM as suggested by the modelling studies (Ashok et al., 2001; Saji et al., 1999). However, palaeorecords (during the Holocene) on IOD are still not available due to lack of sea surface temperature data in the western and eastern Indian Ocean. Therefore, it is unclear how changing IOD frequency and intensity influence towards South Asian summer and winter monsoon rainfall variations during the Holocene.

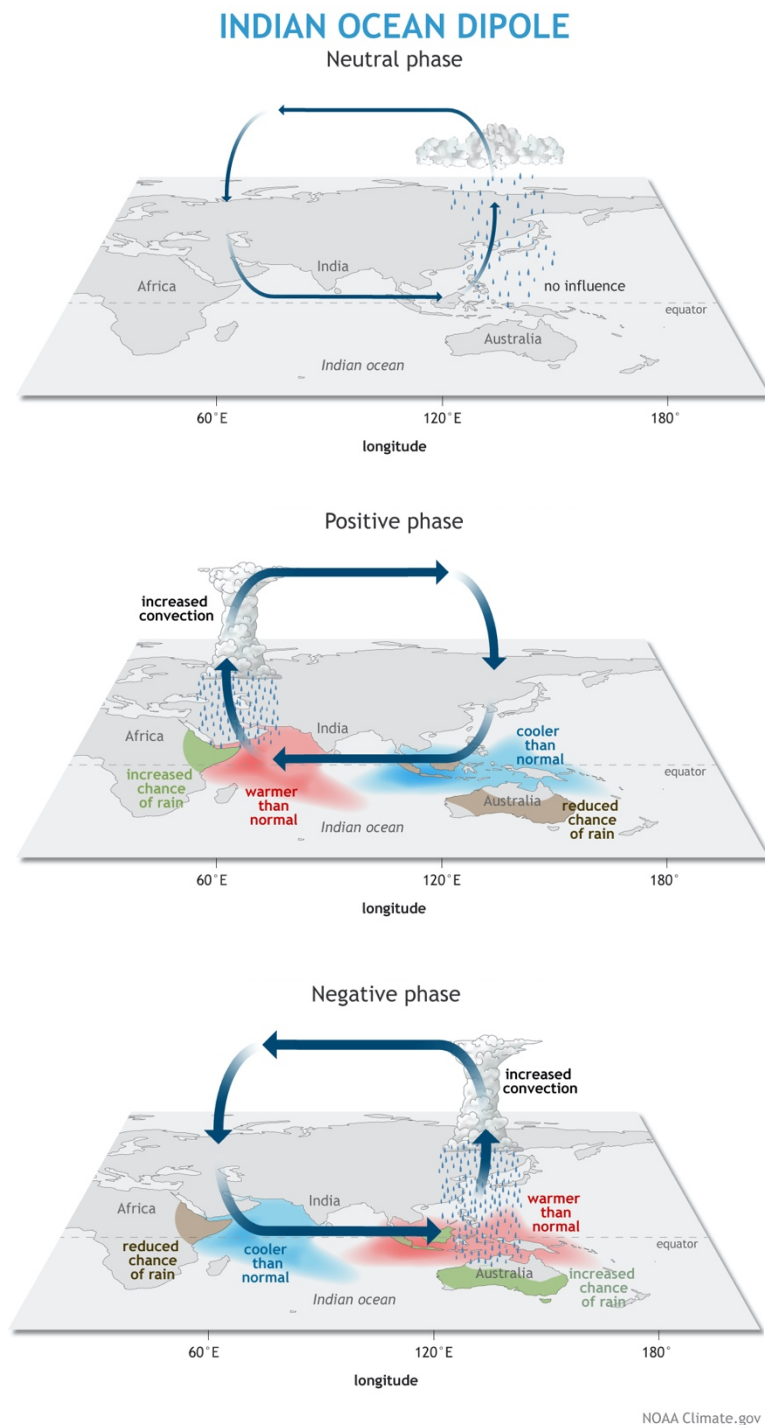


Fig.2.6. Indian Ocean Dipole (IOD). Neutral, Positive and Negative phases and changes to atmospheric circulation.
 (Source: <https://www.climate.gov/news-features/blogs/enso/meet-enso%E2%80%99s-neighbor-indian-ocean-dipole>)

North Atlantic Oscillation (NAO)

In addition, several studies indicate interdecadal to centennial-scale impacts of the North Atlantic Oscillation (NAO) on the ISM (Dutt et al., 2015; Gupta et al., 2003). The NAO is a fluctuation of sea-level atmospheric pressure differences at the surface between the sub-tropical (Azores) high and the subpolar (Icelandic) lows without specific periodicity (Hurrell, 1995). Positive NAO is characterised by high pressure differences where the pressure difference is low during the negative NAO phase. Positive (negative) phases of the NAO are accompanied by relatively mild (cold) winters over northern Europe and a relatively cold (warm) climates in the eastern Mediterranean and the Middle East (Fig.2.7; Wanner et al., 2008).

Bond events indicated by drift ice indices in the North Atlantic during the Holocene refer to periods of enhanced ice sheet formation (Fig. 2.4; Bond et al., 2001) and show general correlation with the solar minima and global dry and cool events during the Holocene (eg; 4.2 ka event, LIA). Bond events and negative NAO conditions are associated with formation of enhanced ice sheets in the sub-polar regions and enhanced snow cover that result increase the albedo. As well, part of solar energy is used for melting ice and snow cover leading a decrease of Northern hemisphere solar insolation. This phenomenon can lead failure of developing low pressure trough in the Northern and central parts of Indian sub-continent reducing the South Asian summer monsoon rainfall over the region (Bamzai and Shukla, 1999; Gupta et al., 2020).

A conspicuous negative excursion of the NAO index at ~ 4.2 ka (Olsen et al., 2012) is associated with regional drought and a reduced summer monsoon that marks the boundary between mid- and late Holocene, which has now been formally recognised (Banerji et al., 2020). These observations suggest that the NAO has an influence on the ISM in the Indian Ocean and the Indian sub-continent by increasing Eurasian ice/snow cover and weakening the land-sea thermal contrast (Gupta et al., 2020). However, the relationship between ISM and

NAO is still not clearly understood. It is generally considered, that about one fourth of abrupt changes of ISM can be related to NAO. As well, it is not clear how the NAO influenced towards changes of IWM.

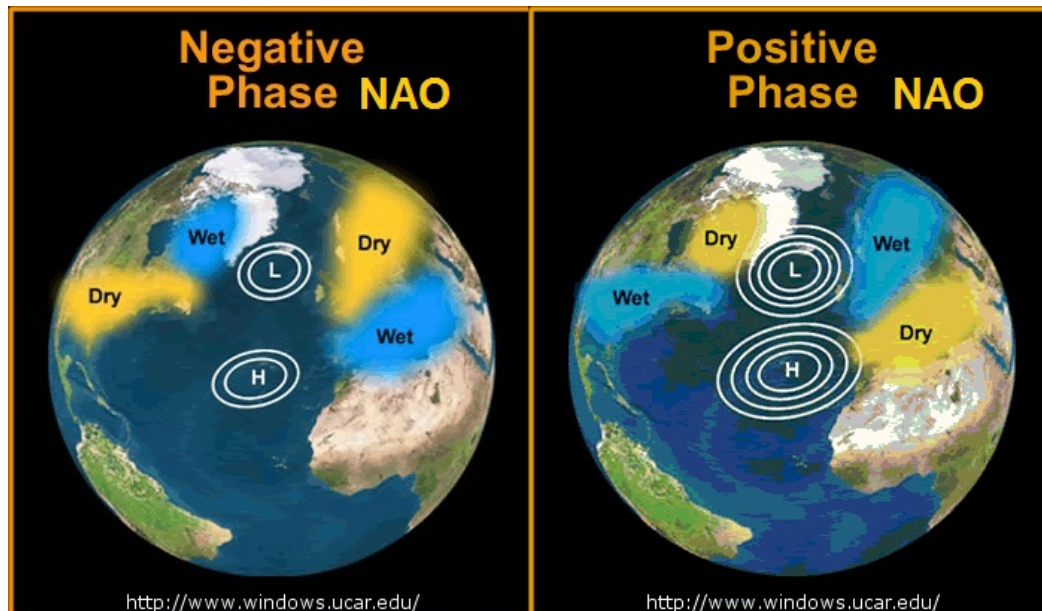


Fig.2.7. North Atlantic Oscillation (NAO) and climate condition in Europe and North America.

(Source: <https://www.windows2universe.org/earth/climate/nao.html&edu=elem>)

2.1.3 Mean Latitudinal Migration of ITCZ

Seasonal migration of the ITCZ to the relatively warmer Northern or Southern hemisphere at different parts of the year regulates the onset, duration, and cessation of tropical and sub-tropical rainy seasons (Schneider et al., 2014). Similarly, over longer timescales, the mean latitudinal position of the ITCZ migrated towards the differentially warming hemispheres as indicated by palaeorecords (Fleitmann et al., 2007; Haug, 2001). The mean latitudinal position of the ITCZ during the Holocene is mainly driven by Earth's precessional cycle that controls interhemispheric solar insolation variability (Banerji et al., 2020).

The early Holocene coincided with perihelion (when Earth's position on its orbit is closest to the sun), and the mean position of the ITCZ shifted north due to intensified summer

insolation over the Northern hemisphere. Subsequently, the ITCZ started migrating southward until the Little Ice Age (LIA, 1350-1800 AD), due to weakening of the Northern hemisphere solar insolation associated with the Earth's precessional cycle (Schneider et al., 2014). This millennial scale Holocene ITCZ migration is witnessed in the Cariaco Basin records, that show variations in runoff inferred from changing Ti content (Haug, 2001), and $\delta^{18}\text{O}$ records of stalagmites from Oman (Fleitmann, 2003) (Fig.2.4). The climatic consequences of these changes were also further strengthened by the southward expansion of evergreen forests during the Late Holocene at the southern margin of Amazonia (Mayle et al., 2000).

Generally, the ISM weakened over the course of the middle and Late Holocene as a result of southward migration of the boreal summer position of the ITCZ according to palaeoclimate reconstructions in ISM domains (Wanner et al., 2008). This is due to the ITCZ moving less far northward in boreal summer, or a weakening of its rainfall intensity, or a combination of both (Schneider et al., 2014). Over the Pacific Ocean, variation of interhemispheric solar insolation during the Holocene might have increased El Niño intensity (Fig.2.4) that further amplified southward migration of the mean ITCZ position. On the other hand, increased El Niño may have further weakened the ISM (Banerji et al., 2020). However, it is not so far investigated how the southward migration of mean ITCZ position influenced towards IWM.

In addition to these atmospheric-ocean circulations and related changes, variation of atmospheric composition as a result of volcanism, forest fires, CO_2 degassing from land and oceans, and anthropogenic activities also can affect Indian monsoon system, although these generally seem to be temporary in a majority of instances. In addition, the predictability of such changes is difficult to resolve in the form of systematic positive or negative swings in the proxies measured to infer precipitation-driven changes (Gupta et al., 2020).

According to the above summary of different forcing factors and their impacts on the South Asian Monsoon (SAM) system, we can see some factors such as solar insolation, total solar irradiance directly influence towards SAM variability through migration of the mean position of ITCZ, changing land-sea thermal contrast, and changing intensity of equatorial convection and evaporation. Some other factors indirectly influenced the SAM by changing general atmospheric circulation (eg; ENSO, IOD), changing albedo, and changing land-sea thermal contrasts (NAO). Their effects can be annual to millennial and can have simultaneous influences. Therefore, the SAM system is highly complex climate phenomenon that that demand spatially well distributed palaeoclimate records in the region for better understanding its key driving factors.

2.2 Proxies Used in Palaeo-monsoonal Reconstructions

Tracking the variations of past rainfall/precipitation is one of the main goals in palaeoclimate reconstructions. Changes in stable hydrogen and oxygen isotopes (δD and $\delta^{18}O$) in meteoric water are recorded in archives such as continental ice cores, speleothems and carbonate or silica producers in lakes (eg; ostracods). However, ice cores are limited to polar regions and high-altitude areas where speleothems are also found only in some cave sites that are formed under special geomorphological settings that are not common in many regions. Carbonate producing microfossils are also not common in many lakes and their availability is also not continuous throughout the whole period (Sachse et al., 2012).

Therefore, measuring the hydrogen isotope ratios (δD values) in a certain organic compound that can be traced to a certain photosynthesizing organism or group of organisms (i.e. biomarker) is a promising method that has been developed recently. Sedimentary leaf wax *n*-alkane are the most commonly used in this purpose due to their relative easiness to separate from TLE, being unnecessary for further sample preparation or correction to added carbon or

hydrogen during derivatization, and their relatively specific nature of the source (cuticular leaf wax) in sediments (Holtvoeth et al., 2019).

Before applying the compound specific isotope technique to reconstruct past hydrological changes, it is necessary to understand the main controlling factors of hydrogen isotopes fractionation in meteoric water in the SAM with specific focus to Sri Lanka and factors determining leaf wax *n*-alkane carbon and hydrogen isotopes fractionation.

2.2.1 Controls of δD and $\delta^{18}O$ in Monsoon Rainfall in Sri Lanka

As a tropical island in the Indian Ocean, rainfall is the main controlling factor of climatic and environmental conditions in Sri Lanka. Due to its near-equator geographical position and geomorphological conditions, the amount effect and altitude effect are the two main factors that determine the H and O isotopic variations of rainfall in Sri Lanka (Edirisinghe et al., 2017). The amount effect is the relationship between the amount of rainfall and the depletion of heavy isotopes (D and ^{18}O) in rainfall in a certain area (Dansgaard, 1964; Rozanski et al., 1993). With decreasing rainfall comes a greater enrichment of D and ^{18}O in meteoric water. Depletion of heavy isotopes in precipitation as a result of increasing elevation is identified as the altitude effect. This is related to decline in air temperature with increasing altitude that control the condensation of water vapour (Gat et al., 2000). Precipitation in highland areas of Sri Lanka show relatively depleted isotopic values compared to the lowlands (Edirisinghe et al., 2017).

In addition, depending on the seasonality of the monsoons (summer or winter rainfall) H and O isotopic values vary in meteoric water. This is actually related to changes in the moisture source. Generally, winter monsoon rainfall is more depleted in D and ^{18}O in contrast to the summer monsoon in Sri Lanka and India (Edirisinghe et al., 2017; Srivastava et al., 2014). The main source of moisture for the winter (or NE) monsoon is the Bay of Bengal (BOB) where several major rivers from the Indian subcontinent such as Ganges, Brahmaputra

and Irrawaddy discharge their water. Therefore, the water isotopic values are relatively depleted in the BOB (Achyuthan et al., 2013) contrast to the open Indian Ocean which is the moisture source for summer (or SW) monsoon rainfall. In addition, winter monsoon winds start from northern India and travel a long distance over the land compared to the sea (BOB), carrying with it some amounts of land derived moisture that is also highly depleted in D and ^{18}O .

2.2.2 Controls of Sediment Leaf Wax Hydrogen and Carbon Isotopes Composition

Water is the primary source of hydrogen for biosynthesis in different photosynthetic organisms. The source of water will vary depending on the environment in which a species lives and their adaptations for the uptake of water. Terrestrial plants depend on soil water whereas aquatic organisms (cyanobacteria, algae, aquatic plants) take up water accumulating in bogs, lakes and rivers. Precipitation (meteoric water) and atmospheric moisture are the primary sources of water for these environments (Sachse et al., 2012). Therefore, δD in sedimentary OM can primarily provide palaeohydrological information, i.e. amount, trajectory and source of precipitation (Holtvoeth et al., 2019).

Hydrogen isotopic composition in meteoric water and atmospheric moisture/vapour varies mainly as a result of Rayleigh fractionation processes. Several environmental factors such as the continental effect, latitude effect, amount effect, altitude effect and seasonal effect involve in modification of the H and O isotopic compositions of meteoric water. Latitude effect is the depletion of heavy isotopes in precipitation when moving to higher latitudes related to lowering temperature. Depletion of heavy isotopes when air masses move over continents due to progressive loss of moisture, is called the continental effect (also called the distance from coast effect). Rainwater isotope depletion also occurs with increasing altitude related to decreasing temperature that can be identified as the altitude effect. The amount effect is the

isotopic depletion of rainwater with higher rainfall. In areas where significant seasonal temperature differences are available, isotopic fractionation in precipitation also occurs based on the seasonal temperatures. In the tropics, seasonal effects are defined by the changing of the moisture source due to changing the direction of air mass (monsoon) (Dansgaard, 1964; Gat et al., 2000; Rozanski et al., 1993).

Hydrogen isotopes from archived remains of photosynthetic organisms will reflect this hydrological information in the past. Higher plants take up soil water that is derived from meteoric water. Hydrogen isotopes of plant water and plant tissues will, however, be significantly modified due to processes impacting transpiration (i.e., aridity) prior to biosynthesis. Therefore, δD in terrestrial plant lipids reflect a combined signal of precipitation and evaporation (Sachse et al., 2012; Sessions et al., 1999). By contrast, submerged aquatic plant and algae use their surrounding water column as their source of hydrogen and so will reflect average δD value of precipitation in the region unless there is no fluvial inflow from distant areas or they are impacted by strong evapotranspiration in very arid regions (Holtvoeth et al., 2019).

However, a number of other factors are involved in hydrogen isotope fractionation in sedimentary hydrocarbon, in addition to source water composition – including physiological and metabolic processes in organisms that fix water hydrogen into organic molecules (Sessions, 2016). The photosynthetic pathway (C_3 or C_4) can have significant impact towards hydrogen isotope fractionation, and it has been shown that δD values can differ by an average of as much as 40 ‰ between C_3 and C_4 grasses (Gamarra et al., 2016). In addition, differences in the correlation between precipitation and n -alkane δD values between different tree species have been observed in some cases (Tipple and Pagani, 2013). However, such interspecies variations seem to be averaged out in soil because calibration studies have proven to have good correlations between precipitation and soil leaf wax n -alkane δD values (Sachse et al., 2012,

2006). Nevertheless, measuring compound specific $\delta^{13}\text{C}$ isotope together with hydrogen isotope is more helpful for interpretation in palaeoclimate investigations.

Atmospheric CO_2 is the main source of carbon for photosynthesis in many photoautotrophs including terrestrial vascular plants. Carbon fixation during photosynthesis results in strong carbon isotopic fractionation against the heavier isotope, ^{13}C (Diefendorf and Freimuth, 2017). Photosynthetic pathway (i.e., C_3 versus C_4 pathway) and availability of water (especially in land plants) are the two main factors that determine the degree of this fractionation and the resulting isotopic composition. Differences in the enzymes and the pathway used during photosynthesis between C_3 and C_4 plants lead to differential isotopic fractionation (as much as up to 10‰) that occurs during CO_2 fixation into OM. C_3 plants fix CO_2 directly using the Calvin Cycle whereas C_4 plants fix CO_2 through the Hatch-Slack pathway to release CO_2 later to facilitate the Calvin Cycle. The C_4 pathway discriminates against ^{13}C to a lesser extent, resulting higher $\delta^{13}\text{C}$ values in the bulk organic carbon and leaf waxes of C_4 plants (Diefendorf and Freimuth, 2017; Garcin et al., 2014). C_3 and C_4 $\delta^{13}\text{C}$ measurements are distinct and non-overlapping. Moreover, as plants following these pathways have different environmental preferences in the tropics (C_3 in forests, woodlands and shrublands; C_4 in grasslands), measurement of these distinctions can provide extra information in relation to environmental change through time. With regards to leaf wax measurements specifically, interspecies differences in isotopic fractionation and leaf wax synthesis associated with plant community changes can also have some impacts on OM $\delta^{13}\text{C}$ (Diefendorf and Freimuth, 2017).

Water stress strongly influences plant stomatal conductance that controls CO_2 intake from the atmosphere, resulting in less isotopic discrimination against ^{13}C (fractionation) during photosynthesis (Diefendorf and Freimuth, 2017; Holtvoeth et al., 2019). Therefore, during the periods where vegetation changes are minimal (C_3 vs C_4 plants) and no major shifts in

atmospheric CO₂ take place, variations in $\delta^{13}\text{C}$ values in OM derived from higher plants can provide information about water availability such as aridity or drought-like conditions. (eg; Gayantha et al., 2020; Goldstein and Santiago, 2016).

2.3 Indian Ocean Monsoon Variability and Cultural Impacts during Holocene

The Holocene also saw the rise and collapse of several agriculture-based urban societies in Asia that have been argued to have been related to abrupt climate changes. According to palaeoclimatic records, the Early Holocene is characterized by strong ISM rainfall throughout Asia associated with increased solar insolation and northward migration of the ITCZ (Dutt et al., 2015; Fleitmann et al., 2007). The transition from the early to middle Holocene is marked by a cold and dry event ~ 8.2 kyr BP. Farming community density in western Asia appears to have reduced radically around this time (Weninger et al., 2006). However, this event is not so prominent in palaeorecords in the Indian sub-continent (Gupta et al., 2020).

Middle Holocene climate records (8.2 – 4.2 kyr BP) show asynchronized behaviour between ISM records across Asia. Palaeoclimate records suggest consistent weakening of ISM monsoon during this period (Dixit et al., 2014; Dykoski et al., 2005; Fleitmann, 2003; Gupta et al., 2003; Leipe et al., 2014). However, some records have shown that Central and NE India (Core Monsoon Zone; CMZ) witnessed a more sudden weakening at ~ 6.4 kyr BP (Dutt et al., 2015; Prasad et al., 2014) whereas Ponton et al., (2012) suggest a gradual weakening of monsoon rainfall in the same region. The reason for these different observations (gradual vs abrupt) about the ISM variation is unclear. The transition from the middle to late Holocene is marked by a globally widespread abrupt arid phase at ~ 4.2 kyr BP, resulting in reduced precipitation and droughts in Asia roughly between 4500 – 3500 cal yr BP (Staubwasser and Weiss, 2006).

With the exception of central India, this is evident in many records from the Indian sub-continent that lasted about 300 years starting from 4200 cal yr BP (Banerji et al., 2017; Staubwasser et al., 2003). It is considered that this abrupt climate event greatly influenced migration of the Harappan civilization into Makran (West Pakistan) and further into the Indo-Gangetic plains (Staubwasser and Weiss, 2006). It has also been linked to the conversion, around 3950 cal yr BP, from urbanized (mature or urban Harappan) to rural societies (post urban Harappan) in certain areas (Possehl, 1997; Roberts et al., 2016).

Abrupt variations in the ISM have also been observed in some palaeorecords during the Medieval Warm Period (MWP; 1050 – 650 cal yr BP) and Little Ice Age (LIA; 650 – 100 cal yr BP), which are alternate warming and cooling phases occurring in the last two millennia. It has been suggested that these periods are a result of the Eddy solar cycle (Lüning and Vahrenholt, 2016). In general, strengthening of the ISM has been observed during the MWP according to marine and continental palaeoclimate records in the Indian subcontinent (Banerji et al., 2017; Chauhan et al., 2010; Gupta et al., 2003; Rawat et al., 2015; Rühland et al., 2006). This warm period is followed by the LIA, which is characterised by glacial expansion, cool winters, and declines in harvests in South Asia (Banerji et al., 2020). The climate records are somewhat inhomogeneous for the Indian sub-continent during LIA (between 15th and 19th centuries). Weakening of ISM or dry climate conditions were observed in peninsular India (Agnihotri et al., 2002; Bhattacharyya et al., 2015) but central and western Indian and the central Himalayan regions were wet during this period (Banerji et al., 2017; Kotlia et al., 2015; Sinha et al., 2015; Sridhar et al., 2015).

The LIA is associated with southward migration of ITCZ according to global records (Brown and Johnson, 2005; Konecky et al., 2013). Lack of palaeorecords in some regions (especially southern parts of Indian sub-continent) with sufficient resolution make it difficult to get a clear understanding about the behaviour of SAM system during LIA and associated

atmospheric circulations. The period between 1800 AD and today is known the Current Warm Period (CWP) and generally characterised by strong ISM in the Indian sub-continent. This period is associated with enhanced surface evaporation, increased convection in the Indian Ocean, and increased global temperatures due to anthropogenic factors (Gupta et al., 2020; Sinha et al., 2011).

3. Study Areas and Methods

3.1 Study Areas

3.1.1 Climate, Geology, and Vegetation of Sri Lanka

The climate of Sri Lanka is described as a tropical monsoonal climate because the seasonally varying monsoon system and associated air mass circulation are the predominant governing factors of precipitation and temperature across the island (Malmgren et al., 2003).

Rainfall

In Sri Lanka, there are two principle monsoon rainfall seasons separated by two short inter-monsoon periods associated with changing wind direction and governed by the annual/seasonal ITCZ migration. Rainfall distributions in the island during all these four monsoonal seasons are shown in Fig.3.1 (Source: <https://meteo.gov.lk/>).

When the ITCZ migrates in a northerly direction it brings winds from the southwest laden with moisture from the Indian Ocean. The summer monsoon (Southwest Monsoon/*Yala*; SWM) is active in Sri Lanka between May and September and brings > 2500 mm of annual rainfall to the southwestern portion of Sri Lanka (Fig.3.1). The central highlands of Sri Lanka, which reach a maximum height of ~2,500 m a.s.l., act as an orographic barrier to these moisture-laden winds, creating a rain shadow effect to the leeward east and northeast and the prevalence of dry conditions outside of Sri Lanka's southwest during this season. When the ITCZ retreats southwards, the winter monsoon (Northeast Monsoon/*Maha*; NEM) brings rainfall between December and February to the northern and eastern portions of Sri Lanka from the Bay of Bengal. By the time the winter monsoons reach Sri Lanka, having travelled over the Indian subcontinent, these winds contain less moisture than those of the summer monsoon, but nevertheless contribute to the majority of the annual rainfall of < 1750 mm for the northern and eastern portions of the island (Fig. 3.1).

These climatic systems lead to the division of Sri Lanka into three main climate ‘zones’ (sub regions) - wet, dry and intermediate (Fig.3.2). Beyond these main seasons, two inter monsoon rainfall seasons (first and second inter-monsoon rainfall seasons) also exist in Sri Lanka, bringing thunderstorm type convectional rainfall and tropical depressions/cyclones. The First Inter-Monsoon rainfall (FIM) occurs in March through to April and brings rainfall to entire southwestern sector of the island (Fig.3.1). The Second Inter-Monsoon (SIM) rainfall occurs between October and November and is generally distributed throughout the whole island (Fig.3.1). These inter-monsoon rainfalls take place when the ITCZ moves over Sri Lanka (Hapuarachchi and Jayawardena, 2015; Malmgren et al., 2003).

Due to its close proximity to the equator, variation in mean annual temperature, as with many tropical regions, is minimal in Sri Lanka. Regional temperature differences in air temperature are mainly due to altitude rather than latitude. In the lowlands (altitude up to about 150 m) the mean annual temperature is 27.5°C. However, temperature drops quickly when moving to the highlands with mean annual temperature around 16°C at Nuwara Eliya at ~1900 m a.s.l (www.meteo.gov.lk/).

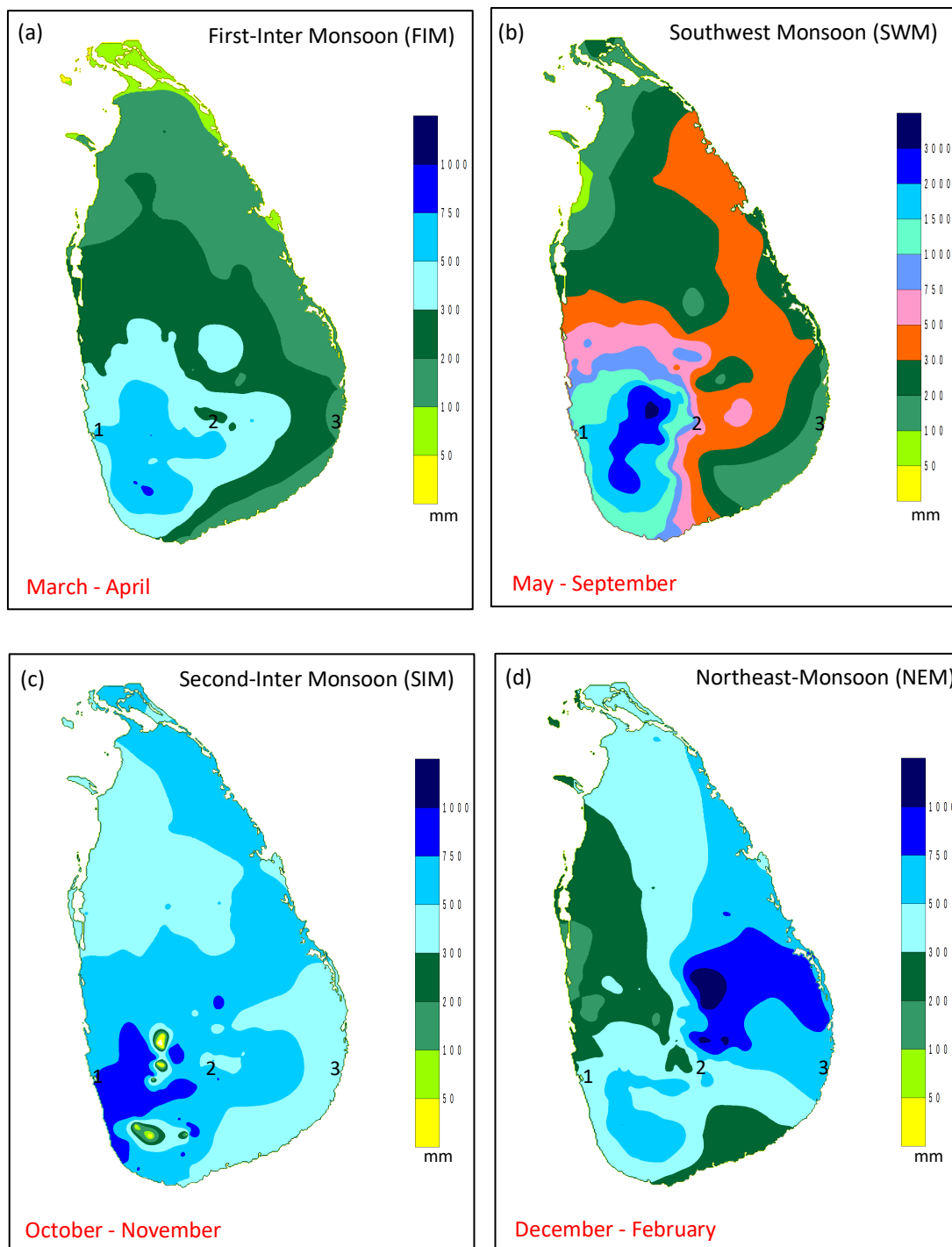


Fig.3.1 Rainfall Distribution in Sri Lanka during (a) First-Inter Monsoon, (b) Southwest Monsoon (Summer monsoon), (c) Second-Inter Monsoon, (d) Northeast Monsoon (Winter monsoon) and locations of selected study sites; 1 = Bolgoda South Lake, 2 = Horton Plains, 3 = Panama Lagoon. (Source: <https://meteo.gov.lk/>)

Geology and Topography

About 90% of the Sri Lankan terrain is made up of highly crystalline Precambrian metamorphic rocks. The remainder is made up of Jurassic (Thabbowa, Andigama, Pallama), Miocene (Jaffna limestone), and Quaternary (beach sand deposits) sedimentary formations in the northwestern region (Cooray, 1978). Three main morphological zones can be identified in Sri Lanka; a). coastal lowlands (altitude up to 270 m), b). uplands (altitude between 270 and 1060 m) and c). highlands (altitude between 1060 and 2420 m) (Vitanage, 1970). The central part of the island is mountainous and consists of complex topographical features such as ridges, peaks, plateaus, basins, valleys, and escarpments. The rest of the island is generally flat except for some small hills in the lowlands (Fig.3.2). As noted above, these topographical features can strongly influence the different climate elements in Sri Lanka.

Vegetation

The three climatic 'zones', as well as topographical features, shape the vegetation cover in Sri Lanka. The lowland wet zone (below c. 900 m) is mainly characterized by tropical rainforests (dominated by Dipterocarpus and Mesua-Shorea communities) and wet zone pastures (grasslands) with species such as *Cynodon dactylon*, *Axonopus compressus* and *Chrysopogon aciculatus*.

The highland wet zone (above c. 900 m) consists of tropical montane rainforest characterised by species such as *Acronychia pedunculata*, *Elaeocarpus montanus*, *Gordonia zeylanica*, *Litsea ovalifolia*, *Olea polygama*, *Plectronia montana*, *Rhamnus arnottianus* and *Syzygium revolutum*. Montane grasslands (Patana) are dominated by species of *Arundinella villosa*, *Chrysopogon zeylanicus*, *Cymbopogon nardus*, *Themeda tremula* and *Andropogon lividus*. The lowland dry zone is characterized by seasonal rainforests (mixed-evergreen forests/dry monsoon forests) dominated by trees of *Manilkara hexandra*, *Chloroxylon swietenia*, *Drypetes sepiaria*, *Diospyros ebenum* and *Syzygium sp.* In addition, dry zone upland

and lowland savannas (Talawa and Damana) consists of grass species such as *Cymbopogon polyneuros*, *Themeda triandra*, *Aristida setacea*, *Cymbopogon polyneuros* and *Panicum sp.* together with trees (eg; *Terminalia sp.*, *Butea monosperma*, *Careya arborea*) and shrubs (*Phyllanthus emblica* and *Zizyphus spp*) (Erdelen, 1988; Fernando, 2012; Perera, 1975).

Significant amounts of mangrove vegetation can also be found along the coastal water bodies, i.e. lagoons and estuaries, in Sri Lanka dominated by species such as *Avicennia marina*, *Rhizophora mucronata*, *Rhizophora apiculate*, and *Lumnitzera racemose* (Amarasinghe and Perera, 2017; Ranawana, 2017).

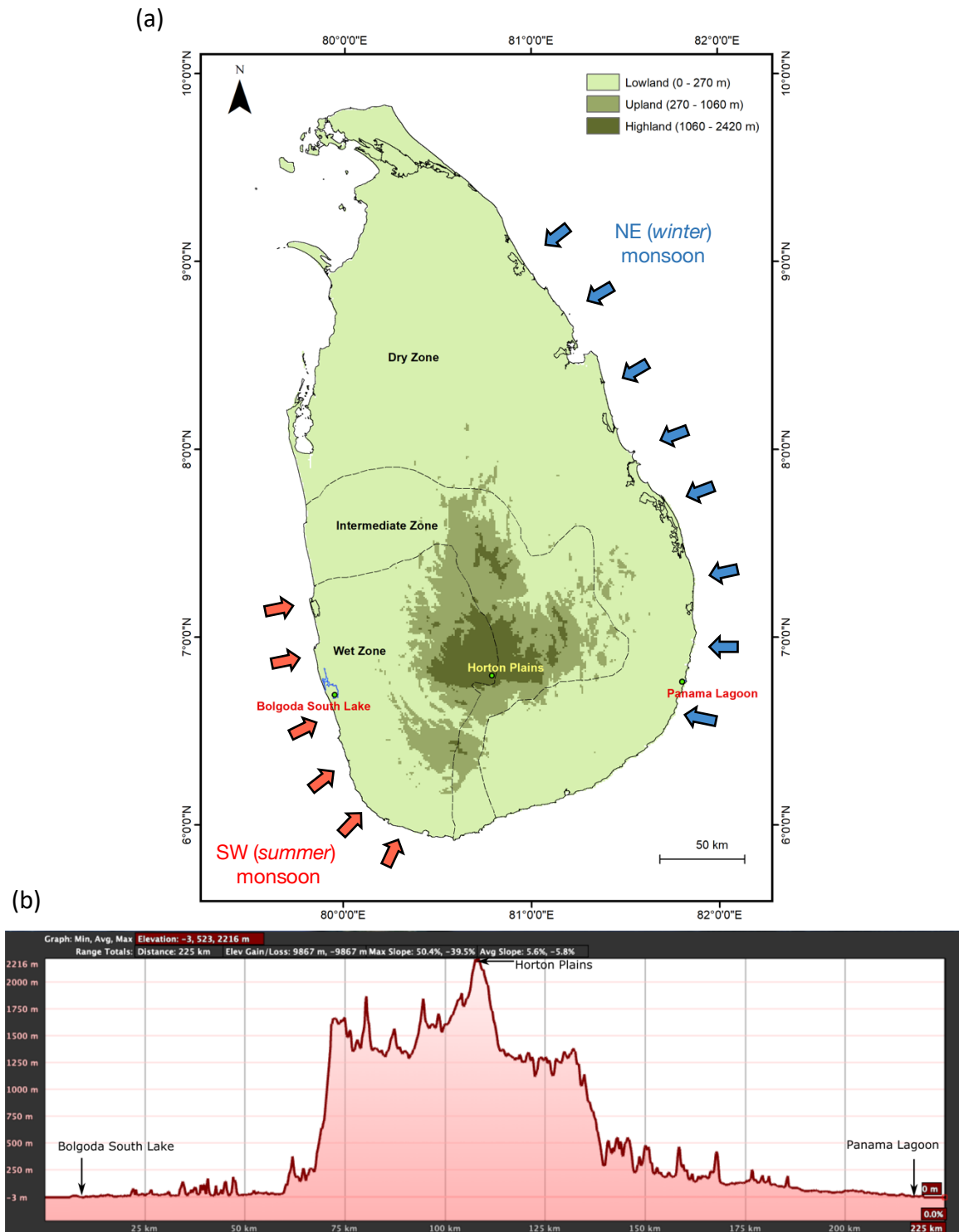


Fig.3.2 (a) Topography, climate zones and influence of monsoon winds of Sri Lanka. (b) Elevation profile along a transect of the three sites (Bolgoda South Lake, Horton Plains and Panama Lagoon) Source of shape file (a): Survey Department of Sri Lanka, Source(b): Google Earth

3.1.2 The Study Sites

The study areas in this investigation were selected in order to cover the main different climate, topographic, and vegetation zones in Sri Lanka (see Fig.3.2).

3.1.2.1 Bolgoda South Lake

Bolgoda South Lake (BGS�) is a part of the Bolgoda Lake system located in the lowland wet zone ($6^{\circ} 40' 57'' - 6^{\circ} 41' 42''\text{N}$; $79^{\circ} 56' 20'' - 79^{\circ} 57' 54''\text{E}$) of western Sri Lanka (Fig. 3.3). The South Lake is located about 8 km south of the Bolgoda North Lake which has been previously investigated (Gayantha et al., 2020, 2017) and is about 2.8 km from the coast. The South Lake has a surface area of $\sim 2 \text{ km}^2$ and an average depth of about 2 m. It is connected to the North Lake via the Bolgoda Ganga river. BGS� is fed by a stream called 'Panape Ela' and the lake is connected to the Indian Ocean via a narrow, artificial stream called 'Thalpitiya Ela' from the western side of the lake. The lake system is drained by a substantial area between the western parts of the Kalu and Kelani river basins (Ranwella, 1995). The lake is currently listed as a slightly brackish water body. Upon direct measurement, the average conductivity of the lake water was found to be about 1.6 mS/cm with a gradual increasing trend towards the sea along Thalpitiya Ela.

The BGS� and its catchment receives an annual rainfall of about 2569 mm mainly from the southwest (summer) monsoon between May and September. The mean annual temperature of the area is 27°C and the mean humidity is 72 % during daytime. The catchment area around BGS� is dominated by flat terrain and bog or half bog soils (paddy clays) associated with paddy fields. Sandy, lateritic gravel can be found as superficial deposits in this area. Charnockitic gneiss, undifferentiated charnockitic biotite gneiss and undifferentiated Proterozoic gneisses are the major rock types of the bedrock in the catchment area (Gayantha et al., 2017). During the peak rainfall season most of the surrounding area becomes seasonal

swamps. A few mangrove swamps can be observed along the southern margin of the lake (Ranwella, 1995) (Fig.3.3).

Floating and submerged aquatic plants are common in the BGS. In the deepest area of the lake, where lots of soft mud can be found, *Nymphoides* and floating *Utricularia* sp are observed. Other parts of the lake are dominated by *Potamogeton indicus*, *Aponogeton* and *Limnophila*. The surrounding marshes are dominated by *Utricularia*, *Bacopa*, *Monochoria* and *Ceratopteris*. These wetlands are surrounded by shrubs and woodlands with *Sonneratia*, *Dillenia*, *Hibiscus*, *Thespesia* and *Cerbera* being the most common (Ranwella, 1995). Paddy rice is the major food crop grown in the area. However, increasing salinity, marshland, and seasonal flooding of grasslands have led to the recent abandonment of many locales. The surrounding higher lands are mainly under rubber and coconut cultivation. Mangrove vegetation is common around the lake and is dominated by *Avicennia*, *Rhizophora*, *Bruguiera* and *Sonneratia* (Ranawana, 2017; Ranwella, 1995).

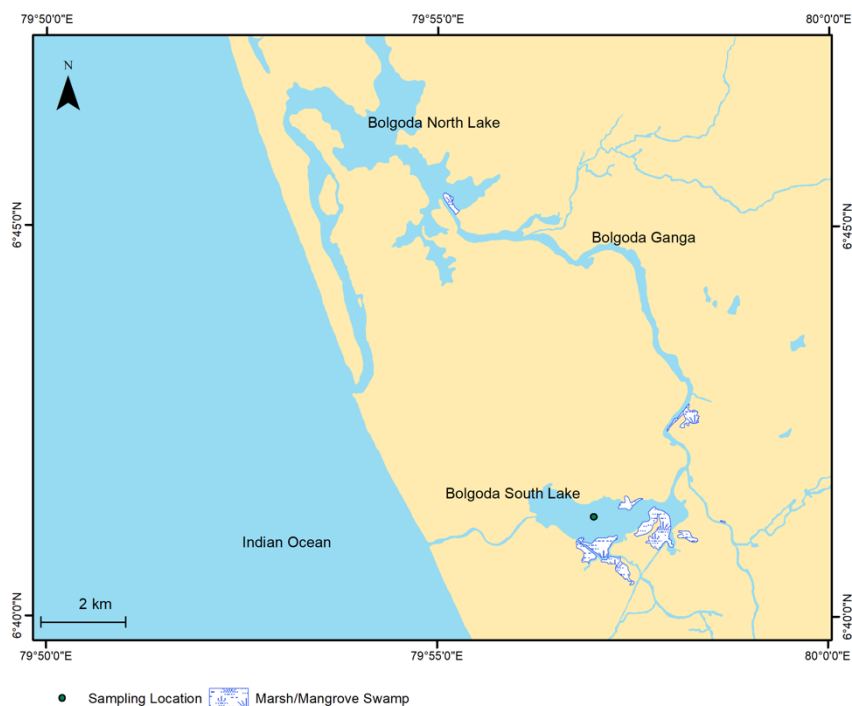


Fig.3.3 Bolgoda Lake System and surrounding area
(Source of shape file: Survey Department of Sri Lanka)

3.1.2.2 Panama Lagoon

Panama Lagoon (PN) is a shallow estuarine lagoon located on the southeastern coast of the dry zone ($6^{\circ} 45'52'' - 6^{\circ} 46'29''\text{N}$; $81^{\circ}48' 20'' - 81^{\circ}49'31''\text{E}$; Fig.3.4). It has a surface area of $\sim 0.73 \text{ km}^2$ and an average depth of 1.48 m. The lagoon is separated from the sea by a coastal sand dune that is about 500 m wide and 30 m high. Wila Oya, a tributary of Heda Oya, brings fresh water into the lagoon from the upland region to the west (Fig.3.4). The lagoon is connected to the sea through a narrow channel (lagoon mouth) which is about 52 m wide. Seasonal closing of the lagoon's mouth takes place during September and mid-November. Nevertheless, at present, artificial breaching is undertaken near to the mouth to facilitate the transport of boats between the ocean and lagoon and to control flooding in upstream agricultural areas (Ellepola and Ranawana, 2015).

The catchment area/watershed is about 480 km^2 and drains about $218 \text{ Mm}^3\text{yr}^{-1}$ freshwater into the Panama lagoon (Silva et al., 2013). The salinity average ranges between 4.5 and 26.6 ppt with significant monthly variation (Ellepola and Ranawana, 2015). Panama lagoon is mainly influenced by northeastern (winter) monsoon rainfall that occurs between November and January and brings 90 % of rainfall into this region with an annual average of 800 mm yr^{-1} . The mean annual temperature is 32°C . The period between mid-May and September is fairly dry and windy with high temperatures and evaporation rates (Chandrajith et al., 2014).

Inland of the lagoon, the area is mostly composed of flat terrain with an underlying bedrock consisting mainly of high-grade Precambrian granitic gneisses that are underlain by Quaternary sediments of dune sand and lagoonal deposits. The barrier beach of the area is formed by the accumulation of unconsolidated sediments transported by wind and waves (Panabokke, 1996). The catchment area of PN is covered by tropical dry evergreen forests (dry monsoon forests). Mangrove vegetation occurs as fringes around a significant part of the

lagoon (Fig.3.4), and *Avicennia marina*, *Lumnitzera racemosa*, *Exoecaria agallocha* and *Rhizophora mucronate* are the most common mangrove species in the area. Paddy rice cultivation is the major economic activity around the lagoon today (Ellepolra and Ranawana, 2015).

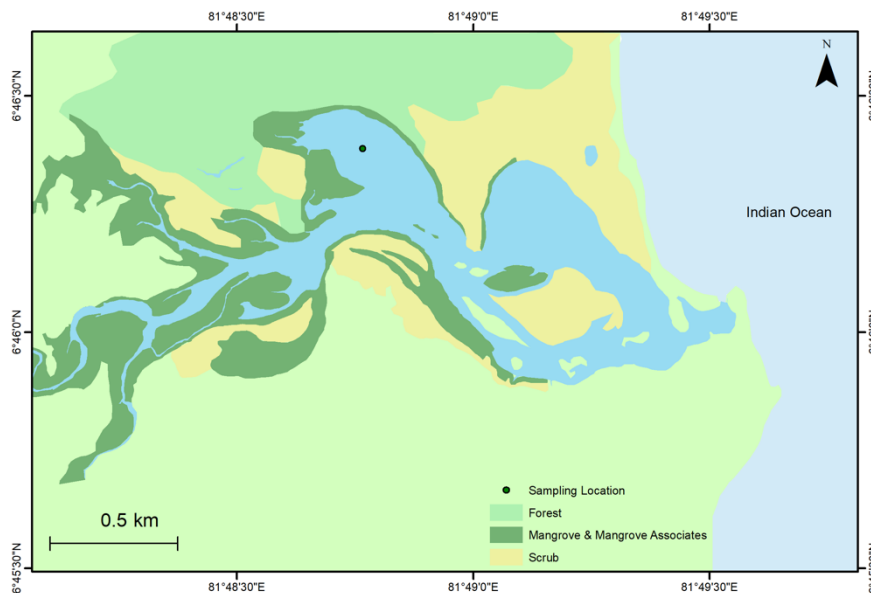


Fig.3.4 Panama Lagoon and surrounding vegetation
(Source of shape file: Survey Department of Sri Lanka)

3.1.2.3 Horton Plains

The Horton Plains is a national park and a UNESCO World Heritage site located at the eastern extremity of the Central Highlands of Sri Lanka ($6^{\circ} 47' - 6^{\circ} 50' N$, $80^{\circ} 46' - 80^{\circ} 51' E$; Fig.3.5). The national park covers an area of 31.6 km^2 and is located at an altitude between 2100 - 2300 m a.s.l. The Horton Plains (HP) is a gently undulating highland plateau with diverse landscapes including mires, plains, forested hilltops, grassy slopes, precipices, brooks, and waterfalls (Premathilake and Risberg, 2003). Tributaries of three of the major river systems of Sri Lanka (Mahaweli, Kelani and Walawe) start in the Horton Plains, forming an important component of the hydrological regime of the island.

The HP lies at the eastern extremity of the wet zone of Sri Lanka and is one of the few areas of the island that is strongly influenced by both southwest monsoon (SWM/summer

monsoon) and northeast monsoon (NEM/winter monsoon) rains. Nonetheless, SWM rainfall has the dominant impact on climate and vegetation in HP today. Although the mean annual rainfall in the wet zone is about 2540 mm, for the HP it can exceed 5000 mm. Due to its higher elevation and precipitation, the HP has a markedly colder and wetter climate in contrast to the rest of the island, with an unpredictable mountainous microclimate (Chandrajith et al., 2009). The mean annual temperature is 15°C and January and February are, on average, the driest months of the year.

The basement rock of the HP is made up of highly crystalline Precambrian metamorphic rocks of quartzite, charnockites, quartzo feldspathic gneisses, hornblende-biotite gneisses and garnet-sillimanite-biotite gneisses (GSMB, 1995). At the end of southern boundary of the HP, well-defined mural fault scarps called the Small and Big ‘World’s End’ can be found. Soils in the HP contain predominantly red yellow podzolic soils, wet mountain regosols, bog soils, and half bog soils. A layer of ironstone gravel, 20-30 cm thick, is found below the black organic-rich surface soil (Chandrajith et al., 2009; Ranasinghe et al., 2007). The HP national park is home to many endemic flora and fauna species that include 57% of plants, 93% of amphibians, 83% of reptiles, 20% of birds and five mammal species that exist in Sri Lanka (DWC, 2007).

The vegetation in HP mainly consists of Upper Montane Rain Forests (also referred to as Cloud Forests) and Wet Patana grasslands. In addition, a narrow ecotonal belt consisting of shrubs and herbs can be identified. The Cloud Forests can be seen on the hilltops and upper or mid slopes of the area whereas grasslands and dwarf bamboo flourish on the lower slopes and valleys. Wetland habitats occur in waterlogged depressions and surrounding smaller streams. Cloud Forests are dominated by *Calophyllum walkeri*, *Michelia nilagirica*, *Syzygium rotundifolium*, *S. revolutum*, *Elaeocarpus montanus*, *E. glandulifer*, *E. coriaceous*, *Ilex walkeri*, *Cinnamomum ovalifolium*, *Litsea ovalifolia* and *Photinia integrifolia*. Wet Patana

grasslands consist of tussock grass (*Chrysopogon nodulibarbis*, *Andropogon Polyptychos*, *Garnotia exaristata*, *Rhododendron arboreum*), carpet grass (*Axonopus fissifolius*) that have currently spread in areas with abundant potato cultivation (started during the British colonial period) and dwarf bamboo (*Arundinaria densifolia*) (Fig.3.5; DWC, 2007).

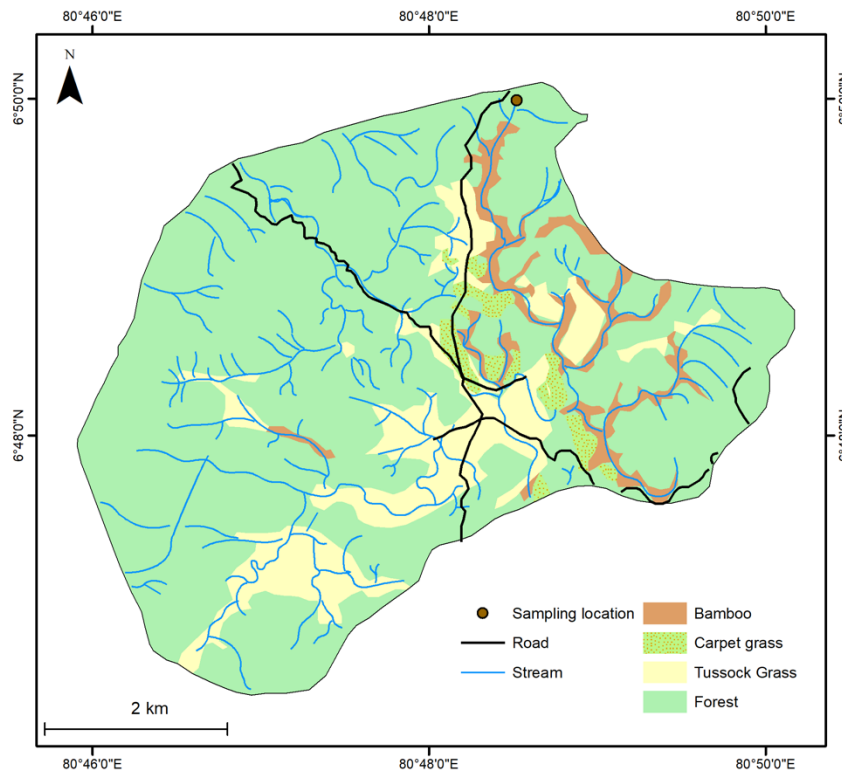


Fig.3.5 Horton Plains National Park and main vegetation types (Digitized map with the data source DWC, 2007)

3.2 Materials and Methods

3.2.1 Sampling/ Sediment Core Collection

The sampling campaign was conducted in the year 2017. Information about specific site locality, coring techniques used, and sample retrieval are detailed in Table 3.1.

Table. 3.1 Site information and coring techniques used in the study

<i>Site Name (abbreviation)</i>	Bolgoda South Lake (BGSL)	Panama Lagoon (PN)	Horton Plains (HP)
<i>Locality</i>	Wet zone, West coast	Dry zone, East coast	Wet zone, Central Highlands
<i>Corer/Method</i>	UWITEC free- fall gravity corer (core diameter: 90 mm)	UWITEC free- fall gravity corer (core diameter: 90 mm)	Russian Peat Corer (50 mm core diameter x 50 cm length core chamber)
<i>Length of sediment core</i>	0.7 m	1 m	1.5 m
<i>GPS coordinates of the sampling point</i>	06° 41' 18" N 79° 57' 08" E	06° 46' 20" N 81° 48' 47" E	06° 50' 14" N 80° 48' 39" E

During the sampling campaign, water quality parameters (i.e. temperature, pH, conductivity and dissolved oxygen) were measured *in situ*. δD and δO values of collected water samples from the sites were measured later at the Stable Isotope Laboratory, MPI-BGC, Jena using in High-Temperature Conversion – Isotope Ratio Mass Spectrometer (HTC-IRMS).

The sediment cores retrieved from Bolgoda South Lake (BGSL) and Panama lagoon (PN) were split into two identical longitudinal sections and one section was archived at the German Research Centre for Geosciences (GFZ), Potsdam, Germany after photographs were taken of the core and lithological characteristics, such as grain size variations, colour variations and availability of shells and other macro fossils, were visually recorded. The remaining split

section was sliced into 1-cm intervals for geochemical analyses. Using a Russian peat corer, only half cores can be retrieved, so no archived sections are available for the Horton Plains (HP) core. The HP cores were also sliced into 1-cm intervals for geochemical analyses. All of the sub-samples were freeze-dried and stored in zip-lock bags in the laboratory at room temperature prior to pre-treatment and analysis.

3.2.2 ^{14}C dating and Construction of Age-depth Models

Mollusc shells and bulk organic carbon were extracted from sediment samples and analysed by ^{14}C dating to establish the chronology and produce age-depth models for the different sites. Considering the diverse organic matter/carbon sources at Panama lagoon, we selected only mollusc shells for ^{14}C dating the PN core. In the BGS� core, no shells or other microfossils were available for ^{14}C dating. In BGS�, terrestrial OM sources are dominant (see below) and there is minimum direct influence from the sea. Hence, bulk sediment (bulk organic carbon) was selected for ^{14}C dating. Ten mollusc shells were selected from the PN core and 12 bulk sediment samples were selected from BGS� core for ^{14}C dating. In the HP core, 15 peat/organic-rich bulk sediment samples were used for ^{14}C dating after sieving the freeze-dried material with a 1-mm sieve to remove rootlets that could be observed primarily in the top ~50 cm of the core.

^{14}C dating was carried out using an Accelerated Mass Spectrometer MICADAS (Ionplus, Dietikon, Switzerland) at the ^{14}C Laboratory, Max Planck Institute for Biogeochemistry, Jena, Germany (see details about sample preparation in Steinhof et al., 2017). Age-depth models were developed using the R- software package BACON (rbacon) (Blaauw and Christen, 2011). BACON uses Bayesian statistics to reconstruct age-depth models. BACON divides a core into many vertical sections (of default thickness = 5 cm), and through millions of Markov Chain Monte Carlo (MCMC) iterations estimates the accumulation rate (in

years/cm) for each of these sections. Combined with estimated starting dates for the first section, these accumulation rates in each section is compiled together to form the age-depth model (Blaauw and Christen, 2011).

The shell ^{14}C dates of shells in the PN core were calibrated using the Marine13 curve (Reimer et al., 2013) and the post-bomb curve NH Zone 3 was applied for negative ^{14}C ages (Hua et al., 2013). In addition, ^{14}C ages in shells were corrected for the local marine reservoir age ($\Delta\text{R} = 133 \pm 65$) based on the data from the online Marine Reservoir Database at Queen's University, Belfast, UK. Bulk organic carbon ^{14}C dates in the BGSL core and HP core were calibrated using the IntCal13 curve (Reimer et al., 2013). Surface samples from the BGSL core (bulk organic carbon) showed an (old carbon) reservoir age of 599 ± 19 ^{14}C years. This value was applied for the reservoir age offset correction to all ^{14}C ages before calibration, assuming that reservoir effect was mostly constant over time.

3.2.3 Grain Size Analysis

Grain size analysis was performed on 10 sediment samples from BGSL and 11 samples from PN. 4-6 g of freeze-dried sediment from each layer were used and the analysis was carried out according to the protocol by Kilmer and Alexander, 1949. First, 0.05% sodium hexametaphosphate was added to the sample to separate the grains. Then, sediment grains greater than $63 \mu\text{m}$ (sand fraction) were separated by wet sieving using a $63 \mu\text{m}$ mesh. The sieved extracts, consisting of particles $< 63 \mu\text{m}$ (i.e. silt and clay), were homogenised using a Sonic Vibra-Cell VC 750, ultrasonic stirrer, and analysed for grain size in a Sedigraph Micromeritics III Particle Size Analyser at Linköping University, Sweden. The results were expressed as weight percentages of sand, silt, and clay.

3.2.4 X-Ray Fluorescence Core Scanning

XRF core scanning was conducted only for the BGSL and PN sediment cores as high organic and water content in peat cores, such as those from HP, creates high analytical uncertainties. XRF core scanning was conducted with the ITRAX μ -XRF core scanner at GFZ, Potsdam Germany at 5-mm resolution. Element intensities (c.p.s.) of Al, Si, S, Cl, K, Ca, Ti, V, Mn, Fe, Ni, Cu, Rb, Sr, Zr, and relative variations in the coherent and incoherent radiation, were obtained non-destructively using the μ -XRF core scanner with a Chromium X-ray source operated at 30kV and 55 mA for 10 S to generate energy dispersive XRF radiation. The elemental intensities (c.p.s.) were non-linearly correlated to the elemental concentrations because direct conversion of intensity of a single element to its concentration is problematic. This is due to many factors such as matrix effects and varying physical properties of sediments throughout the core (e.g. water content and grain-size distribution, irregularities of the split core surface, spatial variations in thickness of an adhesive pore-water film which forms directly below a protective foil covering the core surface) (Weltje and Tjallingii, 2008). To eliminate these effects, the results are presented as log ratios of two element intensities that are linearly correlated with the log ratios of two elemental concentrations. Log ratio transformation of elemental intensities eliminates difficulties associated with closed-sum constraints that can influence multivariate statistical analysis. In this study, I used the centralized log ratio (CLR) of transformed element intensities to perform multivariate analysis of the data (Martin-Puertas et al., 2017; Weltje and Tjallingii, 2008) (see below).

3.2.5 Biomarker Extraction and Analysis

The sediment sub samples were freeze-dried and homogenized prior to geochemical analysis (lipid extractions). In addition, mollusc shells were removed from the sediment by sieving with a 2-mm sieve or through manual extraction using tweezers, where necessary. 5 to 15 g of freeze-dried sediment were used for extraction, depending on the TOC content of samples.

Higher amounts of sample were used for lipid extraction in the PN core due to relatively low TOC content in the core. Nineteen samples from the PN core, 26 samples from the BGS� core, and 21 samples from the HP core were selected for lipid extraction. Lipid extraction was done using dichloromethane (CH₂Cl₂) and methanol (CH₃OH) (9:1 v/v mixture) in a Büchi Speedextractor (E-916, Büchi Labortechnik AG, Switzerland). The total lipid extracts (TLE) were then concentrated on a Büchi Syncore under reduced pressure.

The TLE was then separated into four fractions: F1 (alkane/non-polar hydrocarbon); F2 (aromatic hydrocarbon and ketone); F3 (alcohol and sterol); and F4 (fatty acids and other polar lipids) using the Solid Phase Extraction (SPE) technique on silica gel (0.040–0.063 mm mesh; Merck, Darmstadt, Germany) according to the modified method from Rach et al., 2014). The F1 fraction containing alkanes was eluted with 12 ml of hexane and subsequently desulphurized by elution through activated copper powder (with 1 M HCl) in a glass pipet column. The F2 fraction containing aromatic hydrocarbons and ketones was eluted on the same column using 12 ml of hexane: dichloromethane (DCM) (1:1, v/v) mixture. Subsequently, the alcohols and sterols (F3 fraction) were eluted with 12 ml of DCM: acetone (9:1, v/v) mixture and finally fatty acids and other polar compounds (F4 fraction) were eluted with 12 ml of DCM: Methanol (1:1, v/v) mixture. The F3 fraction was derivatized with bis(trimethylsilyl)trifluoroacetamide (BSTFA) and pyridine and heated at 75 °C for 2 hours. All extracts were then dried under a gentle stream of nitrogen before being re-dissolved in an equal volume (1 ml or 1.5 ml) of the solvent/solvent mixture.

An aliquot of the extracts (180 µl of F1, F2 and F3 fractions) was spiked with androstane (20 µl) as an internal standard for quantification. The samples were analysed on an Agilent 6890N gas chromatograph (GC) interfaced with a 5973 MSD quadrupole mass spectrometer (MS) with a DB-5 (5% phenyl methyl siloxane) fused silica capillary column (30 m length, 0.25 mm inner diameter, 0.25 µm film thickness) at Linköping University, Sweden.

The samples were injected in splitless mode (1 μ l inlet pressure of 10 psi with a flow rate 54.3 ml/min) and injector temperature was maintained at 300 °C. A constant flow (1.3 ml/min) of He was used as the carrier gas. The GC oven was initially maintained at 35 °C for 1 min. The temperature was increased first to 130 °C at 20 °C/min and then to 320 °C at 6 °C/min where it was maintained isothermally for 15 minutes. The MS was operated at 70 eV under full scan mode (m/z 40 – 600) and ion source and MS quadrupole temperatures were maintained at 230 °C and 150 °C, respectively. Compounds in the samples were identified based on their retention times relative to an external *n*-alkane standard mixture (*n*-C₁₅ to *n*-C₃₃) and fragmentation patterns in the NIST MS Library (Version 2.0) and Lipid library (2011). Quantification of the biomarkers was done relative to the peak area of androstane (internal standard quantification).

3.2.6 Bulk Organic Stable Carbon Isotope Analysis and Total Organic Carbon (TOC) Analysis

22 samples from BGSL, 19 samples from PN and 70 samples from HP were selected for TOC and bulk stable carbon isotope analysis. 5 – 10 mg of freeze-dried sediment was weighed into tin capsules based on the total organic carbon content of the core. Inorganic carbon was removed by the gradual addition of 120 μ l HCl (Bisutti et al., 2004). Bulk $\delta^{13}\text{C}_{(\text{org})}$ and TOC were measured at the Stable Isotope Laboratory, MPI-BGC, Jena, Germany. All tin capsules were introduced into an Elemental Analyzer (NA 1110, CE Instruments, Milan, Italy) and the gases produced were transferred to a Delta⁺XL isotope-ratio mass spectrometer (Thermo Finnigan, Bremen, Germany) via a ConFlow III interface (Werner et al., 1999). Each sample was measured in duplicate and in-house standards (acetanilide and caffeine) were measured with the samples for quality control of the respective analyses. Average and standard deviation of standards for $\delta^{13}\text{C}$ was -30.06 ‰ and 0.06 ‰, respectively whereas for TOC it was 71.09 % and 2.05 %, respectively.

3.2.7 Compound Specific Isotope Analysis of *n*-alkanes

The volume of the *n*-alkane fraction was reduced to 50 μ l to increase the concentration by drying under gentle stream of nitrogen before compound specific isotope analysis, due to relatively low concentrations of the compounds in samples. Stable hydrogen and carbon isotope (δ D and δ^{13} C) analysis of individual *n*-alkanes (*n*-C₁₅ to *n*-C₃₃) was performed using a coupled gas chromatograph isotope ratio mass spectrometer (GC-IRMS system) equipped with a 7890A gas chromatograph (Agilent Technologies, Palo Alto USA) linked via GC Isolink and ConFlo IV interface to a Delta V Plus Isotope Ratio Mass Spectrometer (Thermo Fisher Scientific, Bremen Germany) at the Max Planck Institute for Biogeochemistry, Jena, Germany. The GC was equipped with a DB1-MS column (60 m length, 0.25 mm inner diameter, 0.25 mm film thickness) for hydrogen isotope measurements and DB-1 MS column (30 m length, 0.25 mm inner diameter, 0.25 mm film thickness) for carbon isotope measurements. The sample was injected in splitless mode at 280 °C and 2 μ l of the extract was injected. The He carrier gas flow was maintained at 1.3 ml/minute. The GC oven was maintained for 1 minute at 110 °C, before the temperature was increased to 320 °C, at 5 °C/minute and held isothermally for 9 minutes.

Each sample was measured in triplicate at the MPI-BGC, Jena with a standardised mixture of *n*-alkanes (C₁₅ to C₃₃ *n*-alkane standard mixture) of known isotopic composition measured after every sample (3 GC injections). Only peaks with an amplitude >150 mV were used for evaluation. The carbon and hydrogen isotopic values were converted to the Vienna Pee Dee Belemnite (V-PDB) and Vienna Standard Mean Ocean Water (V-SMOW) scales, respectively, using the values of the above-mentioned *n*-alkane standard mixture (offset correction). In addition, drift corrections were applied, determined by the standards run after every sample (Werner and Brand, 2001). The standard deviation of replicate measurements for

all peaks in the standard mixture was 1.2‰ for carbon and 6.4‰ for hydrogen. In addition, the H_3^+ factor was determined on a daily basis (5.50 ± 0.5 ; $n = 25$). It was found to remain constant over the measurement period which indicates a stable condition in the ion source.

3.2.8 Statistical Analysis

Multivariate statistical techniques were used to understand the correlation between *n*-alkane data and XRF elemental data and their distribution in the cores. To identify the subsections/zones based on *n*-alkane distribution, a hierarchical cluster analysis according to Ward's method was performed for *n*-C₁₅ to *n*-C₃₃ for all alkanes in each site. A Principal Component Analysis (PCA) was also performed for *n*-alkane distributions at each site to identify the correlation between different *n*-alkanes within the zones identified by the cluster analysis. To avoid visual overloading of variables (*n*-alkane) in the PCA biplot, only *n*-alkanes with a relative abundance > 5% in any sample were shown in the PCA biplots of each site. The statistical analyses were performed using the R statistical software package (R Core Team, 2020) together with R package 'factoextra' for visualization (Kassambara and Mundt, 2020). The PCA was also done for the XRF (CLR) data, but due to high number of elements with intermediate loadings showed poor correlation between variables (elements) in each component. Therefore, to make the data more interpretable Principal Component Analysis (PCA), followed by varimax orthogonal rotation, was performed using the R software package 'psych' (Revelle, 2019) separately for PN and BGSL. The rotation minimizes the number of elements with intermediate loadings. Major correlations in the rotated component matrices of XRF data were used to identify specific element assemblages (latent variables) that helps to identify the provenance of the deposits and physicochemical processes influencing the distribution. The variation of the PC scores in first 5 rotated components were used to trace the variation of the elemental combinations and their relationship to the provenances and physicochemical processes.

4. Results

4.1 Present Status of the Study Sites

Table 4.1: Average water quality parameters at three sampling sites along a E-W transect in Sri Lanka (samples collected in 2017)

	Panama Lagoon	South Bolgoda Lake	Horton Plains
Conductivity (mS/cm)	36.6	1.6	14
pH	8.7	8.2	6.7
Temperature (°C)	30.1	31.1	17.3
Dissolved Oxygen (mg/L)	8.7	7.3	7.5
δD and $\delta^{18}O$ (‰)	+7.6 and +2.6	-6.9 and -1.7	-39.8 and -6.7

Panama lagoon (PN) showed the highest conductivity values of its surface water, implying high salinity due to its direct connection with the Indian Ocean. Positive δD and $\delta^{18}O$ values for water at PN also indicate high marine influence and evaporation in the lagoon. In contrast, negative δD and $\delta^{18}O$ values in water at the Bolgoda South Lake (BGS�) and at the Horton Plains (HP) indicate the dominant input of freshwater/ meteoric water to the lake/site from their catchments. More negative (depleted) isotope values in water at the HP reflect the altitude effect on precipitation in this highland region. Significant differences in pH and dissolved oxygen were not observed between the sites but the low water temperature at HP can be explained by its high altitude relative to the other water bodies (Table 4.1).

4.2 Stratigraphy

South Bolgoda Lake

The bottom section between 70 cm and 46 cm (section B1) of the core consisted of light greyish coarse sand with the amount decreasing towards the core top. From 46 cm to 5.5 cm (section B2) the core was characterized by dark greyish sandy clay. No shells were found in this section except a single horn gastropod (~ 3 cm long) between 39 and 41 cm. This shell was identified as a gastropod species belonging to the family Potamididae that lives in brackish water environments such as mud flats and mangrove habitats. A brownish sand layer was identified

with some tiny mollusc shells between 5.5 cm and 2 cm (section B3) and an uneven (not uniform) upper boundary. This was identified as a layer deposited during the 2004 Indian Ocean tsunami (see Discussion). The uppermost 2 cm layer (section B4) was characterized by dark grey clayey sediments without shells (Fig. 4.1(c)).

Panama lagoon

From 102 cm (core bottom) to 90 cm (section P1), the core consisted of a greyish silty clay with some intact shells. The shells are relatively low in number in this section in contrast to the upper section P2. From 90 to 37 cm (section P2), the core was characterized by a very large number of intact and semi-intact mollusc shells, including both gastropods and bivalves, with horn gastropods being the most abundant. These gastropods were identified as *Cerethedia cingulate*, a species found today in brackish water mudflats and mangrove habitats. Besides the high frequency of shells, this section consisted of a greyish sandy-silty clay. Between 37 and 10 cm (section P3), the core consisted of greyish sandy-silty clay, and shells were rare. Few bivalves were found in the upper part of the section. From ca. 10 to 5 cm (section P4), a light-coloured sandy layer was present with some shell fragments and an uneven lower boundary that which was similar to South Bolgoda Lake. This deposit was linked to the 2004 tsunami in the Indian Ocean (see Discussion). The uppermost layer (P1; ca. 5 cm to the top of the core) was characterized by a dark brown layer rich in partially decomposed organic detritus (see below; Fig. 4.2 (c)).

Horton Plains

From 150 - 50 cm (H1), the core consisted of dark brown non-laminated peat deposit. The coring was stopped at 150 cm depth because it was difficult to penetrate the sandy layer. Between ca. 50 cm and the core top (H2), the peat deposit indicated dark brown non-laminated organic-rich fine-grained sediments together with partially decomposed or undecomposed rootlets (Fig. 4.3 (c)).

4.3 Chronology

The three sediment cores retrieved revealed a depositional history extending up to the mid-Holocene.

For the South Bolgoda Lake (BGS�) core, ages ranged between 6320 cal yr BP (model maximum age) and 1355 cal yr BP (model minimum age) according to the BACON age-depth model constructed based on bulk sediment ^{14}C ages (Fig. 4.1a). Sedimentation rates varied between 0.08 and 0.28 mm/yr in this core with a general decreasing trend from 46 cm to the core top (Fig. 4.1 (b)). The negative ^{14}C age of shell fragments in section B3 indicated the modern ages; it is likely the sand layer was deposited during the 2004 tsunami event (see appendix Table. 01; Fig.4.1(c)). Therefore, the age-depth model truncated just below the sand layer (section B3) at 5 cm that represent ca.1469 cal yr BP. This suggests that there is a hiatus of deposition present at 5 cm depth that is possibly due to erosion of the topmost sediment layers during the tsunami. Based on the ^{14}C age of the topmost 1cm layer (present surface layer) in the BGS�, it indicated an (old carbon) reservoir age of 599 ± 19 ^{14}C years existed for the lake that was subsequently used for reservoir correction. The marshlands or mangrove swamps located adjacent to the south of the lake should probably cause this old carbon reservoir effect (see Fig.3.2)

The age model of Panama lagoon (PN) constructed based on ^{14}C ages of mollusc shells (Fig. 4.2 (a)), showed a chronology extending from 7242 cal yr BP (model maximum age) to the present with a sedimentation rate varying between 0.06 and 0.37 mm/yr (Fig. 4.2(b)). The bottommost part (102 – 90 cm) and the section between 10 and 20 cm from the top were characterized by very low sedimentation rates that were below 0.1 mm/yr. The age model truncated at 7 cm, just below the sand layer that was identified as a deposit left behind by the 2004 tsunami. Therefore, unconsolidated sediments above this layer (the upper 5 cm) were considered as recently deposited sediments after the 2004 event. In Panama lagoon regional

marine reservoir age of the shells (133 ± 65 yr BP) was applied for the reservoir correction of the ^{14}C shell dates.

The retrieved HP core revealed a depositional history spanning from 5868 cal yr BP (model maximum age) to the present based on the age-depth model constructed based on the bulk ^{14}C dates in the peat sequence (Fig. 4.3(a)). However, at HP, the peat accumulation rate is significantly variable throughout the core. Relatively slower accumulation rates below 0.5 mm/yr was observed between 150 and 75 cm (ca. 5500 – 600 cal yr BP) of the core (Fig. 4.3(b)). After that, the accumulation rate increased rapidly (between ca. 75 cm and the core top; ca. 600 cal yr BP - present) to a maximum value of 2 mm/yr. HP showed an overall increasing trend in its sedimentation rate from bottom to the top (except the decline from ~ 60 – 300 cal yr BP).

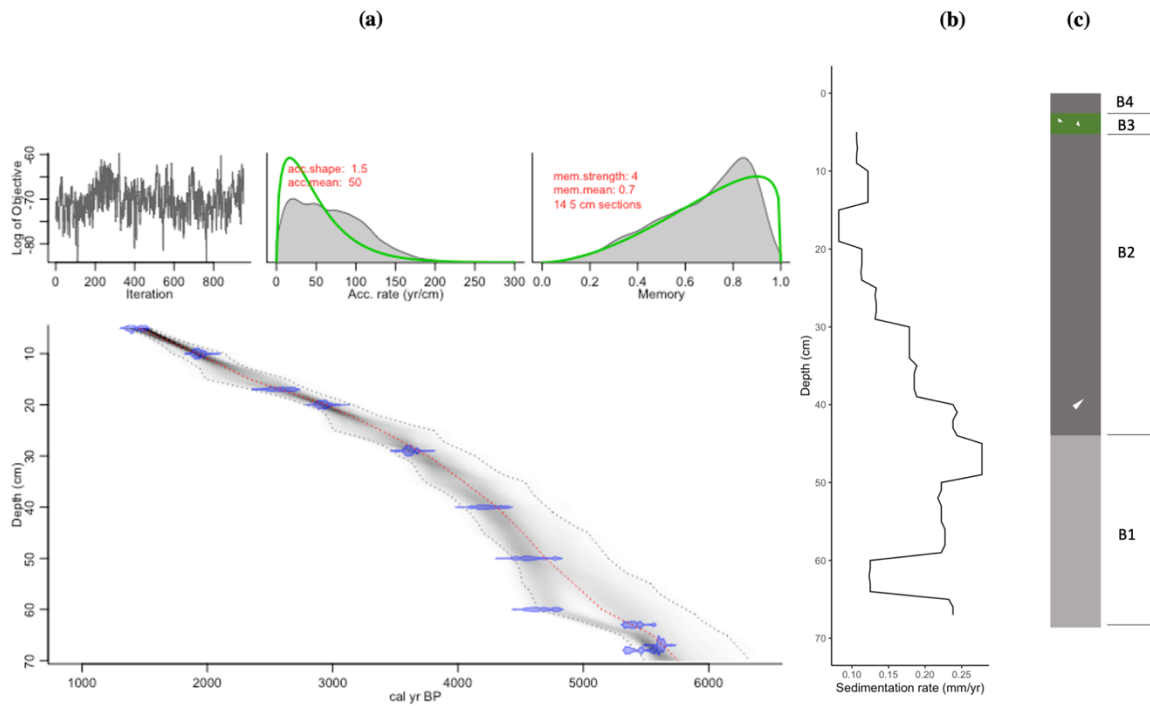


Fig. 4.1. (a) BACON age-depth model; (b) sedimentation rate and (c) sediment core stratigraphy of Bolgoda South Lake (BGS), Sri Lanka

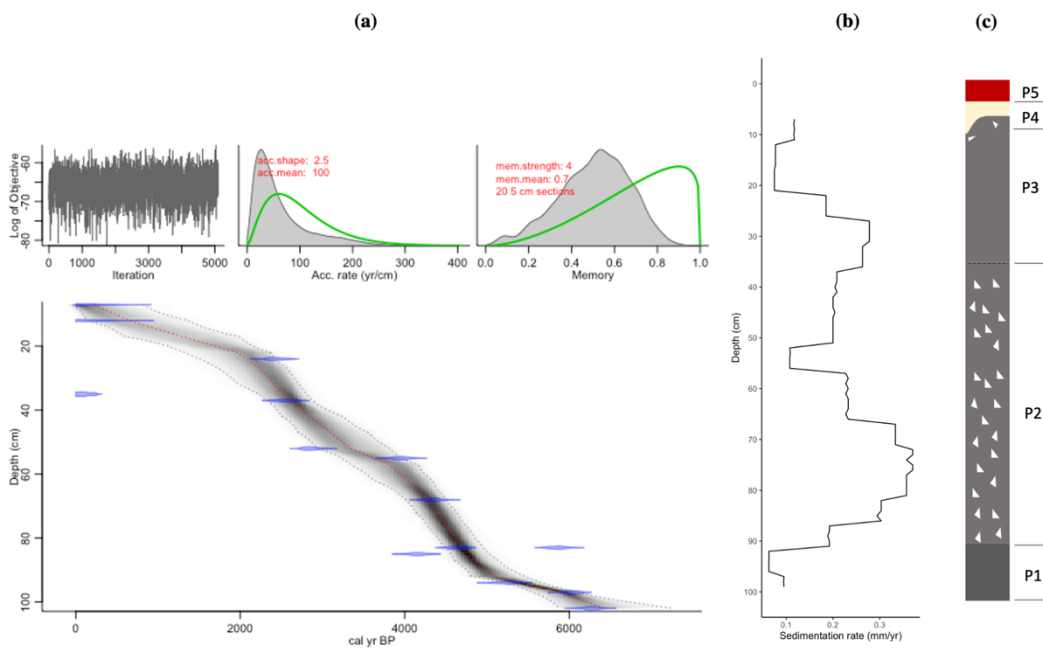


Fig. 4.2. (a) BACON age-depth model; (b) sedimentation rate and (c) sediment core stratigraphy of Panama Lagoon (PN), Sri Lanka

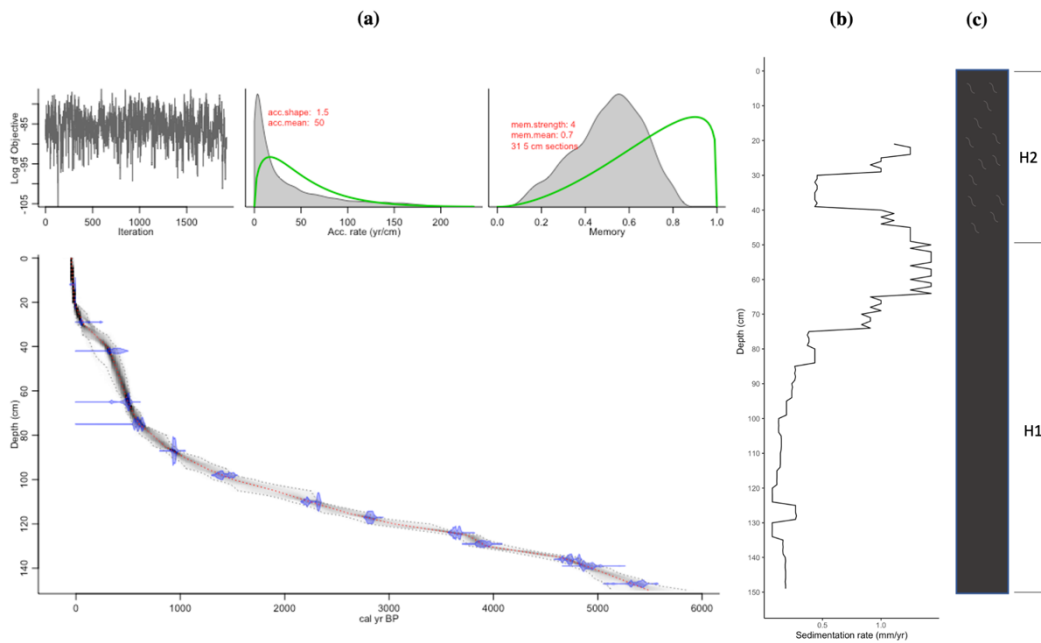


Fig. 4.3. (a) BACON age-depth model; (b) accumulation rate and (c) sediment core stratigraphy of Horton Plains (HP) peat sequence in the Central Highlands in Sri Lanka

4.4. Grain Size Distribution

Both the BGS� and PN cores showed very high contributions from sand that represented 94 % and 93 % of the mean values, respectively. However, for the finer fraction (silt and clay), the silt fraction dominated at BGS� whereas the clay fraction dominated in the PN core. In the BGS� core, both silt and clay fractions showed core upward increasing trends. By contrast, at PN, the clay fraction is relatively high and extended from ~6000 to 4700 cal yr BP. After that clay fraction decreased and showed a slightly decreasing trend until present (Fig.4.4).

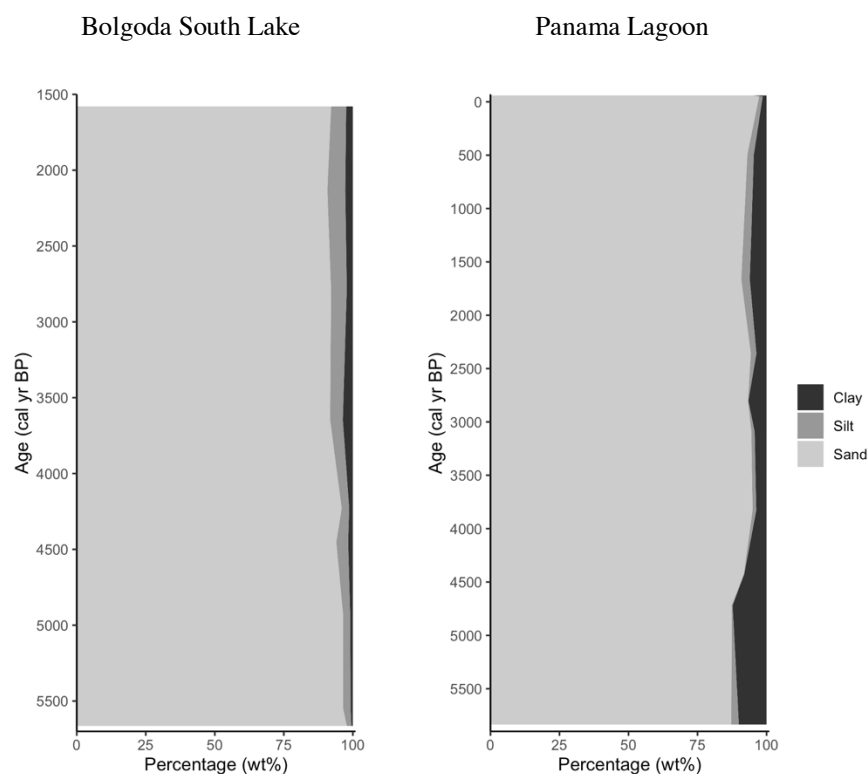


Fig. 4.4. Grain size distribution (weight percentages) of Bolgoda South Lake (left) and Panama Lagoon (right)

4.5. Elemental Composition

XRF data is only available for the Bolgoda South Lake and Panama Lagoon sediment cores. Varimax rotated principal components showed 80% and 86% cumulative variance for the first five rotated components (RCs) at BGS� and PN, respectively (Table. 4.2).

Table 4.2: Varimax Rotated components and their variance

Bolgoda South Lake			Panama Lagoon		
Component	% variance	% cumulative	Component	% variance	% cumulative
RC2	20	20	RC1	32	32
RC1	18	38	RC2	20	52
RC4	16	53	RC4	15	66
RC3	15	68	RC3	11	77
RC5	12	80	RC5	9	86

Table 4.3: PCA loadings for Bolgoda South Lake (correlations greater than 0.65 are bold)

Element	RC2	RC1	RC4	RC3	RC5
Al	-0.153	0.141	0.913	-0.026	0.162
Si	-0.335	0.706	-0.090	0.225	0.452
K	0.524	-0.129	0.767	-0.023	-0.060
Ca	0.710	0.172	0.023	0.083	0.271
Ti	0.121	0.698	-0.155	0.473	0.341
V	0.542	0.502	-0.213	-0.022	-0.127
Mn	0.848	0.042	-0.030	-0.186	0.036
Fe	0.788	-0.244	0.232	0.369	-0.126
Ni	0.030	-0.097	0.275	-0.730	-0.021
Cu	-0.050	0.087	-0.128	-0.817	0.031
Rb	-0.154	-0.866	-0.190	0.322	0.067
Sr	-0.121	-0.075	-0.075	0.054	-0.934
Zr	0.028	0.402	-0.594	0.392	0.418

Table 4.4: PCA loadings for Panama Lagoon (correlations greater than 0.65 are bold)

Element	RC1	RC2	RC4	RC3	RC5
Al	0.907	-0.214	0.007	0.150	0.041
Si	0.673	-0.615	-0.009	-0.031	0.056
K	0.524	-0.686	0.286	-0.140	0.246
Ca	-0.116	-0.142	-0.921	-0.157	0.131
Ti	0.796	-0.134	0.396	0.017	0.263
V	0.197	0.764	0.329	0.040	0.017
Mn	0.070	0.863	0.058	-0.096	-0.079
Fe	0.823	0.351	0.214	0.185	0.073
Ni	-0.030	0.096	0.147	-0.028	-0.969
Cu	-0.246	0.269	0.443	-0.698	-0.097
Rb	-0.077	0.131	0.270	0.850	-0.022
Sr	-0.647	-0.062	-0.581	0.303	0.153
Zr	-0.867	-0.276	0.163	0.148	0.212

In the Bolgoda South Lake core, RC2 explained 20% of the variance (highest variance; Table 4.2). The loadings of Mn, Fe, and Ca showed strong positive correlations with RC2. RC1 explained 18% of the variance and Rb correlated highly negatively, while Si and Ti correlated positively, with RC1. RC4 explained 16% of the variance and was characterised by high

positive loadings of Al and K. RC3 was characterised by high negative loadings of Ni and Cu that explained 15% of the variance. RC5 explained 12% of variance and Sr showed strong negative correlation with RC5 (Table 4.2).

RC2 and RC4 scores showed general trend towards positive scores when moving core upward (Fig. 4.5). In contrast, RC3 showed general trend towards negative scores core upward. RC1 scores showed positive scores from ~ 5700 to 5000 cal yr BP and generally negative scores between 5000 and 1500 cal yr BP where they reached lowest values around 4000 cal yr BP. RC5 scores showed a slight core upward trend towards negative scores (Fig. 4.5).

In the Panama Lagoon core, RC1 explained 32% of the variance (highest variance; Table 4.2). Loadings of Al, Fe, and Ti were strongly positively correlated with RC1 whereas Zr was negatively correlated with RC1. RC2 explained 20% of the variance and was characterised by high positive loadings of Mn and V. RC4 explained 15% of variance and was characterised by a strong negative correlation with Ca. RC3 explained 11% of the variance and showed a strong positive correlation with Rb and negative correlation with Cu. RC5 explained 9% of the variance and was characterised by high negative loadings of Ni (Table 4.2).

The RC1 scores showed generally positive values from ~ 6200 to 4300 cal yr BP (from core bottom to 70 cm) except for a sharp peak with high negative scores at ~ 4800 cal yr BP. After that, RC1 scores shifted to negative scores until present (Fig.4.6). By contrast, RC3 scores show a general core upward trend towards positive scores. RC2 and RC4 scores were mostly negative from 4700 to 3500 cal yr BP. RC5 did not show clear trends in the Panama lagoon core (Fig.4.6).

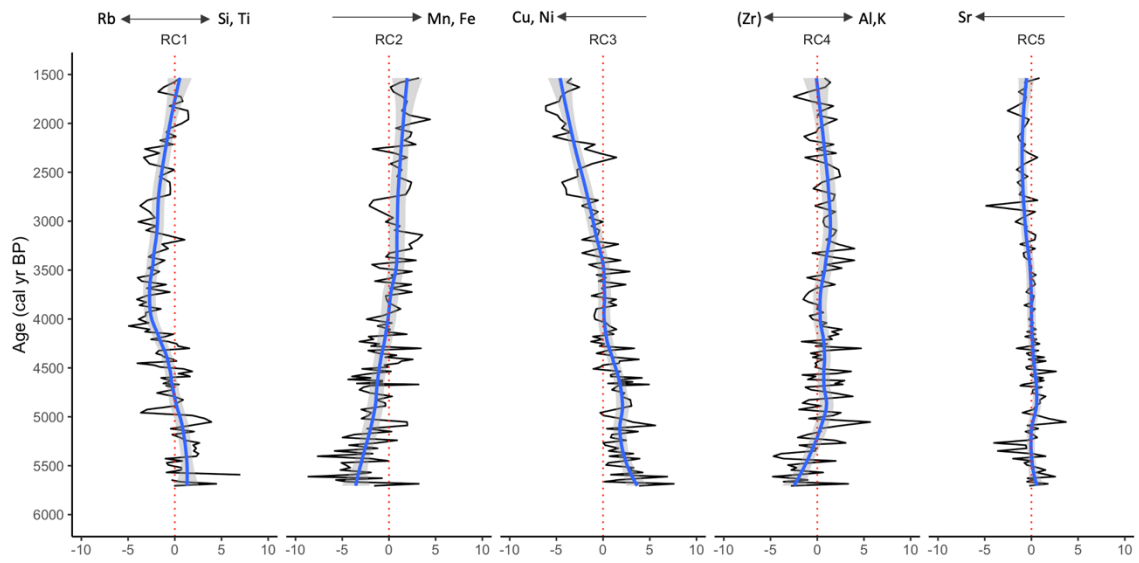


Fig. 4.5. Variations of RC scores in Bolgoda South Lake (BGSL) sediments, Sri Lanka.

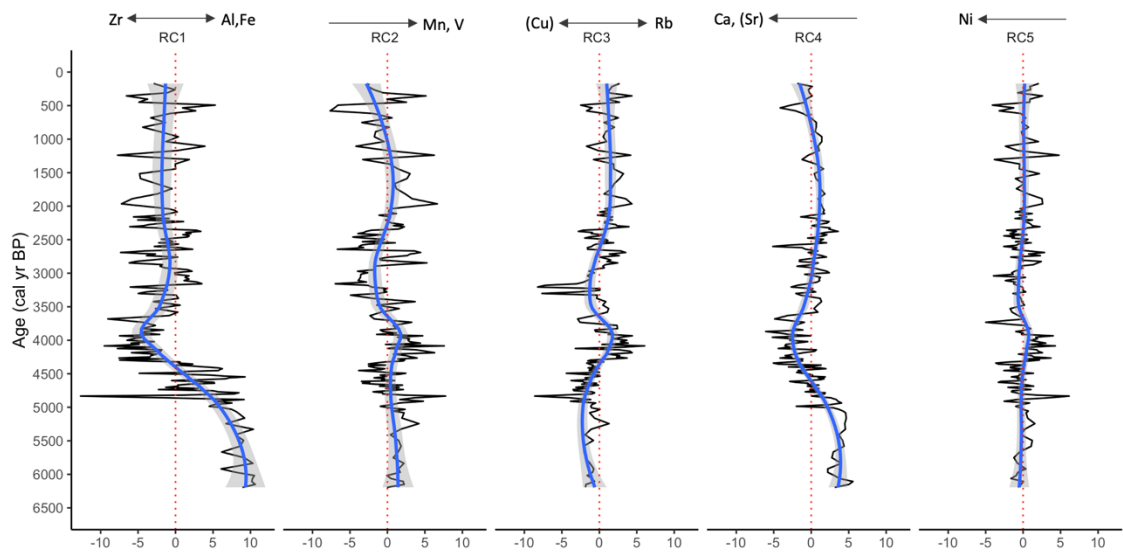


Fig. 4.6. Variations of RC scores in Panama Lagoon (PN) sediments, Sri Lanka

4.6 Biomarker Variation

4.6.1 *n*-Alkane

In sediment cores retrieved from the three sites along a transect, we identified and measured the concentrations of *n*-alkanes extending from *n*-C₁₅ to *n*-C₃₅ chain-length. The total *n*-alkane (*n*-C₁₅ to *n*-C₃₃) content varied between 9.45 – 0.92 ng/mg dry weight (dw) in Bolgoda South Lake, 5.46 – 1.30 ng/mg dw in Panama Lagoon and 159 – 23.8 ng/g dw for the Horton Plains. The chromatograms for both PN and BGSL cores showed a bimodal distribution pattern of *n*-alkanes, with even carbon number short-chain (*n*-C₁₆, C₁₈ and C₂₀) alkanes and odd carbon number long-chain (*n*-C₂₉, C₃₁ and C₃₃) alkanes dominating in the extracts (see Appendix Fig. 2). Contribution from the mid chain *n*-alkanes (*n*-C₂₁ – C₂₇) was low in both BGSL and PN cores. In contrast to BGSL and PN, the HP peat core was dominated by mainly odd carbon numbered *n*-alkanes from C₂₃ to C₃₃ with relatively high contributions from mid-chain (*n*-C₂₅ and C₂₃) alkanes (see Appendix, Fig. 2).

BGSL and PN both showed inverse patterns between their relative distribution of short and long-chain *n*-alkanes in the sediment cores (Fig. 4.7). In PN, the relative abundance of long-chain *n*-alkanes (mainly *n*-C₂₉, C₃₁ and C₃₃) increased up the core whereas short-chain *n*-alkanes (mainly *n*-C₁₆, C₁₈ and C₂₀) decreased. In BGSL, this variation was less predictable. However, overall, long-chain *n*-alkanes increased in abundance and short-chain *n*-alkanes decreased in the upper half section of the core (ca. 35 cm to top). In the Horton Plains, significant variation between the relative abundances of *n*-alkanes was not observed in the core except for in *n*-C₃₃ and C₂₉ (Fig. 4.7).

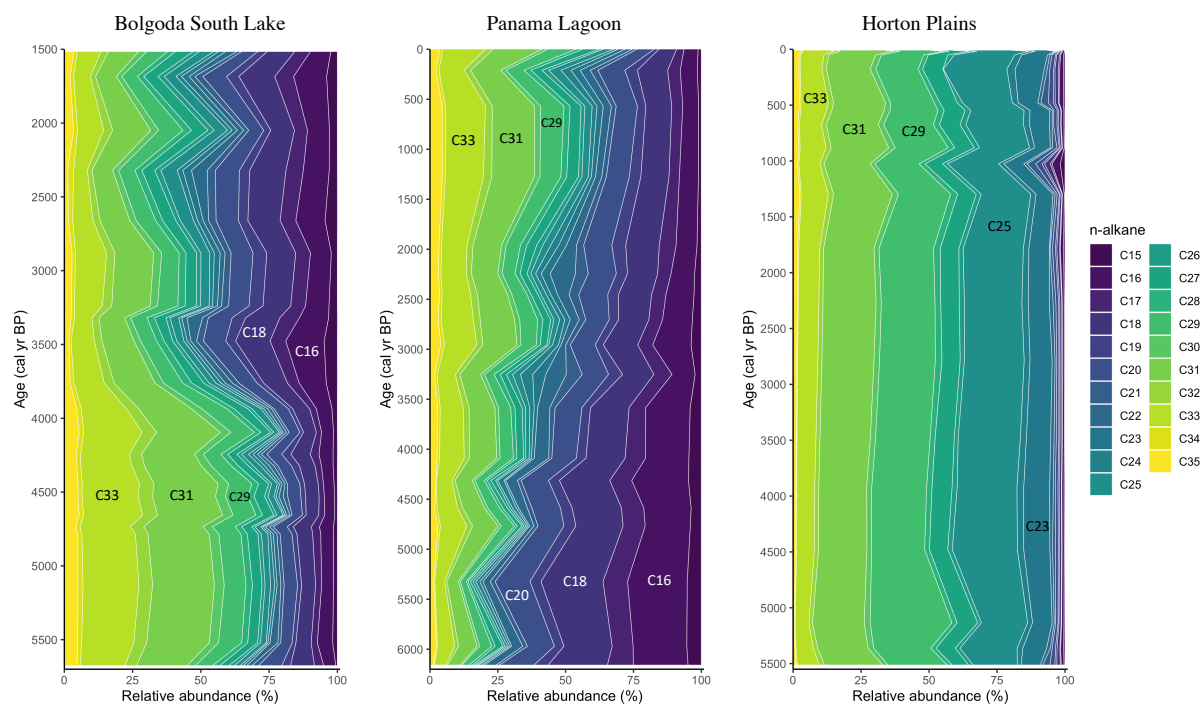


Fig. 4.7. Relative distribution of *n*-alkane (n -C₁₅ to C₃₅) in Bolgoda South Lake (BGS), Panama Lagoon (PN) and Horton Plains (HP)

Each sediment core was divided into two clusters by hierarchical cluster analyses, based on the relative distribution of *n*-alkanes that is taken to indicate different OM sources for the cores. Dominant *n*-alkanes in these clusters were identified using PCA biplots for each core. In BGS, PC1 accounted for 62.3% variance and was characterized by high positive loadings of short-chain *n*-alkanes from C₁₆ to C₂₂ (predominantly even chain *n*-alkanes) and high negative loadings of long chain *n*-alkanes from C₃₁ to C₃₅ (odd chain *n*-alkanes predominant). Cluster 1 in BGS showed positive scores with PC1 whereas cluster 2 showed negative scores (Fig. 4.8(a)). This implies that cluster 1 in BGS is characterized by mainly *n*-C₁₆, C₁₈ and C₂₀ alkanes whereas cluster 2 is mainly consisted of *n*-C₃₁, C₃₃ and C₃₅ alkane. In PN, an inverse pattern of *n*-alkane distributions can be identified based on the hierarchical cluster analyses and PCA. PC1 in PN core accounted for 60.3% variance that was characterized by high negative loadings of short-chain *n*-alkanes from C₁₅ to C₂₀ (predominantly even chain *n*-alkanes) and high positive loadings of long chain *n*-alkanes from C₂₇ to C₃₃ (predominantly odd chain *n*-

alkanes). Cluster 1 in PN, showed positive scores with PC1, whereas cluster 2 indicated negative scores (Fig. 4.8(b)). This trend implied that cluster 1 in PN was characterized mainly by n -C₂₇, C₂₉, C₃₁ and C₃₃ alkanes whereas in cluster 2 it consisted of by n -C₁₆, C₁₈ and C₂₀ alkanes. The variation of PC1 scores both in BGSL and PN therefore, at least in part, represents the variation in abundance of short-chain and long-chain n -alkanes over the time.

A different pattern of n -alkane distribution was identified in the HP peat core based on multivariate statistical analysis. According to the PCA biplot of HP, PC1 and PC2 accounted for 33.6% and 23.7% of total variance, respectively (Fig. 4.8(c)). The loadings of dominant n -alkanes correlated with the PC2 axis rather than the PC1 axis in the PCA biplot. Longer chain n -alkanes (namely C₃₁ and C₃₃) correlated positively with PC2 whereas mid-chain n -alkanes C₂₃ and C₂₅ correlated negatively with PC2. In addition, n -C₂₇ and C₂₉ showed a moderate negative correlation with PC2. Therefore, PC2 scores at HP appear to generally represent variation between long-chain (n -C₃₁ and C₃₃) and mid chain (n -C₂₃, C₂₅) n -alkanes. The majority of cluster 1 depths showed positive scores with PC2, whereas cluster 2 depths showed negative scores with PC2 (Fig.4.8(c)).

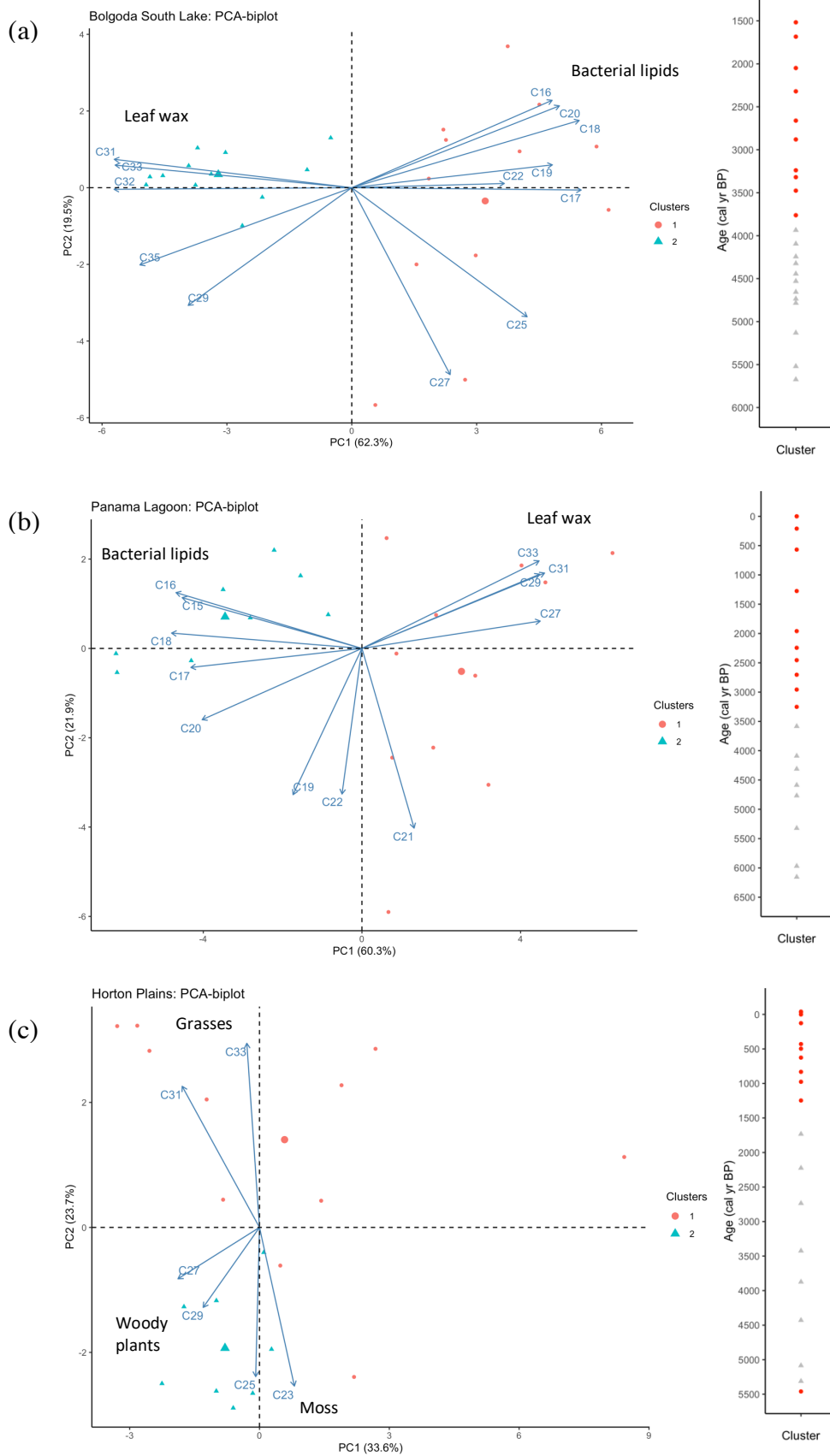


Fig. 4.8. PCA biplots (left) and cluster distributions (right) in (a). Bolgoda South Lake, (b). Panama Lagoon and (c). Horton Plains

PC1 scores changed from negative to positive values in the BGSL core ~ 3800 cal yr BP (32 cm; Fig. 4.9) and ~ 3200 cal yr BP (52 cm in PN; Fig. 4.10). The Carbon Preferential Index (CPI) for *n*-alkanes was used to assess the odd/even predominance of *n*-alkanes in sedimentary organic matter (OM) (Meyers, 1997; Ouyang et al., 2015). Due to the bimodal distribution of *n*-alkanes in the BGSL and PN cores, the CPI for *n*-alkanes (CPI_T) was calculated for *n*-alkanes ranging from C₁₅ to C₃₅ range, as shown below:

$$\text{CPI}_T = (\sum (C_{15} - C_{33}) + \sum (C_{17}-C_{35}))/ (2 \times \sum (C_{16} - C_{34}))$$

BGSL showed an average CPI value of 2.52 that varied between 1.41 and 3.69 and shifted to relatively low value (1.8) ~ 3800 cal yr BP (Fig. 4.9). CPI_T values in PN varied from 0.70 – 3.10 with an average value of 1.55 and a core upward increasing trend (Fig. 4.10).

At HP, PC2 scores were positive between ~ 1500 and 500 cal yr BP and also in the topmost and bottommost layers of the core. *n*-Alkanes showed a unimodal distribution at HP and, therefore, CPI was calculated for *n*-alkanes from C₂₁ to C₃₃ as below:

$$\text{CPI} = (\sum (C_{21} - C_{31}) + \sum (C_{23}-C_{33}))/ (2 \times \sum (C_{22} - C_{32}))$$

CPI values in HP varied between 9.58 and 13.6 with an average of 11.3. An overall core upward decreasing trend of CPI values was observed in the HP core with some fluctuations (Fig. 4.11).

4.6.2 Sterols

The BGSL and PN cores included mangrove-derived triterpenols, primarily taraxerol and β-amyrin. Due to the different total organic carbon (TOC) ranges at BGSL and PN, taraxerol and β-amyrin contents were expressed as TOC normalized values to enable comparison between the two sites. According to the results, high average values of taraxerol and β-amyrin were observed in the PN core relative to BGSL.

In the BGS� core, taraxerol varied from 717 – 2578 ng/g dw TOC and β -amyrin ranged from 67 – 424 ng/g dw TOC. Neither taraxerol nor β -amyrine displayed a clear trend through the BGS� core (Fig. 4.9). In the PN core, taraxerol varied from 626 – 4801 ng/g dw TOC, and β -amyrin ranged from 77 - 1462 ng/g dw TOC. A clear increasing core upward trend of taraxerol and β -amyrin was identified in PN until the tsunami layer (Fig. 4.10).

In the HP core several sterols and stanols were identified, namely cholesterol, cholestanol, campesterol, campestanol, stigmasterol, sitosterol, and sitostanol. The sterol to stanol ratio of these compounds in HP showed a general core upward decreasing trend.

4.7 Bulk Organic Carbon and $\delta^{13}\text{C}_{\text{org}}$ Variation

The highest average total organic carbon (TOC wt%) values were observed in the HP peat deposit, which was followed by the BGS� and PN cores, respectively. In the HP peat deposit, TOC values varied between 2.13 – 14.20 % with an average of 5.49%. The BGS� core had an average TOC value of 3.11%, and varying between 0.71 and 5.09%. In both BGS� and HP sites the TOC showed a core upward increasing trend (Fig. 4.9 and 4.11). TOC content was relatively low in the PN core with an average of 0.52 wt %. Except for the relatively high value (1.94%) in the organic-rich surface layer at the top of the core, TOC content was < 1% and showed a gentle core upward increasing trend (Fig. 4.10).

Bulk organic $\delta^{13}\text{C}$ values ($\delta^{13}\text{C}_{\text{org}}$) in the HP core varied between -27.4 and -23.6 ‰ (with an average of -25.3 ‰). Bulk $\delta^{13}\text{C}_{\text{org}}$ showed an increasing trend until 500 cal yr BP (from the core bottom to 65 cm), stabilizing after this age (Fig. 4.11). The $\delta^{13}\text{C}_{\text{org}}$ values in the BGS� core varied between -29.3 and -26.8 ‰ (average = -27.9 ‰) and showing only subtle variation through the core. However, after ~ 3000 cal yr BP $\delta^{13}\text{C}_{\text{org}}$ showed a slight increase in the values. In the topmost layer (between 1-2 cm) $\delta^{13}\text{C}_{\text{org}}$ decreased to -29.3 ‰ (Fig. 4.9). In the PN core, $\delta^{13}\text{C}_{\text{org}}$ varied between -28.3 and -21.6 ‰ (average = -23.5 ‰). A decreasing core upward trend

of $\delta^{13}\text{C}_{\text{org}}$ was observed with an exceptionally low value of -28.3‰ occurring between 3 and 4 cm, which coincided with carbon-rich sediment with partially decomposed plant debris (Fig. 4.10).

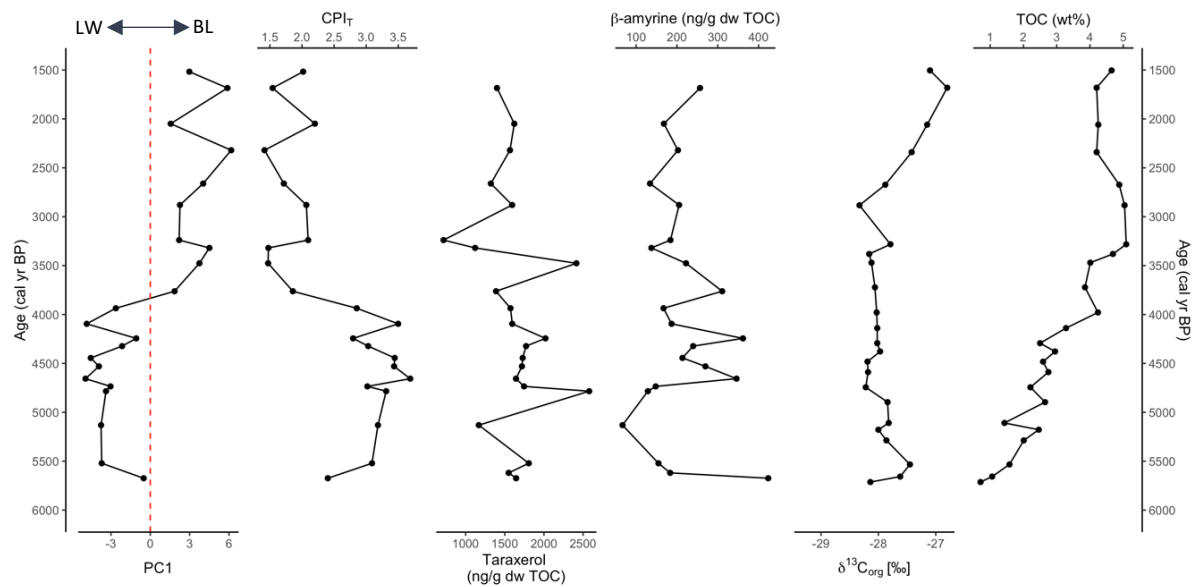


Fig. 4.9. Variations of PC1 scores (LW= Leaf wax, BL= Bacterial lipids), carbon preferential index for total *n*-alkane (CPI_T), triterpenols (taraxerol and β -amyrine), bulk organic carbon isotopes ($\delta^{13}\text{C}_{\text{org}}$) and total organic carbon (TOC) in the Bolgoda South Lake (BGS) core

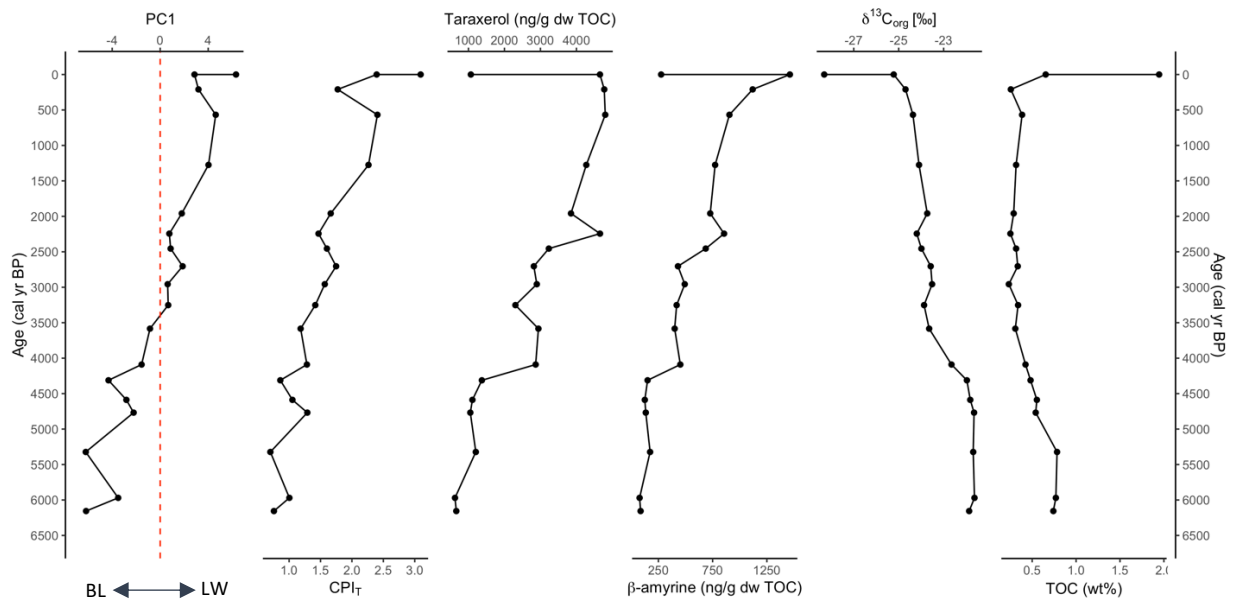


Fig. 4.10. Variations of PC1 scores (LW= Leaf wax, BL= Bacterial lipids), carbon preferential index for total *n*-alkane (CPI_T), triterpenols (taraxerol and β -amyrine), bulk organic carbon isotopes ($\delta^{13}C_{org}$) and total organic carbon (TOC) in the Panama Lagoon (PN) sediments.

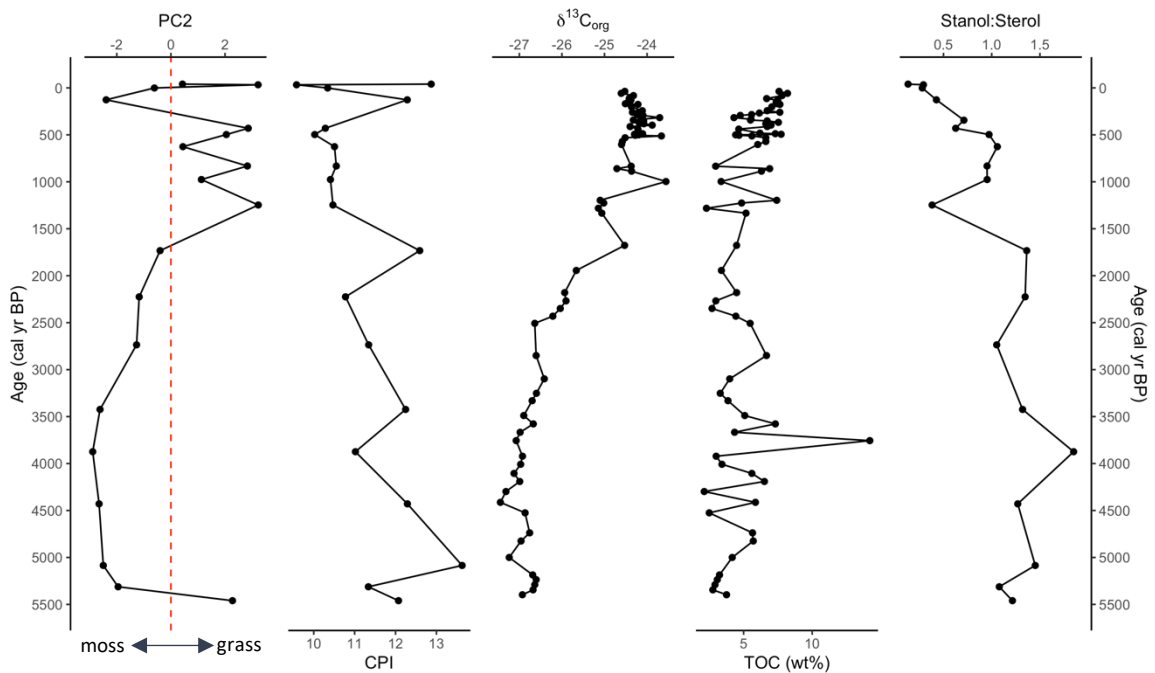


Fig. 4.11. Variations of PC2 scores, carbon preferential index (CPI), bulk organic carbon isotopes ($\delta^{13}C_{org}$), total organic carbon (TOC) and stanol:sterol ratio in the Horton Plains (HP) peat deposit.

4.8 Compound Specific Carbon and Hydrogen Isotope Variation in *n*-Alkanes

Among the three sites, average *n*-alkane δD values of long-chain *n*-alkanes (*n*-C₃₃, C₃₁ and C₂₉) in HP showed the lowest values (most depleted) followed by PN. BGSL showed the highest (most enriched) average δD values in long-chain *n*-alkanes (Table 4.5). Comparison of the average $\delta^{13}C$ values of long-chain *n*-alkanes at the three sites, indicated no significant differences between the core average values. However, at PN slightly higher average values were found compared to BGSL and HP (Table 4.5).

Short-chain *n*-alkanes (*n*-C₁₆ and C₁₈) that were only present in the coastal sites (BGSL and PN). These sites indicated relatively higher average $\delta^{13}C$ values in BGSL relative to PN, particularly for *n*-C₁₈ alkanes. Average δD values were also relatively high in BGSL short-chain *n*-alkanes, particularly for *n*-C₁₆ alkanes (Table. 4.5). Due to the relatively low peak amplitude of *n*-C₂₅ and C₂₇ alkanes in BGSL and PN, δD and $\delta^{13}C$ values were recorded with higher standard error and so not used for interpretations (also not shown in the table).

Long chain *n*-alkane carbon and hydrogen isotopic variations showed very different relationships in the BGSL and PN cores (see Fig. 4.12 and 4.13). In the BGSL core, δD and $\delta^{13}C$ values for *n*-C₃₃, C₃₁ and C₂₉ alkanes showed a general core upward increasing trend in their values that is particularly clear for *n*-C₃₃ alkanes. Particularly high δD and $\delta^{13}C$ long chain *n*-alkane values were observed at ca. 3450 (26 cm) and 3740 cal yr BP (30 cm), respectively, that are most clearly visible in *n*-C₃₃ alkanes (Fig. 4.12). In contrast to the overall core upward increasing trend at BGSL, δD and $\delta^{13}C$ values of *n*-C₃₃, C₃₁ (and C₂₉) showed general core upward decreasing trends in PN. Deviating from this general trend, relatively low δD and $\delta^{13}C$ values were identified at ~ 4770 cal yr BP (depth at 85 cm) in *n*-C₃₃ alkanes (Fig. 4.13). No clear trend was identified in δD and $\delta^{13}C$ values of *n*-C₁₆ and C₁₈ alkanes at BGSL (Fig. 4.12). In contrast, δD and $\delta^{13}C$ values of *n*-C₁₆ and C₁₈ alkanes in PN show generally core upward increasing trends (Fig. 4.13).

Trends for $\delta D_{(n-C_{23} - C_{25})}$ values in the HP core varied somewhat differently to the $\delta^{13}C$ trends in same *n*-alkanes. Higher δD occurred between 1000 and 500 cal yr BP whereas the higher $\delta^{13}C$ values occurred between 500 and 0 cal yr BP. With regards to the δD values in *n*-alkanes, a core upward increasing trend for *n*-C₂₃ and C₂₅ was observed with the maximum values at ~ 610 cal yr BP followed by a gradual decline (Fig. 4.14). $\delta D_{n-C_{29}}$ reached a peak at ~ 810 cal yr BP with a similar core upward increasing trend followed by a decline until present. $\delta D_{n-C_{31}}$ and $\delta D_{n-C_{33}}$ showed core upward increasing trends, reaching their peak values ~ 970 cal yr BP (Fig. 4.14). The δD peak appeared slightly earlier in long-chain *n*-alkanes than in mid-chain *n*-alkanes. $\delta^{13}C$ of *n*-C₂₃, C₂₅ and C₂₉ alkanes showed relatively low (below average) and stable values between ~ 5480 – 430 cal yr BP followed by a sharp peak between 430 and 1 cal yr BP and a gradually decreasing trend after that towards the top of the core. However, $\delta^{13}C_{n-C_{33}}$ showed relatively low values (below -30 ‰) between ~ 5300 and 1250 cal yr BP and shifted to relatively higher values (above -30 ‰) to the present (Fig. 4.14).

Table 4.5: Average, minimum and maximum $\delta^{13}\text{C}$ and δD values of dominant *n*-alkanes in each core

	<i>n</i> -alkane	Panama Lagoon			South Bolgoda Lake				<i>n</i> -alkane	Horton Plains		
		Average ‰	Min ‰	Max ‰	Average ‰	Min ‰	Max ‰			Average ‰	Min ‰	Max ‰
$\delta^{13}\text{C}$	<i>C33</i>	-31.2	-32.4	-29.1	-34.1	-38.0	-29.5	$\delta^{13}\text{C}$	<i>C33</i>	-31.2	-34.4	-28.0
	<i>C31</i>	-32.3	-34.3	-29.3	-33.8	-37.4	-30.0		<i>C31</i>	-34.0	-35.9	-31.9
	<i>C29</i>	-29.7	-31.4	-27.3	-31.3	-34.7	-28.0		<i>C29</i>	-31.7	-33.4	-27.7
	<i>C16</i>	-29.8	-31.3	-28.2	-28.1	-30.4	-23.0		<i>C25</i>	-34.1	-36.5	-29.5
	<i>C18</i>	-29.5	-32.5	-25.7	-17.4	-22.6	-12.4		<i>C23</i>	-33.4	-35.6	-28.1
δD	<i>C33</i>	-130	-144	-107	-100	-117	-78	δD	<i>C33</i>	-138	-159	-85
	<i>C31</i>	-133	-152	-99	-133	-140	-106		<i>C31</i>	-144	-166	-111
	<i>C29</i>	-221	-239	-206	-197	-217	-177		<i>C29</i>	-237	-253	-209
	<i>C16</i>	-75	-92	-57	-40	-75	-5		<i>C25</i>	-249	-275	-208
	<i>C18</i>	-92	-116	-49	-73	-109	-47		<i>C23</i>	-145	-180	-86

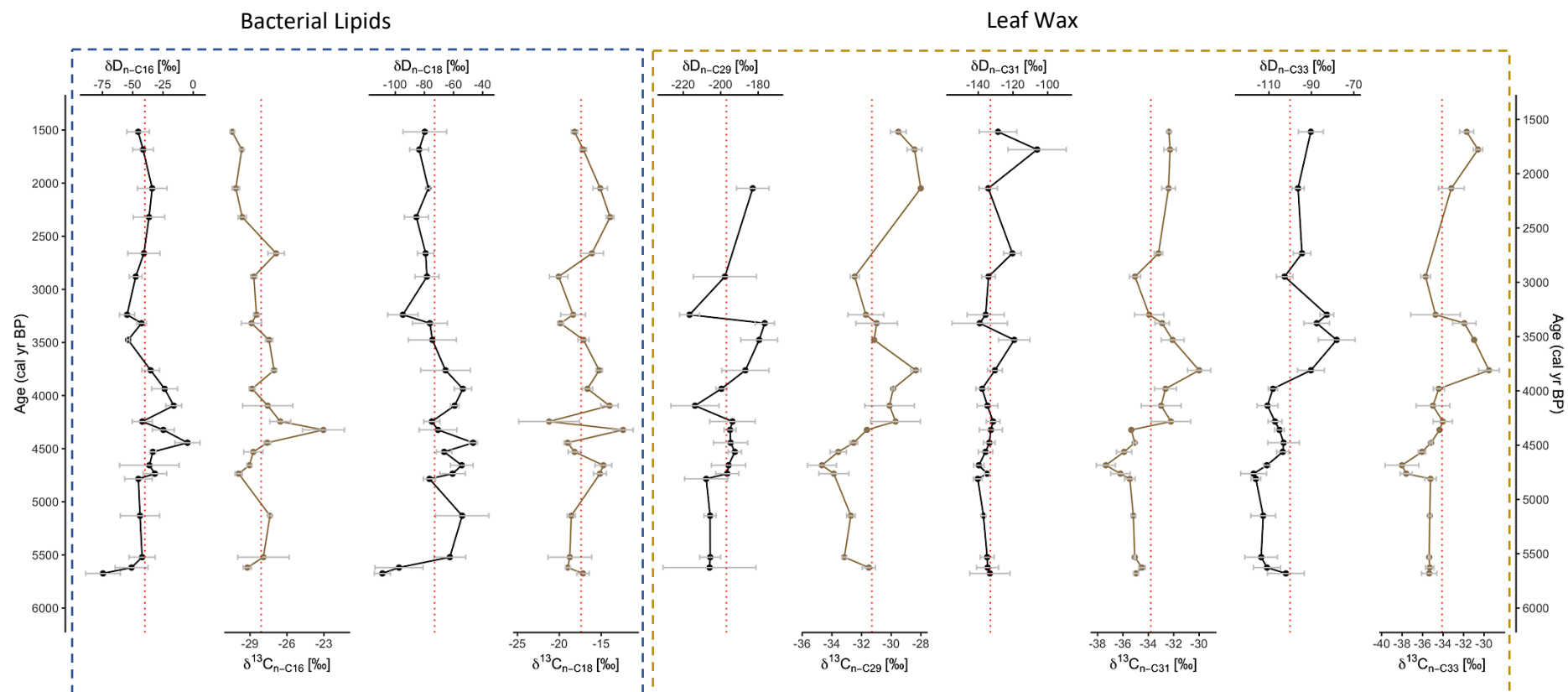


Fig.4.12. Variation of bacterial lipids ($n-C_{16}$ and C_{18}) and leaf wax n -alkane ($n-C_{29}$, C_{31} and C_{33}) D (black) and $\delta^{13}C$ (brown) values in Bolgoda South Lake (BGS) core. (Dotted vertical lines indicate the core average values)

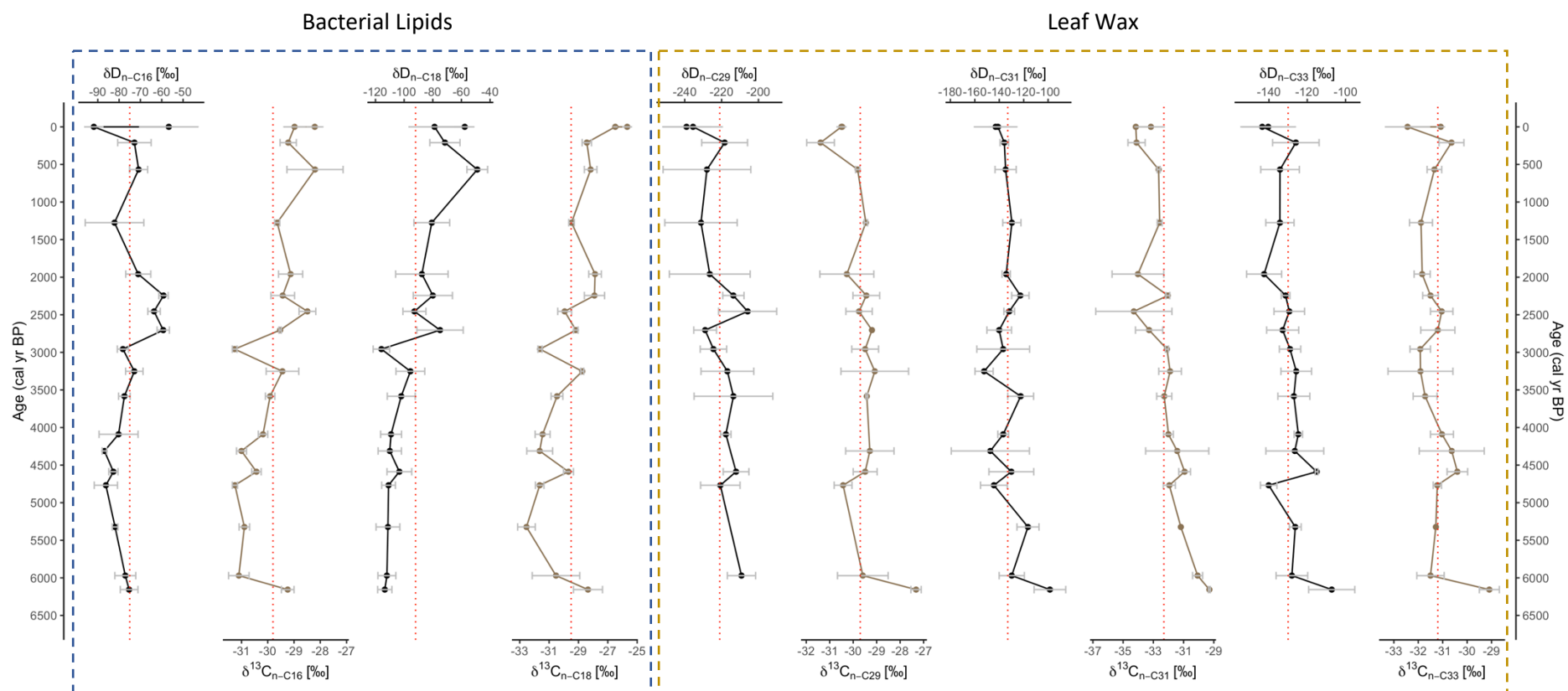


Fig.4.13. Variation of bacterial lipids ($n\text{-C}_{16}$ and C_{18}) and leaf wax n-alkane ($n\text{-C}_{29}$, C_{31} and C_{33}) D (black) and $\delta^{13}\text{C}$ (brown) values in Panama Lagoon (PN) core. (Dotted vertical lines show the core average values)

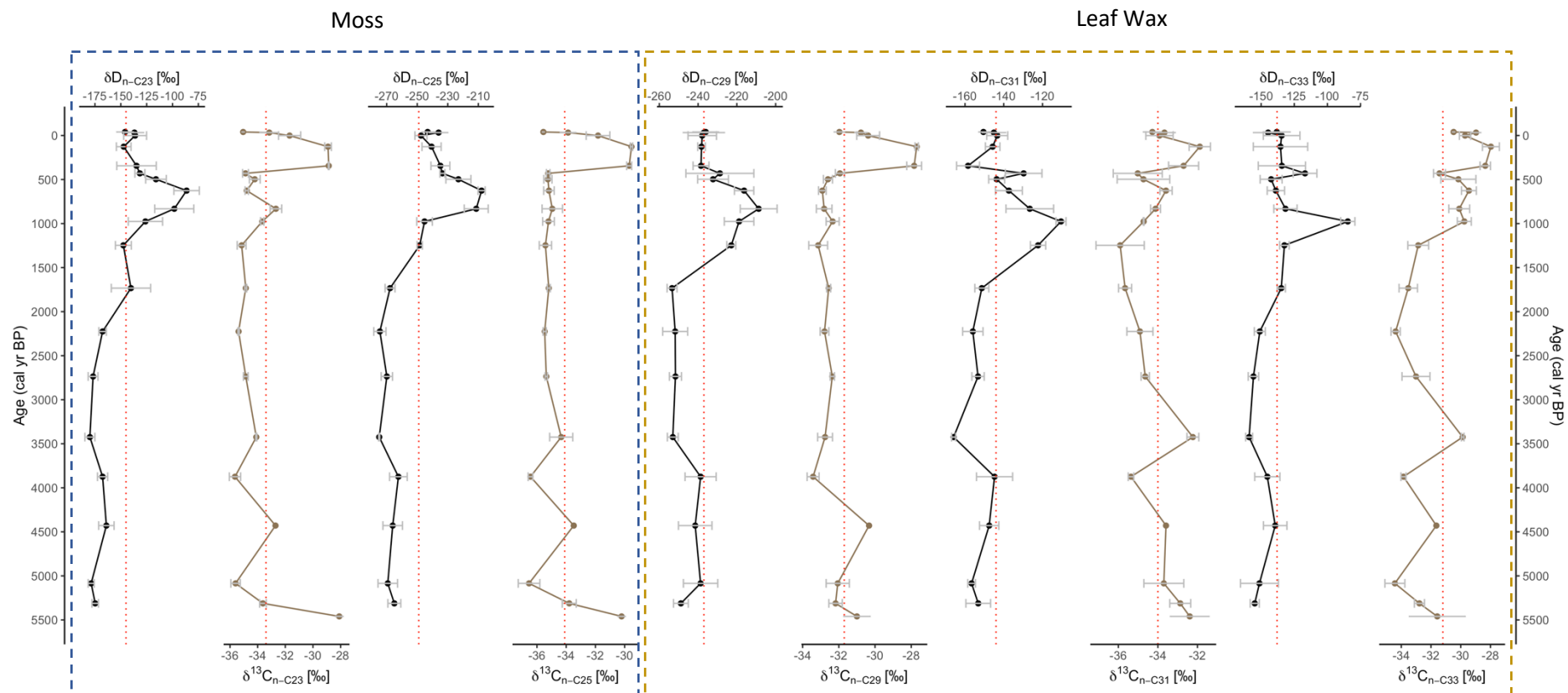


Fig.4.14. Variation of moss ($n-C_{23}$ and C_{25}) and leaf wax n-alkane ($n-C_{29}$, C_{31} and C_{33}) D (black) and $\delta^{13}C$ (brown) values in Horton Plains (HP) core. (Dotted vertical lines show the core average values)

5. Discussion

Along the transect from the west coast to east coast, running through the central highlands of Sri Lanka, these three sites namely Bolgoda South Lake, Horton Plains and Panama Lagoon indicate palaeoenvironmental changes stretching from the mid-Holocene to the present. Based on high-resolution ^{14}C age-depth models of these sites and various geochemical proxies, these sedimentary archives trace the variations in monsoon intensity and its impacts on climate, vegetation, depositional history and the development of a sedentary life focused on agriculture and farming practices. Here we discuss the main climate and environmental implications based on the trends of these diagnostic proxies at each site to understand the general monsoonal trends and environmental responses to the natural and human-induced changes.

5.1 ^{14}C Chronology and Depositional Conditions/Events

According to the lithostratigraphic observations, the very high sand content at the bottom section of BGS (B1; between ~ 5700 and 4500 cal yr BP) indicate sedimentation under a high energy environment that is also supported by the relatively high observed sedimentation rate in this section (Fig. 4.1). These observations suggest enhanced stream discharge that brought coarser particles to the lake as a result of increased rainfall in the catchment. Section B2 (between ~ 4500 and 1500 cal yr BP) is characterized by decreased sand with gradually decreasing trend of sedimentation rate, suggesting the termination of this high energy depositional condition (weakening of catchment rainfall) around 4500 cal yr BP. The modern (negative) ^{14}C ages of shell fragments in the sand layer (section B3) indicate this layer is a recently deposited short-lived high-energy event most likely linked to the 2004 tsunami which is known to have impacted the region (Wijetunge, 2006). The hiatus at 5.5 cm depth (~ 1500 cal yr BP just below the sand layer) could be due to the erosion of surface sediment layers during the tsunami event (Fig.4.1(a)). These kind of tsunami deposits are frequently identified

by a sand layer near the surface, uneven stratigraphical boundaries, and fragmented mollusc shells that yielded modern ^{14}C ages (Goff et al., 2012; Jackson, 2008). The effect of a tsunami on the coastal water body may vary depending on various factors such as direction of the waves, coastal morphology and vegetation, resulting in different impacts even within the same water body (Goff et al., 2012; Morton et al., 2008; Wijetunge, 2006). Tsunami waves can sometimes erode the surface sediments in a coastal water body resulting in relatively older ^{14}C ages in the sediment deposited just below the tsunami deposit (eg; Jackson et al., 2014). The uppermost section B4 can be considered as recently deposited sediments (after 2004) and reveal the old carbon reservoir age (599 ± 19 ^{14}C age BP) for the lake.

In Panama Lagoon, the bottommost section (P1; $\sim 6400 - 5000$ cal yr BP) is characterized by a high amount of clay with few intact shells and a very low sedimentation rate in contrast to the upper sections (Fig. 4.2). Based on the geomorphological setting of the PN site, we suggest two possibilities for this. One is a low rate of freshwater stream flow as a result of weak rainfall in the catchment. Alternatively, the area was inundated by seawater due to marine transgression coinciding with a high sea level. Section P2 ($\sim 5000 - 2600$ cal yr BP) was characterized by a high abundance of brackish water-adapted mollusc shells that indicate a rich nutrient supply and brackish water conditions for the lagoon at this time. In addition, the high sedimentation rate at this time could suggest high rate of stream flow associated with high rainfall in the catchment. Only a few shells were found in section P3 (~ 2600 cal yr BP – present), with less clay also observed, perhaps due to high freshwater input lowering the optimal salinity for molluscs. Similarly to BGSL, the sand layer observed between 10 – 5 cm with an uneven lower boundary could represent the 2004 tsunami event (Goff et al., 2012; Wijetunge, 2006). The shells found just below the sand layer had negative ^{14}C ages (modern ages) so no significant erosion can be identified here due to the tsunami waves.

At HP, a relatively low peat accumulation rate below ca. 75 cm is probably due to the compaction from upper peat layers because no significant stratigraphic difference was observed between these two sections (H1 and H2; Fig. 4.3). Negative ^{14}C ages appeared above ~ 20 cm in HP core, indicating that this section of the core consists of recently deposited OM and acrotelm that contain living plant material (Naafs et al., 2019).

5.2 Implications about Catchment and in Lake Processes by Physical and Inorganic

Geochemical Parameters

Sediment grain size distribution and variations in inorganic element contents provide crucial information on catchment dynamics and regional climate variability in the form of insights into sediment provenance, transportation, and oxic-anoxic conditions in lacustrine environments (Croudace and Rothwell, 2015).

Grain Size Distribution

Grain size variation primarily reflects energy driven processes in a given lake catchment. High rates of precipitation trigger enhanced erosion and stream discharge that bring coarse particles (sand) to the lake bottom. Weaker precipitation or dry climatic conditions lead to the accumulation of more of the fine clay particles in sedimentary sequences (Gayantha et al., 2017; Peng et al., 2005). However, stream and catchment morphological alterations and human impacts can also influence erosional processes, and thereby, the grain size distribution in sediments (Gayantha et al., 2017).

A contrasting relationship between the trends of grain size distribution (sand and clay) in the BGSL and PN cores reflect the inverse trends of rainfall variation in the catchments (Fig.4.4). General increasing trends of clay and silt content relative to sand content (representing a low energy environment) towards the top of the core in the BGSL core reflects

the weakening of inland summer precipitation over time (as discussed above). In contrast, a general core upward decreasing trend of clay content relative to its sand content in PN (representing a high energy more erosive environment) document an increasing trend of winter monsoon precipitation in the catchment (Fig. 4.4). In both the BGSL and PN cores, grain size (variation of clay fraction) is an important factor controlling the distribution of TOC (Fig. 4.9 and Fig. 4.10) because organic carbon is mainly associated with the fine fraction (Meyers and Teranes, 2001).

Element composition

Lithogenic elements, such as Al, Si, K, Ti, Fe, Rb and Zr can be used to understand catchment processes such as weathering and erosion due to their geochemical stability and incorporation as part of resistant minerals that are conservative in most environments (Davies et al., 2015). In BGSL, RC1 and RC4 are defined by these elemental assemblages and reflect grain size distribution and related processes in the catchment. In BGSL, RC 1 is mainly represented by rubidium (Rb) that shows the highest negative RC1 loadings (Fig. 4.5/Table 4.3). Rb is chemically similar to K and adsorbs to the clay fraction in sediments (Kylander et al., 2011). Accordingly, the highest clay content can be observed in BGSL ~4000 cal yr BP indicating lowest stream discharge and catchment erosion due to weakening of the monsoon (Fig.4.5). RC4 is characterized by high positive loadings of Al and K that are detrital elements associated with clay minerals (Davies et al., 2015; Kylander et al., 2011). Variation in RC4 scores further indicate that an increase of the clay fraction in the sediment between 5000 and 1500 cal yr BP occurred as a consequence of decreasing stream discharge and low rainfall in the catchment (Fig. 4.5).

Mn, Fe and V are redox sensitive elements that vary in their solubility depending on the bottom water oxic-anoxic conditions. Therefore, during periods with less bottom water oxic conditions these elements show high solubility in water, decreasing their contents in the

sediment. Water level changes, organic matter degradation, and biological productivity can influence the bottom water oxygenation process in lakes (Davies et al., 2015; Davison, 1993). An increasing trend of Mn and Fe in BGSL according to RC2 scores denote increasing oxic conditions in the bottom water, possibly due to lowering the lake water level as a result of less stream discharge to the lake and decreasing rainfall in the catchment (Fig. 4.5). Thus, RC1, RC2 and RC4 in BGSL, denote changes in elemental composition in sediment associated with decreasing stream discharge and catchment rainfall.

The degree of sorption of trace metals such as Cu, Zn, Co, Cd and Ni depends on the pH and ionic strength in water. Adsorption of these elements to the clay-rich sediments increases when the pH and ionic strength are low in water (e.g.; fresh or brackish water environments in contrast to seawater) (Hao et al., 2020). When the sea water enters into the estuarine or lagoonal environment its pH and ionic strength decreases leading to enhanced trace element adsorption to the clay particles. Hence, Cu and Ni in this study can be used as a proxy for sea water intrusion into coastal water bodies. RC3 in BGSL is characterised by high negative loadings of Cu and Ni where it shows a generally increasing trend of these elements in sediments and increasing sea water intrusion/marine influence with time. Also, Sr is common in sea water and is represented by high negative scores for RC5 in BGSL. A slight increase in Sr levels between 3500 cal yr BP and present indicates an increase in sea water intrusion in BGSL during this period. Thus, RC3 and RC5 indicate the marine influence in BGSL.

In Panama Lagoon (PN), RC1 is characterized by high positive loadings of Al, Fe and Ti that are often associated with clay minerals, and negative loadings of Zr linked with the coarse sand or silt fraction (Kylander et al., 2011). Therefore, RC1 in PN denotes sediment grain size variation over time and high clay content (positive scores) with a decreasing trend from ~ 6200 to 4500 cal yr BP. This indicates low sedimentation rate in the lagoon during this period as a

result of low stream discharge and/or marine transgression (Fig. 4.6). This however needs to be ascertained based on evidence from other proxies too.

RC3 is characterised by high positive loadings for Rb that is a detrital element and associated with clay fraction. In contrast, Cu that possibly originated from the sea water shows a negative loading. Therefore, RC3 can generally reflect changing marine and terrestrial influence on PN over time. According to these elemental trends a higher marine influence on the lagoon can be observed between 6200 and 4500 cal yr BP and also around 3250 cal yr BP. However, in general, the marine influence shows an overall decreasing trend with the time in PN according to the variation in RC3 scores (Fig. 4.6). Finally, in the PN core, high negative loadings of Ca and Sr observed in RC4 indicate biogenic carbonate deposition in the sediments. This is supported by the negative RC4 scores between ~ 4500 and 3000 cal yr BP that agree with the abundance of mollusc shells in the layer (between 90 and 37 cm) in the PN core (Fig. 4.6).

5.3 Sources of Organic Matter

Based on the *n*-alkane distributions at Bolgoda South Lake (BGSL) and Panama Lagoon (PN), both of these sites can be inferred as having two similar types of OM sources. The two clusters identified in both sites are characterized by predominantly even carbon numbered short-chain *n*-alkanes (*n*-C₁₆, C₁₈ and C₂₀) and odd carbon numbered long-chain *n*-alkanes (*n*-C₂₉, C₃₁ and C₃₃).

Bacterial Lipids

Predominance of even chain *n*-alkanes is not so common in the geosphere and, elsewhere, has been related to microbial degradation in inter-tidal hypersaline environments such as lagoons, estuaries, and bays (e.g.; Aghadadashi et al., 2017; Aloulou et al., 2010; Ekpo et al., 2005; Elias et al., 1997; Nishimura and Baker, 1986). In addition, such *n*-alkane distributions have also been found in carbonate (petroleum) source rock types (Peters et al., 2007), though this factor

is not relevant for the sites under consideration. It has been suggested that some reducing and halophilic bacteria such as *Desulfovibrio desulfuricans* and *Coryne bacterium* sp. produce even carbon-numbered short-chain *n*-alkanes. They are also responsible for the biodegradation of compounds dominant in marine algae, yielding predominance of even carbon-numbered short chain *n*-alkanes (Aghadadashi et al., 2017; Nishimura and Baker, 1986). Therefore, the dominant *n*-C₁₆, C₁₈ and C₂₀ alkanes could derive from autochthonous bacterial lipids, as a product of reductively-decaying algal mats in saline environments (Aghadadashi et al., 2017; Ekpo et al., 2005; Nishimura and Baker, 1986). It can be assumed that the origin and abundance of these bacterial lipids depends on the salinity of the water bodies that is, in turn, controlled by marine influence (sea water intrusion). Hence, the variation of their abundance can be used as a proxy to trace marine influence in coastal water bodies connected to the sea.

Terrestrial Plants

Odd carbon numbered predominant long-chain *n*-alkanes are derived from leaf waxes in terrestrial plants and represent the allochthonous fraction of sedimentary OM (Eglinton and Eglinton, 2008; Meyers, 2003). Variation in long-chain *n*-alkanes distributions can indicate different types of terrestrial plant matter that contributed to the OM pool in these sediments (Meyers, 1997). Generally, tropical grasses are dominated by long-chain *n*-alkanes that are C₃₁, C₃₃ and C₃₅. Meanwhile, woody plants are generally characterized by *n*-C₂₇, C₂₉ and C₃₁ alkanes (Bush and McInerney, 2013; Garcin et al., 2014; Gayantha et al., 2020; Meyers, 2003).

Based on this distribution of *n*-alkanes, it can be identified that Bolgoda South Lake (BGS�), from ~ 5700 to 3800 cal yr BP (cluster 2) is dominated by leaf wax *n*-alkanes whereas from ~ 3800 – 1500 cal yr BP period (cluster 1) it is dominated by bacterial lipids (Fig. 4.8(a)). By comparison, in the Panama Lagoon (PN), the period ~ 6400 – 3600 cal yr BP (cluster 2) is dominated by bacterial lipid *n*-alkanes whereas leaf wax *n*-alkanes dominate from 3600 cal yr BP to present (cluster 1) (Fig. 4.8(b)). According to the variation of PC1 scores in the PN core,

leaf wax *n*-alkanes content gradually increases relative to bacterial *n*-alkanes towards the core top (Fig.4.10). In BGSL, bacterial *n*-alkanes are abundant in the upper section of the core (cluster 1), with a dramatic increase of their abundance around 3800 cal yr BP, relative to lower section (cluster 2) (Fig.4.9).

The different OM sources and their change within the cores is also supported by CPI_T trends at BGSL and PN. CPI_T trends vary in line with PC1 trends at both sites (Fig.4.9 and 4.10). In BGSL, the odd-even *n*-alkane predominance of *n*-alkane weakens when moving core upward due to increasing the relative abundance of bacterial lipids. By contrast, at PN CPI_T increases core upwards indicating a relative decrease of bacterial lipids at the site near the present. These variations in OM source in BGSL and PN show that the marine influence in PN is, overall, generally higher than at BGSL that is also indicated by modern salinity measurements in the sites (Table. 4.1). Furthermore, in PN the marine influence gradually decreases overtime whereas at BGSL the marine influence increases between ca. 3800 and 1500 cal yr BP.

Mangrove

Taraxerol and β -amyirin are reliable proxies for the presence of mangrove vegetation surrounding a lake/lagoon (Gayantha et al., 2020; Ranjan et al., 2015). Both the BGSL and PN cores show a strong signal for taraxerol and β -amyirin throughout the core, implying the presence of mangrove vegetation around both sites during the whole period (Fig.4.9 and 4.10). Modern day vegetation cover observations show that PN is surrounded by a higher amount of mangrove vegetation relative to BGSL, something that also appears to have been the case in the past based on average values for taraxerol and β -amyirin in the cores. Notably, taraxerol and β -amyirin show a gradual core upward increasing trend in PN (Fig. 4.10) implying an increase of the mangrove vegetation around the lagoon (Englong et al., 2019). At BGSL, although there is overall less mangrove vegetation on average, a lack of variation in taraxerol

and β -amyrin relative to their core average suggests that the mangrove vegetation at this site may have been stable over time (Fig. 4.9).

Organic matter sources in Horton Plains

Three main OM sources can be identified in HP based on the *n*-alkane distributions in the PCA biplot (Fig. 4.8 (c)). *n*-C₂₃ and C₂₅, that negatively correlate with PC2, represent mosses (like *Sphagnum*) which generally live in cool and moist environments (Naafs et al., 2019). In addition, these mid-chain *n*-alkanes can also be biosynthesized by aquatic macrophytes (Ficken et al., 2000). It is difficult to distinguish between these two sources based on their *n*-alkane chain length distribution or isotopic signatures. However, given the present-day environment at HP, and the observation of abundant *Sphagnum* growing near the HP coring location, we can reasonably assume that the source of C₂₃ and C₂₅ *n*-alkanes are *Sphagnum* mosses for the remainder of the core. *n*-C₂₉ and C₂₇ alkanes that showed moderate negative correlations with both PC1 and PC2 (Fig.4.8(c)) and are most likely derived from woody plants. *n*-C₃₃ and C₃₁ alkanes, that show high positive correlations with PC2 (Fig.4.8(c)), are likely to be predominantly from grasses (graminoids) (Bush and McInerney, 2013; Rommerskirchen et al., 2006).

Clusters 1 and 2 in the HP core are characterized by grasses and mosses, respectively (Fig.4.8 (c)). Therefore, variation of PC2 scores in HP represent the variation in the relative proportions of mosses and grasses, and indicate a period ~ 1500 – 500 cal yr BP that is dominated by grasses in HP (Fig. 4.11). CPI values in HP also reflect a shift in vegetation (OM sources) rather than temperature-induced microbial degradation at this time. Generally, *Sphagnum*-dominated peat has higher CPI values (between 10 and 35), whereas graminoid- and woody angiosperm-dominated peat has relatively low values (between 5 and 15) (Naafs et

al., 2019). The low CPI values between 1500 – 500 cal yr BP supports the idea that grasses dominate the vegetation in the area during this time (Fig. 4.11).

In addition, bulk $\delta^{13}\text{C}$ variations reflect changing OM source conditions in the HP peat deposit, supporting the *n*-alkane trends. Relatively depleted $\delta^{13}\text{C}$ values (below -25.5‰) observed between ~ 5500 and 1900 cal yr BP possibly indicate moss- and woody plant-dominated peat, whereas enriched values (above -25.5‰) between 1900 cal yr BP and present reflect moss- and graminoid-dominated peat (Fig. 4.11).

The presence of sterols such as cholesterol, campesterol, stigmasterol and β -sitosterol can provide additional insights into input from higher plants and mosses (Ronkainen et al., 2014). Stanols are saturated counterparts of their respective sterols produced by microbial hydrogenation (Routh et al., 2014). Hence, the Σ stanol: Σ sterol ratio can be used to trace the degree of microbial degradation or humification in peat (Naafs et al., 2019; Routh et al., 2014). The Σ stanol: Σ sterol ratios in HP are very low (below 0.5) in the acrotelm (top-most 20 cm) that yielded modern ages (negative ^{14}C values). In the cattotelm (below 20 cm), the Σ stanol: Σ sterol ratio showed a downcore increasing trend that is normal for peat, indicating that microbial degradation increases over time (Fig. 4.11). TOC content also decreases downcore further supporting the post-diagenetic changes after deposition (Fig. 4.11).

5.4 Climate and Environmental Implications Inferred by ^{13}C and D Isotopes in Leaf Wax *n*-Alkane

It is possible to apply leaf wax *n*-alkane hydrogen isotopes together with *n*-alkane carbon isotopes to track changes in rainfall intensity/amount and related climate and environmental conditions in Sri Lanka – an approach applied successfully in regions worldwide (Günther et al., 2016; Jin et al., 2015; Sarkar et al., 2015; Strobel et al., 2019; Yamoah et al., 2016). Since the hydrogen isotopic fractionation in leaf waxes is controlled by several factors, in addition to

the source water isotopic signal, it is preferred to analyse leaf wax carbon isotopes together with hydrogen isotopes for palaeohydrological reconstructions.

In ecosystems where mixed C₃-C₄ vegetation is present with significantly high fraction of C₄ vegetation, such as in tropical African savannah, photosynthetic pathway (C₃ or C₄) and plant functional type become the major controlling factors towards leaf wax $\delta^{13}\text{C}$ and δD variations rather than precipitation changes (Garcin et al., 2014; Wang et al., 2013). However, unlike tropical African ecosystems, the C₄ vegetation is very low in Sri Lanka and dominated by C₃ vegetation due to high annual rainfall (Still et al., 2003). Hence, it can be safely ruled out the biological effects (i.e., changing photosynthetic pathway of vegetation and plant functional types) towards leaf wax δD and $\delta^{13}\text{C}$ variations in Sri Lanka. In this case, precipitation changes and soil water stress (aridity) become the first order factors that determine leaf wax hydrogen and carbon isotopic composition.

Leaf wax *n*-alkane (C₂₉, C₃₁ and C₃₃) $\delta^{13}\text{C}$ values vary between -37.4 ‰ and -28.0 ‰ in Bolgoda South Lake and -34.4 ‰ and -27.3 ‰ in Panama lagoon (Table. 4.5). The ranges of leaf wax *n*-alkane $\delta^{13}\text{C}$ values indicate that catchment vegetation in both the lowland dry and wet zones are dominated by C₃ vegetation over the last ~ 6000 yrs, similar to present day conditions.

Seasonal impacts (moisture source) of rainfall on H isotope fractionation in meteoric water is also reflected by leaf wax *n*-alkane (C₂₉ and C₃₃) δD values in BGSL and PN (Table. 4.5). Summer monsoon-fed BGSL showed relatively higher (enriched) average $\delta\text{D}_{\text{C}_{29}}$ and $\delta\text{D}_{\text{C}_{33}}$ values than the winter monsoon fed PN. In addition, the lowest average leaf wax δD values (most depleted) in HP relative to both BGSL and PN reflect the altitude effect towards rainfall in the central highlands. Considering the general gradient of the altitude effect for H isotopes (~ -1.5 ‰ /100 m ; Gat et al., 2000), and correction of the HP record on this basis to reveal the source water values, it is clear that HP (located at ~ 2500 m altitude) was mainly

influenced by summer monsoon rainfall rather than winter monsoon rainfall back then, as it is today.

Leaf wax *n*-alkane (*n*-C₂₉, C₃₁ and C₃₃) δD and $\delta^{13}C$ showed a core upward increasing trends in their values at BGSL, indicating a weakening of rainfall in the catchment and increasing aridity from ~ 6000 to ~ 1500 cal yr BP (Fig. 4.12). Relatively higher δD and $\delta^{13}C$ values deviated from the general trend between ca. 3800 and 3200 cal yr BP and suggest prevalence of drought-like conditions due to significant weakening of the summer monsoon rainfall (Fig. 4.12). In contrast at the PN site, leaf wax δD and $\delta^{13}C$ values showed a general core upward decreasing trend that indicate strengthening of the winter monsoon rainfall over the last ~ 6200 cal yr BP in the catchment (Fig.4.13). Deviating from this general trend relatively low $\delta D_{C_{33}}$ values can be observed ~ 4700 cal yr BP suggesting a short period of intense rainfall in the PN catchment. At both sites (BGSL and PN), $\delta D_{C_{33}}$ variations are more distinct relative to $\delta D_{C_{29}}$ and $\delta D_{C_{31}}$, possibly due to its predominant origin from grasses that are more abundant and sensitive to climate changes. Based on these trends, we suggest that *n*-C₃₃ alkanes are a better marker for indicating palaeo-precipitation and related climate signals in these tropical environments (e.g.; Gayantha et al., 2020).

Due to the geographical locality of the Horton Plains (HP), the area is influenced by both summer (SWM) and winter (NEM) monsoon rainfalls during the year, though major influence is from summer monsoon. Therefore, *n*-alkane δD records of HP might reflect both the amount effect and the seasonality effect of rainfall if there is no significant shift between vegetation types (C₃ vs C₄). This phenomenon makes interpretations challenging due to the overlapping signals may affect the interpretation of the signals. However, since the leaf wax ^{13}C fractionation is not dependant on source water isotopes but on soil moisture availability, we can compare leaf wax $\delta^{13}C$ and δD isotopic variation simultaneously to identify the seasonality effect on HP.

Horton Plains consists of two OM sources that are mosses (*Sphagnum*) and terrestrial higher plants that indicate palaeohydrological information. Mosses grow in wet environments with higher humidity and have no stomatal openings to control water loss unlike vascular plants. Therefore transpirative enrichment of H isotopes in mosses is relatively less than in vascular plants, meaning that they mainly reflect the isotopic signature of the available water source (Sachse et al., 2006). Therefore, δD values of mid chain *n*-alkanes derived from mosses can indicate rainfall variation and/or changes in moisture sources in the area. However, due to lack of stomatal openings in mosses, $\delta^{13}C_{n-C_{23}}$ and $\delta^{13}C_{n-C_{25}}$ do not indicate aridity in HP core. The sharp increase in $\delta^{13}C_{n-C_{23}}$ and $\delta^{13}C_{n-C_{25}}$ values appears between $\sim 350 - 150$ cal yr BP is probably due to a changing of the dominant OM source of these *n*-alkanes from mosses to grasses. This is confirmed based on the OM source information (see Fig. 4.11) and isotopic values of leaf wax *n*-C₃₃ alkanes (Fig. 4.14). Therefore, during this period $\delta D_{C_{23}}$ and $\delta D_{C_{25}}$ isotopic values might represent the palaeohydrological signal from grasses rather than mosses. Despite the overlapping signals, between $\sim 350 - 150$ cal yr BP, $\delta D_{C_{23}}$ and $\delta D_{C_{25}}$ values at HP indicate an increasing trend of their values towards the present. There is a distinct shift towards enriched δD values ~ 650 cal yr BP indicating a steady decline in rainfall and increasing aridity (Fig. 4.14).

Individual leaf wax *n*-alkane $\delta^{13}C$ values in the central highlands HP records do not indicate any major shifts implying dominant OM contribution persistently came from C₃ vegetation in the area (Table 4.5). However, leaf wax $\delta^{13}C$ and δD values only showed partial similarity to each other, possibly due to the confounding seasonality effect of rainfall source. Notably, the *n*-C₃₁ and C₃₃ alkane isotopic trends show inverse trends ~ 3500 cal yr BP and from ~ 800 cal yr BP to the present. During these periods while $\delta^{13}C$ indicates aridity based on the enriched values, the δD values are depleted due to enhanced relative contribution from the winter monsoon rainfall (due to decrease of summer monsoon rainfall) that consists of highly

depleted rainwater isotopes. Therefore, in HP, $\delta^{13}\text{C}_{n\text{-C}_{33}}$ seems like a promising proxy for tracing water stress/availability in the area. According to $\delta^{13}\text{C}_{n\text{-C}_{33}}$ variations in the HP (increasing trend of values with time), it indicates a steady increase in aridity at HP over the last 5500 cal yr BP. These trends also indicate that aridity increased ~ 3500 cal yr BP and between 1000 cal yr BP and the present. The arid event around 3500 cal yr BP in HP also coincides with the Bolgoda South Lake records implying this to be a more regional signal.

5.5 Marine Influence Inferred by ^{13}C and D Isotopes in bacterial lipids (*n*-alkane)

The even number short chain *n*-alkanes are considered as secondary products that originate in hypersaline environments (Aghadadashi et al., 2017). During biological reactions such as bacterial processes and photosynthesis, lighter isotopes are often enriched in the reaction product relative to the substrate (Hoefs, 2009). Therefore, variation of *n*-C₁₆ and *n*-C₁₈ alkane C and H isotope values can provide information on the rate of bacterial lipid synthesis in lacustrine sediments. Both $\delta^{13}\text{C}$ and δD isotopes of *n*-C₁₆ and C₁₈ alkanes show a core upward increasing trends in the PN core implying a decrease in bacterial lipid synthesis during the last 6200 cal yr BP (Fig. 4.13). This implies that the conditions became gradually more unfavourable for bacterial lipid synthesis due to increasing freshwater input (decreasing water salinity) coupled with higher rainfall in the catchment as inferred by leaf wax *n*-alkane D isotopes. It seems that while the marine influence in Panama lagoon was gradually decreasing from 6200 cal yr BP to the present there was a higher incidence of rainfall in the catchment.

In contrast, at BGSL *n*-C₁₆, C₁₈ alkane C and D isotopes do not show a clear trend except $\delta\text{D}_{\text{C}_{18}}$ which show lower values between $\sim 3500 - 1500$ cal yr BP. This trend indicates that there was little variation in bacterial lipid synthesis in BGSL due to relatively low salinity variation in the lake (Fig. 4.12).

5.6 Behaviour of Monsoon Rainfall and Environmental Impacts in Sri Lanka

The multiple proxies discussed above indicate a complex history of rainfall patterns and related environmental changes in the catchments. Below, we discuss and summarise the key changes inferred based on these proxies at each site to build a comprehensive picture of palaeoclimatic changes since the mid-Holocene.

Bolgoda South Lake

This summer (SW) monsoon fed lowland coastal brackish water lake demonstrated a depositional history spanning between ~ 5700 and 1500 cal yr BP. Leaf wax *n*-alkane hydrogen isotope variation (δD_{n-C33}), together with *n*-alkane carbon isotopes ($\delta^{13}C_{n-C33}$), indicate a general decreasing trend of rainfall (trending aridity) in the area during this time. However, positive excursions of δD_{n-C33} and $\delta^{13}C_{n-C33}$ values between 3800 and 3200 cal yr BP indicate a clear decline of SWM rainfall during this time (starting ~4000 cal yr BP) with peak aridity/drought occurring ~3500 cal yr BP in the lowland wet zone of Sri Lanka (Fig.5.1). High clay content (finer fraction) inferred by increases in Rb (negative RC1 scores) during this period further support the weakening of stream inflow and erosion in the catchment during this period (Fig. 5.1). The main OM sources, which are terrestrial leaf wax (LW) and marine bacterial lipids (BL), changed in line with this interpreted rainfall trend. Bacterial lipids increased rapidly in the lake starting ~3800 cal yr BP indicating higher levels of marine influence (sea water intrusion into the lake) with the decline of SWM rainfall in the catchment (Fig.5.1). Some increase of the rate of bacterial lipid synthesis can also be observed according to δD_{n-C18} variation after ~3500 cal yr BP that also indicate increased marine influence (Fig. 5.1). In addition, an increasing trend of Cu and Ni (negative RC3 scores) with time supports increasing sea water intrusion into BGSL (Fig. 5.1). The lowering of the lake water level, as inferred by

redox sensitive elements (Mn and Fe; positive RC2 scores), may have facilitated increased sea water intrusion to the lake system (Fig. 5.1).

Horton Plains

Central highlands located Horton Plains area is influenced by both SW and NE monsoon rainfall with a dominant impact from SW monsoon rainfall. Therefore, the HP peat deposit can archive mixed signals of both monsoonal precipitations. This high-altitude peat deposit revealed a depositional history of 5500 cal yr BP and indicated a general decreasing trend in rainfall according to leaf wax ($n\text{-C}_{33}$) and moss ($n\text{-C}_{23}$) n -alkane hydrogen isotope records (Fig.5.2). However, the weak SW monsoon period around 3500 cal yr BP identified in BGS L is not visible in Horton Plains according to δD records. Instead, a slight decrease of $\delta\text{D}_{n\text{-C}_{33}}$ and $\delta\text{D}_{n\text{-C}_{23}}$ can be observed at HP during this period (Fig. 5.2). This is probably due to a changing of the dominant moisture source in HP during this period. Since the summer monsoon rainfall was apparently weak around this time, the isotopically depleted winter monsoon rainfall might have briefly become the dominant source of rainfall to the area that brings relatively less amount of precipitation. Therefore, the vegetation (both moss and higher plants) δD values could show slightly depleted values around this time despite low amount of rainfall. Supporting this assumption, $\delta^{13}\text{C}_{n\text{-C}_{33}}$ showed enriched values ~ 3500 cal yr BP suggesting dry conditions in the area through a different mechanism that has no influence from the moisture source (eg; Gayantha et al., 2020). In addition, an inverse behaviour between $\delta\text{D}_{n\text{-C}_{33}}$ and $\delta^{13}\text{C}_{n\text{-C}_{33}}$ variation can be observed between ~ 975 and 120 cal yr BP whereby $\delta\text{D}_{n\text{-C}_{33}}$ values are decreasing, whereas $\delta^{13}\text{C}_{n\text{-C}_{33}}$ show an increasing trend. This observation suggests a decline of SW monsoon rainfall in the area leading to dry conditions during this period. Concurrent to this, there seems to have been an increase in grasses in the catchment that can withstand the dry climate conditions (Fig. 5.2). Peak aridity can be identified $\sim 350 - 150$ cal yr BP. Given

the HP location in the centre of the island, these observations can be abstracted to suggest that many parts of the island went through a water shortage during this period as a result of the radial drainage pattern starting from the central highlands.

Panama lagoon

Panama lagoon is a winter (NE) monsoon fed coastal water body in the dry zone of Sri Lanka that directly connects with the Indian Ocean. During its depositional history of ~6200 cal yr BP, the NE monsoon rainfall shows a generally increasing trend over the time, in contrast to Bolgoda South Lake and Horton Plains as inferred by δD_{n-C33} with $\delta^{13}C_{n-C33}$ signals (Fig. 5.3). However, the increasing trend of NE monsoon rainfall seems a more gradual when compared to the decreasing SW monsoon rainfall trend inferred at BGSL. Concurrent to the rainfall trend, the abundance of bacterial lipids gradually decreased (and leaf waxes increased) indicating a decreasing marine influence with increasing freshwater input to the lagoon due to high rainfall in the catchment (Fig. 5.3). This is also supported by the decreasing trend of the rate of the bacterial lipid synthesis as inferred by δD_{n-C18} and $\delta^{13}C_{n-C18}$ variations (Fig. 5.3). In addition, the period between ca. 6200 and 4500 cal yr BP is characterised by noticeably high clay content and an abundance of elements derived from clay minerals such as Al and Fe (positive RC1 scores; Fig. 5.3). However, the rainfall is not notably low during this period compared to the rest of the time in the PN core according to leaf wax hydrogen isotopes values. Therefore, it is probably a period with a sea level high stand that diminished the energy of stream water discharge into the lagoon. Concurrent to this, an increase of Cu (negative RC3 scores) can also be observed during this period. Other studies of geological features have documented a sea level high stand around this period in Sri Lanka that further supports this interpretation (Katupotha, 1995; Ranasinghe et al., 2013; Weerakkody, 1992). Water level changes in the

lagoon do not seem significant according to RC2 variation, probably due to its direct connection and close proximity to the Indian Ocean (Fig. 5.3).

Overall, climate and environmental proxy trends in BGSL and HP revealed a general weakening trend in the rainfall amount in their catchments. In contrast, the trends in PN showed general strengthening of rainfall in its catchment over the last ~ 6000 yrs. This implies that summer or SW monsoon fed lowland and highland wet zones in Sri Lanka are characterized by general weakening trend of their rainfall during this period. Winter or NE monsoon which fed the lowland dry zone indicates an increasing trend in precipitation.

The multi-proxy results indicate that there is millennial or sub-millennial scale inverse relationship between summer and winter monsoon (SW and NE monsoon) during mid- to late Holocene period. That said, there are some deviations from this general trend in the form of a few centennial scale failures of SW monsoon rainfall (e.g.; 3800 – 3200 cal yr BP and 350 – 120 cal yr BP) are also evident in the BGSL and HP records.

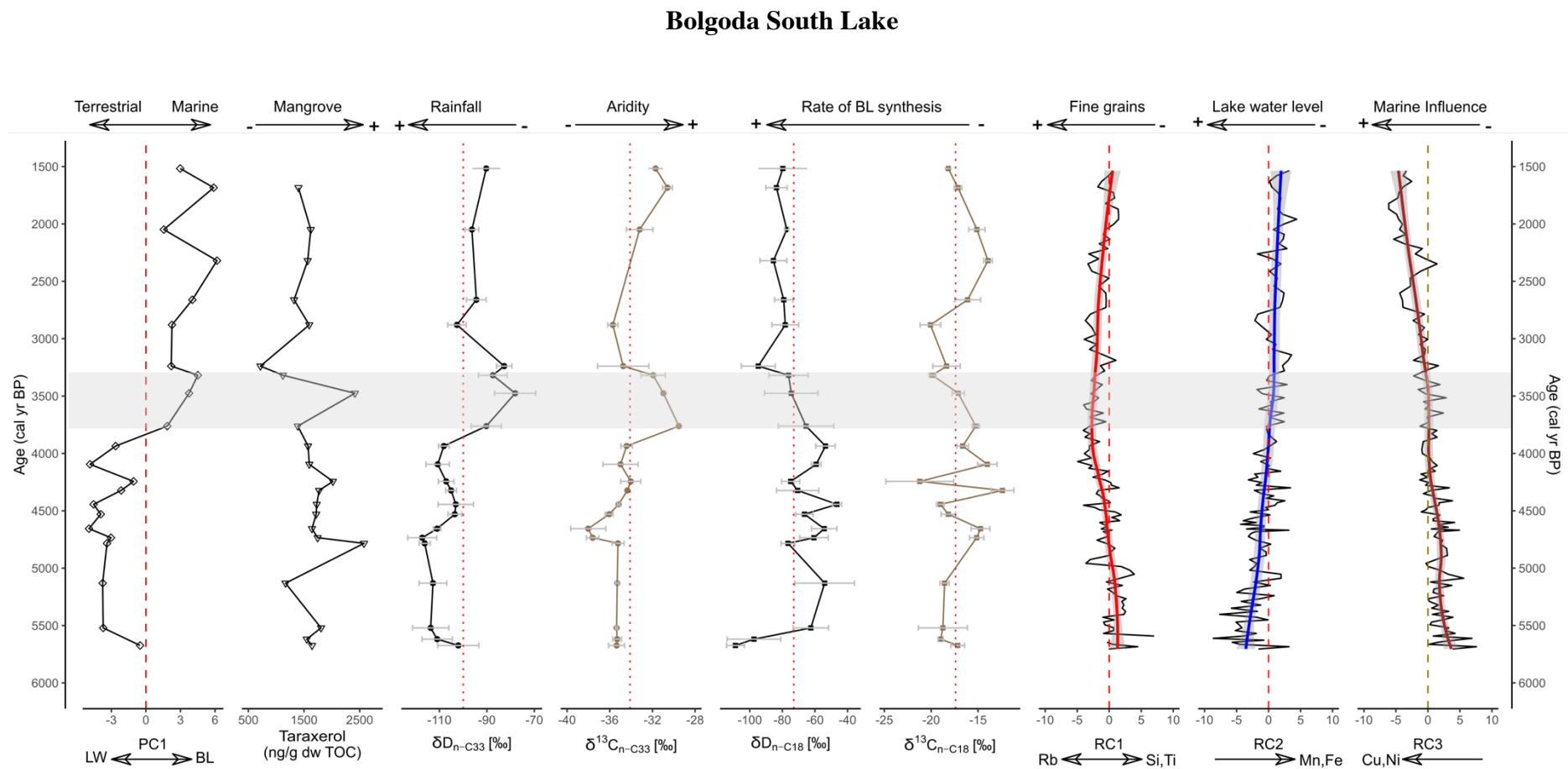


Fig.5.1. Selected multi-proxy trends and their climate and environmental implications in Bolgoda South Lake, Sri Lanka.

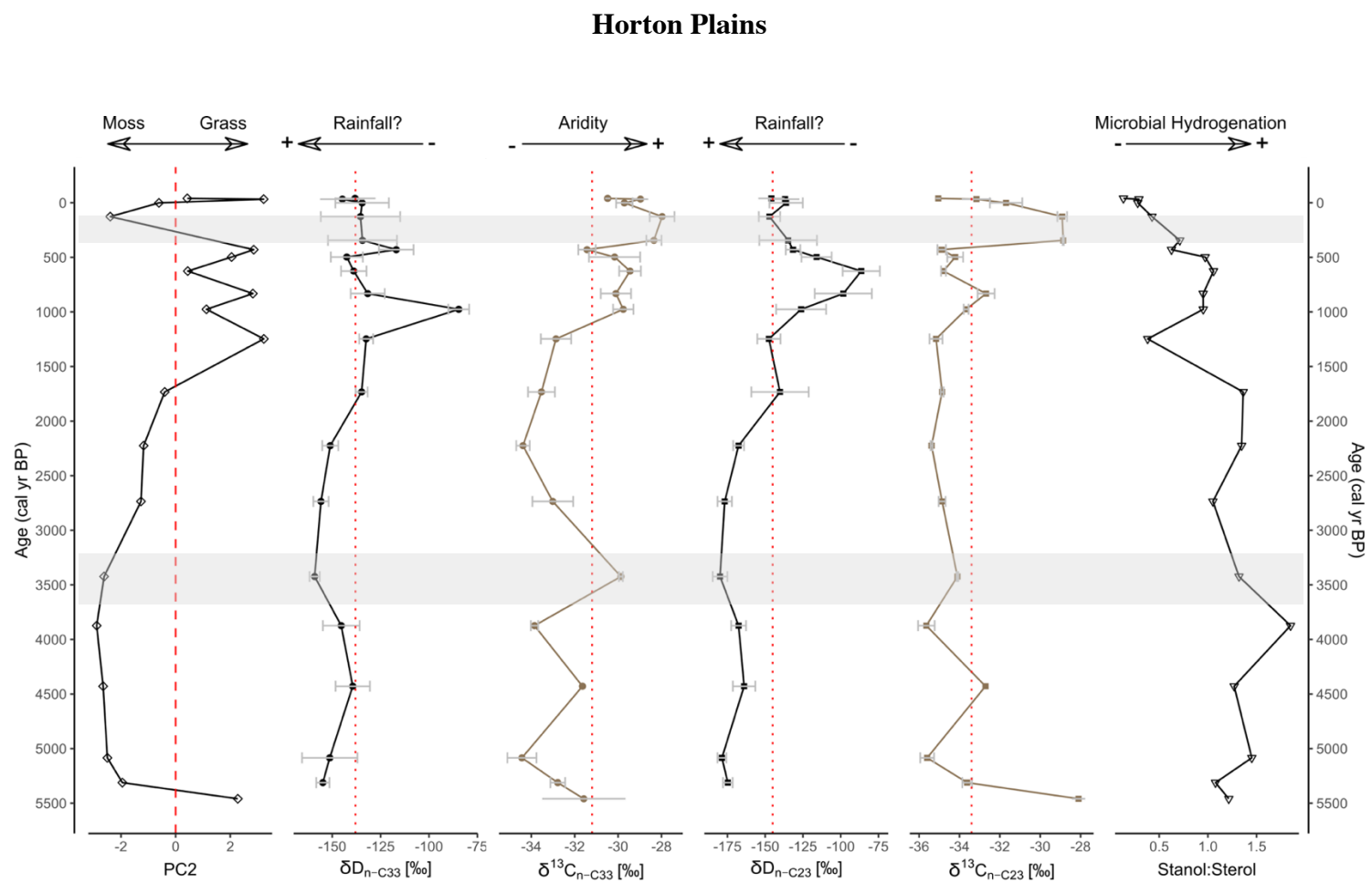


Fig.5.2. Selected multi-proxy trends and their climate and environmental implications in Horton Plains, Sri Lanka

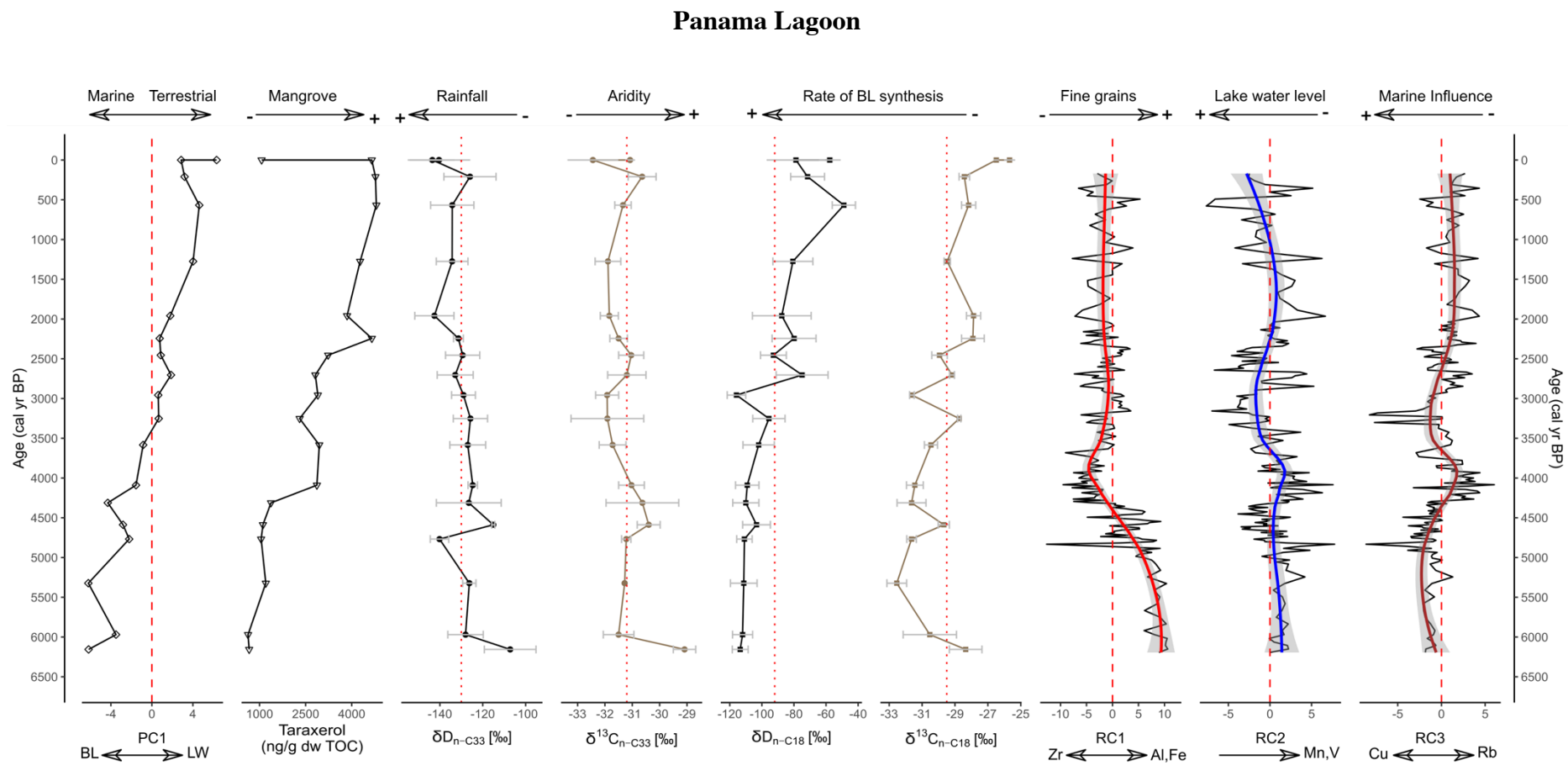


Fig.5.3. Selected multi-proxy trends and their climate and environmental implications in Panama Lagoon, Sri Lanka.

5.7 Regional Comparison of Palaeo-monsoonal Records

Many palaeoclimate records available in Sri Lanka and India imply a general weakening trend of the Indian summer monsoon during the middle and late Holocene period (Ankit et al., 2017; Basavaiah et al., 2015; Gayantha et al., 2020, 2017; Leipe et al., 2014; Ponton et al., 2012; Prasad et al., 2014b, 1997; Premathilake and Risberg, 2003; Ratnayake et al., 2017, see Fig. 5.4). The notable exception to this trend can be observed in the records from the South Indian peninsular region which imply a progressive or stepwise increase in rainfall and/ fluctuation in its intensity in some cases (Rajmanickam et al., 2017; Sandeep et al., 2017; Veena et al., 2014, see Fig. 5.4). However, these regions in South India receive a significant amount of rainfall from the NEM (winter monsoon; between 17 and 49%) in addition to SWM (summer monsoon) rainfall (Sreekala et al., 2012). As well, the proxies used to reconstruct monsoon variability in these studies are unable to distinguish between the source of the monsoon rainfall (SWM or NEM). Regional records for winter monsoon rainfall variation are extremely limited. Some only cover the Late Holocene while others fail to identify a clear trend. Nevertheless, in general, the available records show increasing winter monsoon rainfall towards the present (Böll et al., 2014; Mishra et al., 2019; Ranasinghe et al., 2013; see Fig. 5.4). We compared the summer and winter monsoon records separately in Sri Lanka and the Indian subcontinent (regional) with our study to infer the variability in regional monsoon trends. Further, we selected palaeoclimate records consisting of age models with more than three reliable ^{14}C dates to provide better certainty in the overall interpretation of these changes. The overall trend in these regional studies is consistent with our observations in three sites along an EW transect across Sri Lanka and further detailed below.

The rapid drop of summer monsoon rainfall starts ~ 4000 cal yr BP, and subsequent peak aridity occurs between ~ 3700 and 3500 cal yr BP (according to the Bolgoda South Lake and Horton Plains records; Fig. 5.1), are likely correlated with the arid phase that has been

recognized globally around 4200 cal yr BP (4.2 kyr event; end of middle Holocene) resulting severe and prolonged droughts across various portions of Asia roughly between 3500 and 4500 cal yr BP. This arid phase has been argued to have stimulated human migration and the collapse of some ancient urban societies, such as the Early Bronze Age Harappan civilization in northwestern India and southeastern Pakistan (Berkelhammer et al., 2012; Dutt et al., 2018; Staubwasser and Weiss, 2006). In the Horton Plains, this arid period is visible only in leaf wax carbon isotope values due to the shift of the dominant moisture source from SW to NE monsoon during this period (Fig. 5.2). Meanwhile, in Panama Lagoon, where the catchment is fed by winter monsoon rainfall, there is no sign of a dry or wet event around this time but rather stable rainfall conditions (between 4500 – 3500 cal yr BP; Fig. 5.3), highlighting the fact that the 4.2 ka event was most manifest in SWM-influenced regions, such as the BGSL record. This further indicates the importance of the development of local records in order to determine the material impacts of supposedly ‘global’ climate events on different environments and systems.

The last millennium is marked by globally alternating cold and warm events (MWP; ~ 1000 cal yr BP, LIA; ~ 500 cal yr BP, CWP; ~ 0 cal yr BP), though their age boundaries, and impacts on different regions, are not so certain yet. Generally, the ISM is weak during cold periods such as LIA and strong during warm periods such as MWP (Gupta et al., 2020). Consistent with this, an intense period of maximum aridity can be observed in the Horton Plains leaf wax carbon isotope records roughly between 350 and 120 cal yr BP (Fig. 5.2) that is broadly contemporaneous with the Little Ice Age (LIA) when weak ISM or dry climate conditions have been observed in the Indian sub-continent (Agnihotri et al., 2002; Banerji et al., 2020). The alternating trend of $\delta^{13}\text{C}_{\text{n-C}_{33}}$ values in the Horton Plains probably reflect these weak and strong summer monsoon periods during the last 1000 yrs.

There is, however, no evidence for this period from wet zone lowland (Bolgoda South Lake) due to lack of suitable depositional records during this time (hiatus; Fig. 5.4). In Panama

lagoon, the weakening of rainfall and some aridity is visible around 200 cal yr BP according to leaf wax isotope records concurrent to this event (Fig. 5.3). However, the resolution of the isotopic records is low around this period and caution is recommended in overinterpreting these geochemical trends.

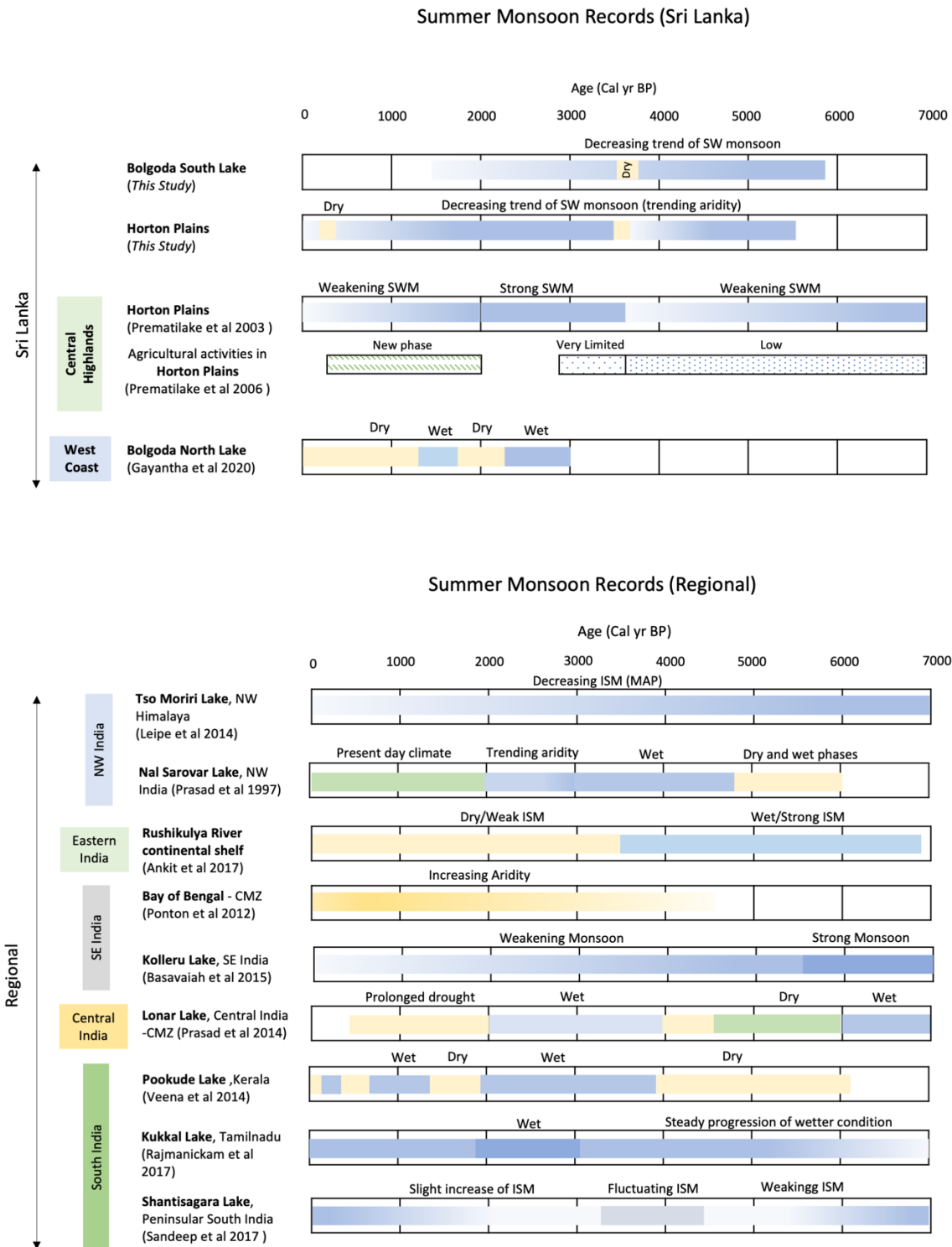


Fig. 5.4 Selected palaeoclimate records in the region (a) Summer (SW) monsoon and climate records from Sri Lanka (including pre-historic agricultural activities in Horton Plains). (b) Regional summer monsoonal and climate records during the middle and late Holocene.

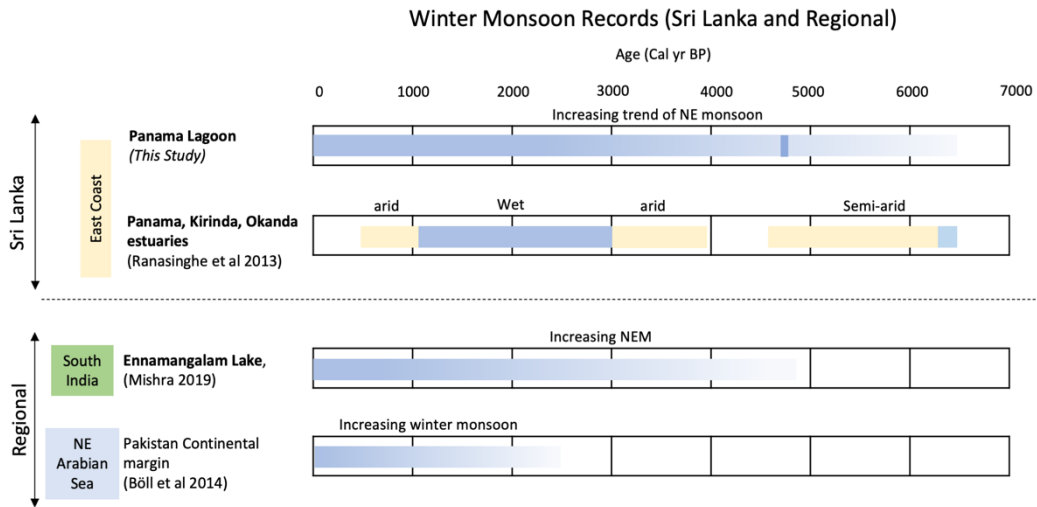


Fig. 5.4 (cont.) Selected palaeoclimate records in the region (c) Winter (NE) monsoon and climate records



Fig. 5.5 Locations of palaeoclimate records mentioned in the Fig. 5.4. (white labels denote summer monsoon records and green labels denote winter monsoon records according to published studies). (Source: Google Earth)

5.8 The Influence of Climate Forcing Factors on Monsoon Variability in Sri Lanka

Various forcing factors directly and indirectly influence the South Asian monsoon system and subsequent rainfall variability as suggested by present-day instrumental records and palaeoclimate records in the region (Banerji et al., 2020; Gupta et al., 2020). Orbital forcing-controlled solar insolation variability causes variations in the interhemispheric thermal contrast, resulting in the expansion or melting of ice sheets in the high latitudes, changing land-sea temperature gradients, and the migration of the mean latitudinal position of the ITCZ. These factors directly influence the intensity, total amount, and duration of monsoonal rainfall (Gupta et al., 2020; Schneider et al., 2014). Notably, solar insolation in the northern and southern hemispheres show an inverse variation during the Holocene relative to the Earth's precession cycle. As a result, the Northern hemisphere solar insolation is gradually decreasing while the Southern hemisphere insolation is increasing during this time period (Fig. 5.6). This is the key driving force of the migration of the mean latitudinal position of the ITCZ/ equatorial trough towards the relatively warmer Southern hemisphere. As a result, the ITCZ moved less far in a northerly direction during the boreal summer and further southward during the boreal winter (Fig. 5.6). This mechanism has been proposed by several researchers for explaining the weakening of summer monsoon rainfall in the Northern hemisphere during the middle to late Holocene period (Fleitmann et al., 2003; Haug, 2001).

Due to its geographical location on the seasonal ITCZ migration path, the hypothesized influence of the southward migration of the mean position of ITCZ on changing durations/lengths of monsoonal seasons can be tested separately for both summer and winter monsoon rainfall in Sri Lanka. In theory, southward migration of the mean position of the ITCZ during the mid and late Holocene would lead to decreases in the length of the summer monsoon season in Sri Lanka, decreasing the amount of summer monsoon rainfall in the wet zone. Meanwhile, the length of winter monsoon season would increase in Sri Lanka, leading to an

increased amount of winter monsoon rainfall in the dry zone (Fig. 5.7). In addition, decreasing Northern hemisphere solar insolation can result in a weakening of the land sea thermal contrast that causes a further weakening of ISM rainfall intensity (Schneider et al., 2014). As can be seen in the reconstructed rainfall variations in this study (Fig.5.6), the amount of summer monsoon rainfall in the wet zone is decreasing whilst the amount of winter monsoon rainfall is increasing in the dry zone of Sri Lanka during the mid to late Holocene, indicating a sub-millennial scale inverse relationship between summer and winter monsoons and supporting the above hypothesis.

In addition to insolation and ITCZ-related processes, other possible mechanisms affecting the observed rainfall variations have also been suggested. An increased ENSO frequency during the Late Holocene, in contrast to the mid-Holocene (Conroy et al., 2008; Moy et al., 2002), may have significantly influenced the weakening of summer monsoon rainfall during the Holocene (Fig. 5.6). Generally, El Niño conditions in the Pacific Ocean cause the failure of Indian summer monsoon rainfall and results in drought conditions in South Asia including Sri Lanka (Kumar et al., 2006; Rasmusson and Carpenter, 1983; Sinha et al., 2011; Zubair et al., 2007). In addition, a positive correlation has been identified between El Niño and the second inter monsoon (SIM) rainfall (October – November) in Sri Lanka (Hapuarachchi and Jayawardena, 2015; Kane, 1998; Malmgren et al., 2003). Therefore, increasing El Niño frequency during the Late Holocene could have diminished the summer monsoon rainfall in Sri Lanka while bringing enhanced SIM rainfall that is a significant part of the dry zone water budget. This phenomenon can also further influence the inverse relationship between summer and winter monsoon rainfalls in Sri Lanka. Increasing the El Niño frequency can further drag the ITCZ southward, as observed during the LIA, that again causes a weakening of the Indian summer monsoon rainfall (Banerji et al., 2019; Brown and Johnson, 2005). However, according to the reconstructed ENSO records (Conroy et al., 2008; Moy et al., 2002), there is

a more abrupt increase in the frequency of El Niño from middle to late Holocene rather than gradual variation. In addition, during the last ~ 1000 yrs BP, it shows a decreasing trend (Fig. 5.6). Therefore, it is obvious that increasing El Niño frequency could only have a partial influence on the observed inverse rainfall trends between the South Asian summer and winter monsoon.

Despite the millennial or sub-millennial scale general inverse trend observed between summer and winter monsoon rainfall in Sri Lanka, summer monsoon rainfall showed additional centennial or multi-centennial scale shifts in contrast to the patterns seen for winter monsoon rainfall (Fig. 5.6). In fact, variation in winter monsoon rainfall seems to generally show a much smoother trend than summer monsoon rainfall. The equatorial trough or ITCZ is not identical when it is over the oceans and continents. Some scientists are against calling it the 'ITCZ' over the continents because the ITCZ and the region of maximum rainfall can be decoupled over the continents (Nicholson, 2018, 2009). Therefore, surface processes can also impact when the land equatorial trough (also called land ITCZ or continental tropical convergence zone; CTCZ) is over the Indian sub-continent (Gadil, 2018) and its teleconnection with other modes of climate variables (eg; ENSO, IOD, NAO) that can result in different impacts on summer and winter monsoon rainfalls in the region.

Firstly, the clear arid phase identified in this study ~ 3500 cal yr BP coincides with a sharp negative excursion of the NAO index (Olsen et al., 2012) and also shows a partial overlap with Bond event number 2 (Fig. 5.6). A negative NAO results in cold winters in northern Europe, causing expanding ice sheets and increased snow cover over Eurasia. Similarly, Bond events represent North Atlantic ice rafting events related to cold periods in the Northern subpolar regions. These conditions lead to failures in the development of a low pressure trough in northern and central parts of India, reducing South Asian summer monsoon rainfall over the Indian sub-continent (Bamzai and Shukla, 1999; Gupta et al., 2020). Therefore, I postulate that

this extreme arid event (~ 3500 cal yr BP) may have been primarily influenced by the negative NAO index. The second arid phase observed between ca. 120 – 350 cal yr BP is clearly visible in the Horton Plains records but also identified in Panama lagoon records as a decrease in winter monsoon rainfall. A sharp negative excursion of NAO index together with Bond event 0 broadly coincide with this event (Fig.5.6). Though the decrease of summer monsoon rainfall can be explained by this extreme NAO and further southward migration of ITCZ (Fig.5.6), the cause for the decrease of winter monsoon rainfall is not clear. Significant decline in El Niño frequency may explain the winter monsoon failure because generally El Niño and winter monsoon rainfall (especially SIM in Sri Lanka) show a positive correlation (Kane, 1998; Malmgren et al., 2003). Another possibility is the influence of Indian Ocean Dipole (IOD) on winter monsoon rainfall, but reconstructed IOD data are still not available in the region for comparison.

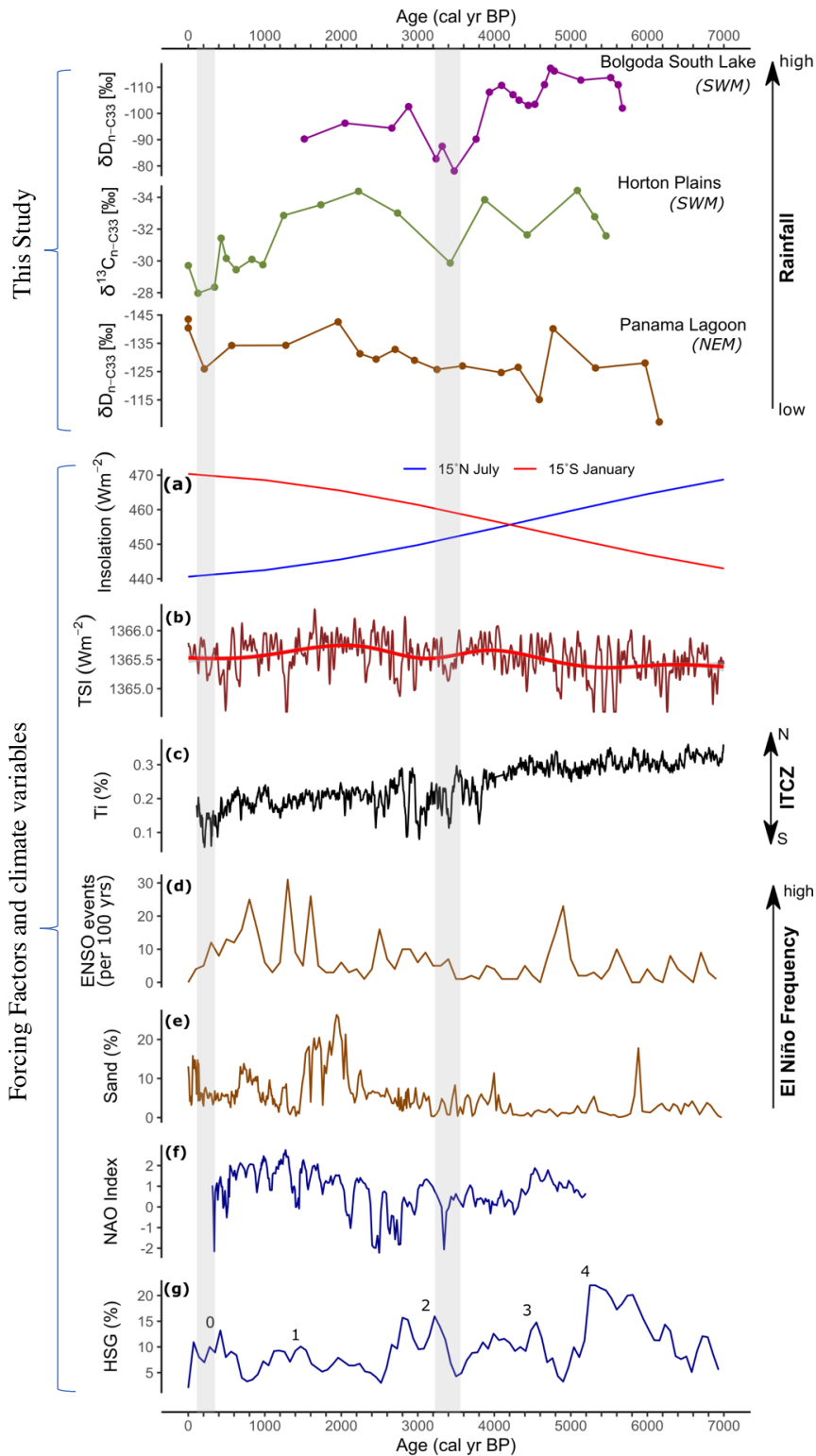


Fig. 5.6 Comparison of reconstructed monsoonal variations in Sri Lanka with different forcing factors/modes of climate variables during last 7000 years. Two grey bars represent the arid phases (a) Solar Insolation (Berger and Loutre, 1994), (b) Total Solar Irradiance (TSI) (Steinhilber et al., 2019), (c) Ti Content of Cariaco Basin sediments (Haug et al., 2002), (d) Number of ENSO events per 100 yrs (Moy et al., 2002), (e) Percentage of sand in El Junco Lake, Galápagos (Conroy et al., 2008), (f) Reconstructed North Atlantic Oscillation Index (Olsen et al., 2012), (g) Hematite-Stained Grains (HSG) percentage in North Atlantic deep-sea sediment and Bond events (Bond et al., 2001)

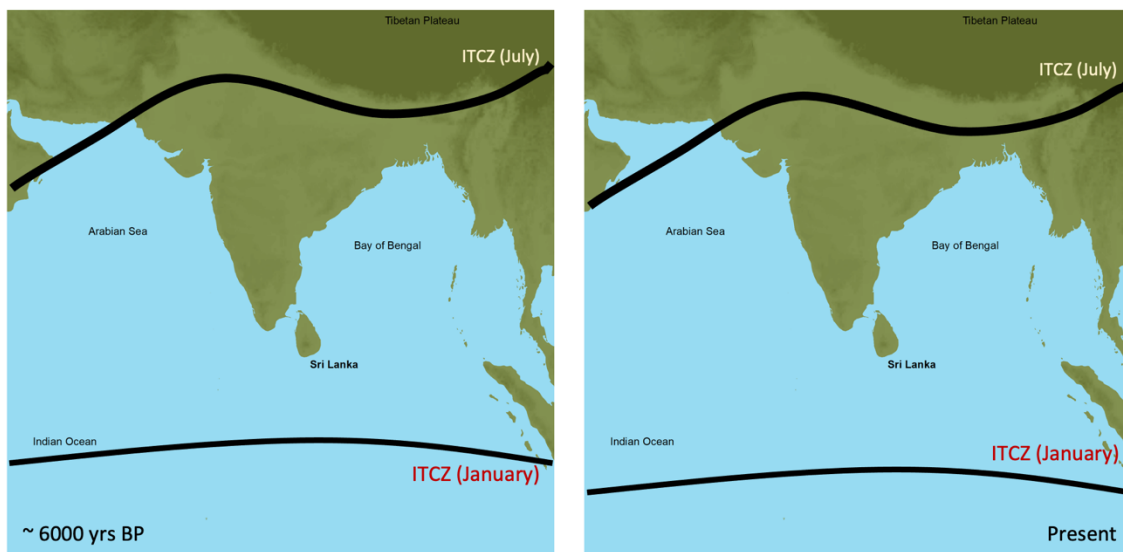


Fig. 5.7 Schematic illustration of the southward migration of mean position of ITCZ over last ~ 6000 yrs. As a result, length (duration) of the SWM season decreases where NEM increases in Sri Lanka (Source of shape file: <https://www.naturalearthdata.com/>)

5.9 Mid-Late Holocene Climate-Cultural Impacts in Sri Lanka

Though well-established archaeological records are available for prehistoric human settlements in Sri Lanka during the late Pleistocene (eg; Deraniyagala, 1989; Roberts et al., 2015; Wedage et al., 2019), there is a paucity of records between the mid-Holocene and the historic period with which to understand human adaptations around the island at this time. A palynological analysis in Horton Plains by Premathilake (2006) suggested prehistoric cultivation activities started in the Horton Plains ~17500 cal yr BP and decreased between 8000 and 3600 cal yr BP coinciding with decreasing SWM rainfall, though these interpretations remain heavily disputed. The period between 3600 and 2900 cal yr BP is characterised by very limited human presence followed by a renewed phase of agriculture between 2000 – 150 cal yr BP (Fig. 5.4 (a)). Our records suggest that a drastic decrease of SWM rainfall around 3500 cal yr BP could have impacted human behaviour although the relatively mesic conditions in the HP mean that changes would likely have been subtle. Further aridity after 0.15 cal kyr BP, may have further

influenced human populations in the region, though the impact of British colonial plantations and hunting is likely to have played a more dominant role (Premathilake, 2012).

By contrast, the arid northern lowland dry zone may have been more prone to changes in rainfall. Here, prehistoric farming activities seem to have been forced to relocate around 2900 cal yr BP (Deraniyagala, 1989; Myrdal-Runebjer, 1996). More stable and increasing NE monsoon rainfall may have initially attracted prehistoric and early historical agriculture to dry zone lowland areas. The kingdoms of Anuradhapura and Polonnaruwa survived until ~ 800 cal yr BP with sophisticated hydraulic technology in the lowland dry zone (Abeywardana et al., 2019; Bebermeier et al., 2017; Jayasena et al., 2011). However, the ancient kingdoms started to migrate towards the southwest and central highland areas (towards the wet zone through the intermediate zones) after that, with invasions and failure in the hydraulic systems both being postulated as potential drivers. Unfortunately, our NEM records are not of sufficient resolution to clearly understand the influence of rainfall on the abandonment of ancient kingdoms in the dry zone during this period (see Lucero et al., 2015), necessitating further work. That said, we can reasonably assume that SWM rainfall in Sri Lanka has been decreasing continuously until present in the lowland wet zone (similar to highland wet zone) due to the key influence of orbital forcing factors. Therefore, this weakening SWM rainfall might have led to a decline in rainforest density (shrinking of the rainforest areas) in the wet zone of Sri Lanka, turning the southwestern areas of Sri Lanka into landscapes more suitable for human settlements and agricultural activities than before (Lucero et al., 2015).

6. Conclusions

This multi-proxy palaeoclimate and palaeoenvironmental investigation revealed an inverse relationship between summer monsoon (Southwest Monsoon; SWM) and winter monsoon (Northeast Monsoon; NEM) rainfall in Sri Lanka during the last ~ 6000 cal yr BP. According to the different physical and chemical proxies, a decreasing trend of summer monsoon rainfall can be identified in the lowland and highland wet zones of Sri Lanka. In contrast, the winter monsoon showed an increasing trend during this period in the dry zone of Sri Lanka. As a result of this change, the average rainfall in the wet zone is decreasing while it is increasing in the dry zone. However, the average trend in rainfall across the whole island was also generally decreasing over the last ~ 6000 years because the winter monsoon rainfall brings less rainfall. According to current knowledge of the South Asian Monsoon system, it can be concluded that this inverse relationship between summer and winter monsoon rainfall during the mid-late Holocene period is mainly governed by the southward migration of the mean latitudinal position of the ITCZ/ equatorial trough driven by decreasing Northern hemisphere solar insolation that is mainly controlled by the Earth's precession cycle. Additionally, increasing frequency of El Niño events from the middle to late Holocene may have had at least a partial influence on this phenomenon.

In addition to these general trends of summer and winter monsoon rainfall, centennial or multi-centennial scale deterioration of summer monsoon rainfall can also be identified based on our proxy records. The first phase started ca. 4000 cal yr BP, leading to peak aridity ca. 3500 cal yr BP that is clearly evident in the Bolgoda South Lake record. The second phase showed aridity between ca. 350 – 120 cal yr BP that is evident in the Horton Plains record. The first arid phase correlates with globally widespread dry climate conditions recorded between 3500 and 4500 cal yr BP related to the 4.2 kyr event. The second arid phase partially correlates

with the LIA that led to failures in summer monsoon rainfall over the Indian sub-continent and severe droughts. Both of these arid phases observed in the records correlate with sharp negative excursions of the NAO index and also, at least partially, with Bond events (North Atlantic cooling events with expansion of polar ice sheets). Therefore, it can be concluded that extreme conditions in the NAO have played a significant role in South Asian summer monsoon failures leading to abrupt arid climate changes in the region. Other regional records also support this interpretation. All in all, our records further demonstrate that the South Asian monsoon system is complex, and the millennial or sub millennial scale changes are controlled by orbital forcing factors whereas the centennial and multi-centennial scale changes or abrupt events are likely governed by interactions with other climate variables such as NAO.

The multi-proxy data also revealed information about the changing marine influence in the coastal water bodies analysed during the last ~ 6000 yr BP. Marine influence refers to the intrusion of excessive sea water into coastal water bodies as a result of decreasing stream discharge to the coastal lake/lagoon or a marine transgression period (sea level high stand). In Bolgoda South Lake it can be seen that sea water intrusion (marine influence) is solely controlled by the variation of stream discharge governed by catchment rainfall. However, in the Panama lagoon, located on the east coast with a direct connection to the Indian Ocean, there is evidence for a period with high sea level (marine transgression) between ~6200 and 4500 cal yr BP. This is not evident in the Bolgoda South Lake probably due to its geomorphological setting and its indirect connection to the Indian Ocean through a narrow opening. However, for the remaining documented period at Panama lagoon, marine influence was also controlled by the catchment rainfall via the amount of stream discharge into the lagoon.

I applied compound-specific hydrogen isotope analysis as a means of palaeohydrological reconstruction in tropical coastal and high-altitude environments in Sri Lanka. Our data suggest that *n*-C₃₃ alkanes (tritriacontane) are the most suitable and promising

leaf wax *n*-alkanes to trace hydrological changes in the catchment via compound-specific isotope analysis in tropical environments like Sri Lanka. The variability of its signals is higher than other leaf wax *n*-alkane to identify clear trend/variation possibly due to its specific origin from tropical grasses that are more sensitive to soil water exchange in contrast to woody plants. However, applying leaf wax *n*-alkane hydrogen isotopes (δD_{wax}) alone to the reconstruction of precipitation changes in the Horton Plains was problematic due to two possible different moisture sources for the rainfall (summer vs winter monsoons) that have distinct water isotopic values.

Human societies across the island were also likely influenced by the observed inverse behaviour between summer and winter monsoon rainfall. According to the available archaeological records, agricultural systems developing in the northern Dry Zone from 2900 cal yr BP may have been linked to overall increasing NEM and decreasing SWM rains at this time. Meanwhile, from 1000 cal yr BP, a decrease in overall rainfall, may have resulted in the shift of the political centre of the island back towards the southwestern lowlands as drier conditions and contracting rainforests may have facilitated more widespread agriculture. Nevertheless, more records are required, in direct association with major archaeological sites, such as Anuradhapura, Polonnaruwa, and Kandy, to truly test these hypotheses.

Limitations of the study and future research

Despite this study revealing a broad range of palaeoclimate and palaeoenvironmental information along an EW transect in Sri Lanka, several limitations have been identified. It is clear that the impact of some forcing factors and climate variables such as solar forcing, ENSO, IOD and NAO on the South Asian Monsoon system can be decadal to multi-centennial scale in many cases. Therefore, it is difficult to compare our 'coarse' reconstructed monsoonal records with these factors, limiting more comprehensive understanding with regards to the

exact influences of these forcing factors and climate variables on the South Asian monsoon system.

In addition, the records analysed in this study only cover the Late Holocene and part of the Mid-Holocene. In Bolgoda South Lake core, there is a hiatus between the present and ~ 1500 cal yr BP (perhaps a washout of the sedimentary record as a result of the 2004 tsunami), resulting in missing information about wet zone lowland climate and environment during this period. The relatively narrow depositional histories of the available sediment cores limit our understanding about the behaviour of the monsoon system during the Holocene epoch that could provide more detailed information for understanding ITCZ dynamics and the impacts of SAM on perceived climate-culture links. The fact that we did not reach the maximum depth of deposits at BGSL and HP suggests that they hold much promise for developing extended records if cored using different techniques in the future.

In terms of, what is known about past human societies in Sri Lanka, the period between 2500 cal yr BP and present is significant for the emergence of agricultural adaptations and urban settlements in different parts of the island. However, our records are not at a sufficient resolution to precisely compare reconstructed climate variabilities with cultural changes during this period. Moreover, these study sites are not proximate to areas where major urban centres, such as Anuradhapura and Polonnaruwa, with their sophisticated water management systems, were located. We were also not able to detect any human specific biomarkers such as coprostanol in these sites (except on the surface layers), implying the sites are isolated from early/ historical human settlements. Deep drilling in selected sites closer to areas of past human settlements might provide a broader range information about climate-culture interactions during the ancient times in Sri Lanka and how ancient water management technologies adapted to varying climate conditions and increasing populations. This is something that is a major priority for future work (see Gilliland et al., 2013; Lucero et al., 2015).

Summary

The South Asian Monsoon is a critical climate phenomenon for the large portion of the world's population that lives in the Indian sub-continent, and it directly influences socio-economic and agricultural activities in the region. However, predicting the nature of monsoonal changes and related extreme events is highly challenging for climate scientists who are reliant on instrumental records that are available only for the last few decades. Therefore, palaeoclimate records are essential to understand the long-term variability in, and mechanisms behind, the functioning of the tropical monsoon system in the region. There has also been a significant knowledge gap specific to the South Asian monsoon system due to a scarcity of winter monsoonal records, high heterogeneity of palaeoclimate records in the region, and difficulties associated with comparing marine and terrestrial records to trace rainfall variability.

In order to fill some of these knowledge gaps, this study reconstructed the summer monsoon (southwest monsoon; SWM) and winter monsoon (northeast monsoon; NEM) rainfall variability in Sri Lanka and its related environmental and cultural influences on the island during the last ~ 6000 years. Being a tropical island located in a central region of the seasonal migration path of the Inter-Tropical Convergence Zone (ITCZ), Sri Lanka is influenced by summer (SWM), winter (NEM) and inter-monsoonal rainfalls throughout the year. The two main rainy seasons, summer (long duration) and winter (short duration) monsoon have a clear spatial distribution over the island due to the central highlands (max altitude ~ 2500 m) that act as an orographic barrier to these seasonal winds. Taking advantage of this unique geographical location and geomorphological setting, I retrieved two sediment cores from summer monsoon rainfall fed Bolgoda South Lake and winter monsoon rainfall dominant Panama Lagoon, respectively. I also retrieved a high-altitude peat core from the Horton Plains where both summer and winter monsoon rainfall occur. I applied compound-specific hydrogen and carbon isotope measurements of individual *n*-alkanes to sediment/peat records to reconstruct

palaeohydrological changes, together with diagnostic biomarkers (*n*-alkane, sterols), bulk geochemical parameters (TOC, $\delta^{13}\text{C}_{\text{org}}$), XRF element intensities, and grain size distributions to understand related palaeoenvironmental changes. Age models were constructed for each core through the ^{14}C dating of mollusc shells and bulk sediment. Bolgoda South Lake, Panama Lagoon and the Horton Plains revealed depositional histories spanning ca. 6000 – 1500 cal yr BP, 6200 – present, and 5500 cal yr BP – present, respectively. Terrestrial plant (leaf wax *n*-alkane) and bacterial synthesized (secondary) lipids are the two main organic matter (OM) sources in the coastal sites; Bolgoda South Lake and Panama Lagoon. In the Horton Plains, mosses (*Sphagnum*), woody plants, and grasses were identified as the main sources of OM in the peat core.

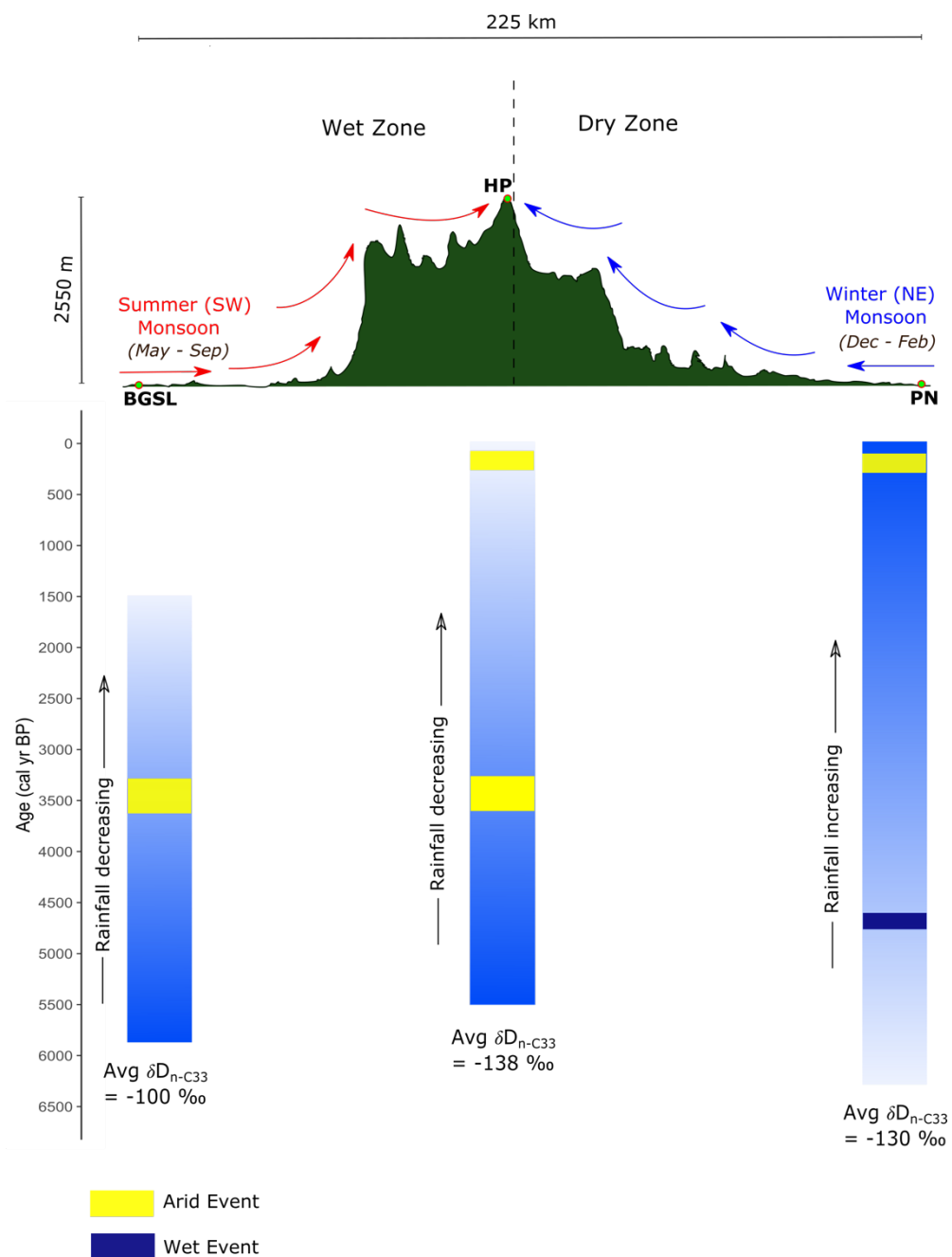
As inferred from the *n*-alkane leaf wax hydrogen and carbon isotope data, the summer monsoon feeding the Bolgoda South Lake catchment showed a decreasing trend in rainfall from the middle to the late Holocene. This is supported by proxies of decreasing lake water level and increasing proportions of fine grains (clay) in the sediment. Concurrent to this decreasing catchment rainfall, marine influence (seawater intrusion) also increased into the lake. A rapid decrease of rainfall occurred around 4000 cal yr BP and an arid event was identified ~ 3500 cal yr BP. A similar rainfall trend was found at Horton Plains, where the area is also dominantly influenced by summer monsoon rainfall in the present. High aridity events are identified at ~ 3500 cal yr BP and ~ 250 cal yr BP in the Horton Plains sequence. The changing of the dominant moisture source from the SWM to NEM also occurred during these times at HP. The relative abundance of grasses increased after ~ 1500 cal yr BP, concurrent to trending aridity in the area. The opposite trend of rainfall variation was identified in the NEM-influenced Panama lagoon that showed a general increasing trend of rainfall during the last ~ 6200 cal yr BP. This was also supported by a decreasing proportion fine grains (clay) in the

sediment, increasing mangrove vegetation, and decreasing marine influence in the lagoon. A high sea level stand is also evident between 6200 and 4500 cal yr BP.

The majority of regional palaeoclimate records infer a gradual or stepwise decreasing trend of Indian summer monsoon (ISM) rainfall over the Indian subcontinent from the middle to late Holocene, except for records from South Indian peninsular. Failures of the ISM and drought-like climate conditions were also recorded in many parts of the Indian sub-continent between 4500 – 3500 cal yr BP, related to the 4.2 kyr arid event, and at ~ 500 cal yr BP, concurrent with the LIA. Our results show agreement with general observed trends of regional summer monsoonal rainfall variability and also some of the abrupt events (droughts) that have been argued to have occurred during the middle and late Holocene in South Asia more widely.

Our proxy records in Sri Lanka indicated a sub-millennial scale inverse relationship between South Asian summer and winter monsoon rainfall during the middle and late Holocene. Orbitally induced southward migration of the mean position of the ITCZ appear to be the key driving force behind this inverse rainfall trend. In addition, increasing ENSO frequency during this time likely partially influenced this phenomenon. The more abrupt failures of the ISM during the last ~ 6000 yrs, leading to droughts in the region, seem to be primarily governed by negative North Atlantic Oscillations.

These observed changes in monsoonal rainfall have also likely influenced past human societies in Sri Lanka. It seems that gradually increasing winter monsoon rainfall in the dry zone attracted agricultural and urban societies to the area starting around 2900 cal yr BP. However, after 800 cal yr BP, declining rainfall may be behind the failure of water management systems in the dry zone and the migration of ancient kingdoms towards the southwestern part of the island. By that time, optimal hydrological conditions for agriculture and a shrinkage in dense rainforest areas, due to decreasing summer monsoon rainfall, may have enhanced the potential for widespread agriculture in the wet zone of Sri Lanka.



Graphical summary of monsoon rainfall variation in Sri Lanka during last ~ 6000 years. (BGS = Bolgoda South Lake; PN = Panama Lagoon; HP = Horton Plains).

Zusammenfassung

Der südasiatische Monsun ist ein Klimaphänomen, welches große Bedeutung für den großen Teil der Weltbevölkerung hat, welcher auf dem indischen Subkontinent lebt. Außerdem beeinflusst er direkt die sozioökonomischen und landwirtschaftlichen Aktivitäten in dieser Region. Die Voraussage von Veränderungen des Monsunsystems und den damit verbundenen Klimaextremen ist jedoch eine große Herausforderung für Klimatologen, die auf Aufzeichnungen von Instrumenten angewiesen sind, welche erst seit wenigen Jahrzehnten verfügbar sind. Daher sind Paläoklimadaten unerlässlich, um die langfristige Variabilität und die mechanistische Funktionsweise des tropischen Monsunsystems in der Region zu verstehen. Beispielsweise gibt es bedeutende Wissenslücken hinsichtlich des südasiatischen Monsunsystems, die darauf zurückzuführen sind, dass ein Mangel an Wintermonsun-Daten besteht, große Heterogenität in den regionalen Paläoklima-Aufzeichnungen vorliegt und es Schwierigkeiten beim Vergleich von marinen und terrestrischen Aufzeichnungen zur Rückverfolgung der Niederschlagsvariabilität gibt.

Um einige dieser Wissenslücken zu füllen, wurde in dieser Dissertation die Sommermonsun- (Südwestmonsun; SWM) und Wintermonsun- (Nordostmonsun; NEM) Niederschlagsvariabilität in Sri Lanka und die damit verbundenen Umwelt- und Kulturveränderungen auf der Insel während der letzten ~6000 Jahre rekonstruiert. Als tropische Insel, die in einer zentralen Region des saisonalen Migrationspfades der intertropischen Konvergenzzone (ITCZ) liegt, wird Sri Lanka das ganze Jahr über von Sommer- (SWM), Winter- (NEM) sowie intermonsunalen Regenfällen beeinflusst. Die beiden Hauptregenzeiten, der Sommermonsun (lange Zeitdauer) und der Wintermonsun (kurze Zeitdauer), haben eine klare räumliche Verteilung innerhalb der Insel, da das zentrale Hochland (maximale Höhe ~ 2500 m) als orographische Barriere für diese saisonalen Winde agiert. Mit Hinblick auf diese einzigartige geographische Lage sowie die geomorphologischen Gegebenheiten, habe ich zwei

Sedimentkerne aus dem vom Sommermonsunregen gespeisten Bolgoda South Lake bzw. aus der vom Wintermonsunregen dominierten Panama Lagoon entnommen. Des Weiteren habe ich einen Torfkern aus den hochgelegenen Horton Plains entnommen, wo sowohl Sommer- als auch Wintermonsun-Regenfälle auftreten. An diesen Sediment- und Torfkernen habe ich komponentenspezifische Wasserstoff- und Kohlenstoff-Isotopenmessungen einzelner *n*-Alkane durchgeführt, um paläohydrologische Veränderungen zu rekonstruieren. Diese habe ich unterstützt durch Analysen von diagnostischen Biomarkern (*n*-Alkane, Sterole), geochemischen Gesamtparametern (TOC, $\delta^{13}\text{C}_{\text{org}}$), XRF-Elementintensitäten und Korngrößenverteilungen, um damit verbundene paläoökologische Veränderungen zu verstehen. Für jeden Kern wurden Altersmodelle durch ^{14}C -Datierung von Molluskenschalen und dem Gesamtsediment erstellt. Der Bolgoda South Lake, die Panama Lagoon und die Horton Plains zeigten jeweils eine zeitliche Ablagerung von ca. 6000 - 1500 cal yr BP, 6200 - heute und 5500 cal yr BP - heute. Terrestrische Pflanzen (*n*-Alkane aus Blattwachsen) und bakteriell synthetisierte (sekundäre) Lipide sind die beiden Hauptquellen für organische Substanz (OM) in den Küstengebieten; Bolgoda South Lake und Panama Lagoon. In den Horton Plains wurden Moose (Sphagnum), Holzgewächse und Gräser als die Hauptquellen für OM im Torfkern identifiziert.

Ausgehend von den Wasserstoff- und Kohlenstoff-Isotopendaten von *n*-Alkanen aus Blattwachsen, zeigte der Sommermonsun, der das Einzugsgebiet des Bolgoda South Lakes speist, einen abnehmenden Niederschlagstrend vom mittleren bis zum späten Holozän. Dieses Ergebnis wird durch Marker für einen abnehmenden Wasserspiegel des Sees sowie einen zunehmenden Anteil an feinkörnigem Sediment (Ton) gestützt. Parallel zum abnehmenden Niederschlag im Einzugsgebiet nahm der marine Einfluss (Meerwasserintrusion) in den See zu. Eine rapide Verringerung der Niederschläge trat um 4000 cal yr BP auf und um ~3500 cal yr BP konnte ein Trockenevent identifiziert werden. Ein ähnlicher Niederschlagstrend zeigte

sich in den Horton Plains, welche auch zurzeit überwiegend von Sommermonsun-Regenfällen beeinflusst werden. Hohe Aridität wurde an spezifischen Events um ~3500 cal yr BP und ~250 cal yr BP im Sedimentkern der Horton Plains identifiziert. Außerdem fanden in den Horton Plains zu diesen Zeitpunkten Wechsel der dominanten Feuchtigkeitsquellen vom SWM hin zum NEM statt. Die relative Häufigkeit von Gräsern nahm nach ~1500 cal yr BP zu, gleichzeitig mit der zunehmenden Trockenheit in diesem Gebiet. In der NEM-beeinflussten Panama-Lagune konnte ein entgegengesetzter Niederschlagstrend identifiziert werden, welcher auf im Allgemeinen zunehmende Niederschläge während der letzten ~ 6200 cal yr BP hindeutete. Dies wurde auch durch einen abnehmenden Anteil feiner Sedimentanteile (Ton), zunehmende Mangrovenvegetation und einen abnehmenden marinen Einfluss in der Lagune unterstützt. Zwischen 6200 und 4500 cal yr BP zeigte sich außerdem ein hoher Meeresspiegelstand.

Die Mehrheit der regionalen Paläoklimaaufzeichnungen lässt auf einen graduellen oder stufenweisen Abwärtstrend der Niederschläge des indischen Sommermonsuns (ISM) über dem indischen Subkontinent vom mittleren bis zum späten Holozän schließen, mit Ausnahme der Aufzeichnungen von der südindischen Halbinsel. Ausfälle des ISM und dürreähnliche Bedingungen wurden außerdem in vielen Teilen des indischen Subkontinents zwischen 4500 - 3500 cal yr BP, im Zusammenhang mit dem 4,2-Kilojahr-Ereignis, und bei ~500 cal yr BP, assoziiert mit der Kleinen Eiszeit, aufgezeichnet. Die Ergebnisse dieser Dissertation zeigen eine Übereinstimmung mit den allgemein beobachteten Trends der regionalen Variabilität der Sommermonsunniederschläge und auch mit einigen der abrupten Events (Dürren), von denen angenommen wird, dass sie während des mittleren und späten Holozäns in Südasien weit verbreitet auftraten.

Unsere Proxy-Aufzeichnungen in Sri Lanka deuten auf eine submillenniale, inverse Beziehung zwischen den Sommer- und Wintermonsun-Regenfällen in Südasien während des

mittleren und späten Holozäns hin. Eine orbital induzierte südwärts gerichtete Wanderung der mittleren Position der ITCZ scheint die treibende Kraft hinter diesem inversen Niederschlagstrend zu sein. Zusätzlich hat die zunehmende ENSO-Häufigkeit während dieser Zeit dieses Phänomen wahrscheinlich teilweise beeinflusst. Die abrupteren Ausfälle des ISM während der letzten ~6000 Jahre, die zu Dürren in der Region führten, scheinen in erster Linie durch negative nordatlantische Oszillationen bestimmt zu sein.

Die beobachteten Veränderungen der Monsunregenfälle haben wahrscheinlich auch die früheren menschlichen Kulturen in Sri Lanka beeinflusst. Es scheint, dass die allmählich zunehmenden Wintermonsun-Regenfälle in der Trockenzone ab etwa 2900 cal yr BP landwirtschaftliche und urbane Gesellschaften in das Gebiet führten. Nach 800 cal yr BP könnten jedoch abnehmende Niederschläge der Grund für das Versagen der Wassermanagementsysteme in der Trockenzone und die Abwanderung der alten Königreiche in den südwestlichen Teil der Insel verantwortlich sein. Zu diesem Zeitpunkt könnten optimale hydrologische Bedingungen für die Landwirtschaft und ein Rückgang der dichten Regenwaldgebiete aufgrund abnehmender Sommermonsun-Regenfälle das Potenzial für eine weit verbreitete Landwirtschaft in der feuchten Zone Sri Lankas erhöht haben.

Bibliography

- Abeywardana, N., Pitawala, H.M.T.G.A., Schütt, B., Bebermeier, W., 2019. Evolution of the dry zone water harvesting and management systems in Sri Lanka during the Anuradhapura Kingdom; a study based on ancient chronicles and lithic inscriptions. *Water Hist.* 11, 75–103. <https://doi.org/10.1007/s12685-019-00230-7>
- Abram, N.J., Hargreaves, J.A., Wright, N.M., Thirumalai, K., Ummenhofer, C.C., England, M.H., 2020. Palaeoclimate perspectives on the Indian Ocean Dipole. *Quat. Sci. Rev.* 237, 106302. <https://doi.org/10.1016/j.quascirev.2020.106302>
- Achyuthan, H., Deshpande, R.D., Rao, M.S., Kumar, B., Nallathambi, T., Shashi Kumar, K., Ramesh, R., Ramachandran, P., Maurya, A.S., Gupta, S.K., 2013. Stable isotopes and salinity in the surface waters of the Bay of Bengal: Implications for water dynamics and palaeoclimate. *Mar. Chem.* 149, 51–62. <https://doi.org/10.1016/j.marchem.2012.12.006>
- Achyuthan, H., Farooqui, A., Gopal, V., Phartiyal, B., Lone, A., 2016. Late Quaternary to Holocene Southwest Monsoon Reconstruction: A Review based on Lake and Wetland Systems (Studies Carried Out during 2011-2016). *Proc. Indian Natl. Sci. Acad.* 82, 847–868. <https://doi.org/10.16943/ptinsa/2016/48489>
- Aghadadashi, V., Mehdinia, A., Molaei, S., 2017. Origin, toxicological and narcotic potential of sedimentary PAHs and remarkable even/odd n-alkane predominance in Bushehr Peninsula, the Persian Gulf. *Mar. Pollut. Bull.* 114, 494–504. <https://doi.org/10.1016/j.marpolbul.2016.10.013>
- Agnihotri, R., Dutta, K., Bhushan, R., Somayajulu, B.L.K.Ā., 2002. Evidence for solar forcing on the Indian monsoon during the last millennium. *Earth Planet. Sci. Lett.* 198, 521–527.
- Aloulou, F., Kallel, M., Dammak, M., Elleuch, B., Saliot, A., 2010. Even-numbered n-alkanes/n-alkenes predominance in surface sediments of Gabes Gulf in Tunisia. *Environ. Earth Sci.* 61, 1–10. <https://doi.org/10.1007/s12665-009-0315-y>
- Amarasinghe, M.D., Perera, K.A.R.S., 2017. Ecological biogeography of mangroves in Sri Lanka. *Ceylon J. Sci.* 46, 119. <https://doi.org/10.4038/cjs.v46i5.7459>
- An, Z., Wu, G., Li, J., Sun, Y., Liu, Y., Zhou, W., Cai, Y., Duan, A., Li, L., Mao, J., Cheng, H., Shi, Z., Tan, L., Yan, H., Ao, H., Chang, H., Feng, J., 2015. Global Monsoon Dynamics and Climate Change. *Annu. Rev. Earth Planet. Sci.* 43, 29–77. <https://doi.org/10.1146/annurev-earth-060313-054623>
- Anderson, D.M., 2002. Increase in the Asian Southwest Monsoon During the Past Four Centuries. *Science (80-.)*. 297, 596–599. <https://doi.org/10.1126/science.1072881>
- Ankit, Y., Kumar, P., Anoop, A., Mishra, P.K., Varghese, S., 2017. Mid-late Holocene climate variability in the Indian monsoon: Evidence from continental shelf sediments adjacent to Rushikulya river, eastern India. *Quat. Int.* 443, 155–163. <https://doi.org/10.1016/j.quaint.2016.12.023>
- Ashok, K., Guan, Z., Saji, N.H., Yamagata, T., 2004. Individual and Combined Influences of ENSO and the Indian Ocean Dipole on the Indian Summer Monsoon. *J. Clim.* 17, 3141–3155. [https://doi.org/10.1175/1520-0442\(2004\)017<3141:IACIOE>2.0.CO;2](https://doi.org/10.1175/1520-0442(2004)017<3141:IACIOE>2.0.CO;2)
- Ashok, K., Guan, Z., Yamagata, T., 2001. Impact of the Indian Ocean dipole on the relationship between the Indian monsoon rainfall and ENSO. *Geophys. Res. Lett.* 28, 4499–4502. <https://doi.org/10.1029/2001GL013294>
- Bamzai, A.S., Shukla, J., 1999. Relation between Eurasian snow cover, snow depth, and the Indian summer monsoon: An observational study. *J. Clim.* <https://doi.org/10.1175/1520->

- 0442(1999)012<3117:RBESCS>2.0.CO;2
- Banerji, U.S., Arulbalaji, P., Padmalal, D., 2020. Holocene climate variability and Indian Summer Monsoon: An overview. *Holocene*. <https://doi.org/10.1177/0959683619895577>
- Banerji, U.S., Bhushan, R., Jull, A.J.T., 2019. Signatures of global climatic events and forcing factors for the last two millennia from the active mudflats of Rohisa, southern Saurashtra, Gujarat, western India. *Quat. Int.* 507, 172–187. <https://doi.org/10.1016/j.quaint.2019.02.015>
- Banerji, U.S., Bhushan, R., Jull, A.J.T., 2017. Mid– late Holocene monsoonal records from the partially active mudflat of Diu Island, southern Saurashtra, Gujarat, western India. *Quat. Int.* 443, 200–210.
- Basavaiah, N., Mahesh Babu, J.L.V., Gawali, P.B., Naga Kumar, K.C.V., Demudu, G., Prizomwala, S.P., Hanamgond, P.T., Nageswara Rao, K., 2015. Late Quaternary environmental and sea level changes from Kolleru Lake, SE India: Inferences from mineral magnetic, geochemical and textural analyses. *Quat. Int.* 371, 197–208. <https://doi.org/10.1016/j.quaint.2014.12.018>
- Bebermeier, W., Meister, J., Withanachchi, C.R., Middelhaufe, I., Middelhaufe, B., 2017. Tank cascade systems as a sustainable measure of watershed management in South Asia. *Water (Switzerland)* 9, 1–16. <https://doi.org/10.3390/w9030231>
- Berger, A., Loutre, M.F., 1994. Precession, eccentricity, obliquity, insolation and paleoclimates, in: *Long-Term Climatic Variations*. Springer, pp. 107–151.
- Berkelhammer, M., Sinha, A., Stott, L., Cheng, H., Pausata, F.S.R., Yoshimura, K., 2012. An abrupt shift in the Indian monsoon 4000 years ago. *Geophys. Monogr. Ser.* 198, 75–87. <https://doi.org/10.1029/2012GM001207>
- Bhattacharyya, A., Sandeep, K., Misra, S., Shankar, R., Warriar, A.K., Weijian, Z., Xuefeng, L., 2015. Vegetational and climatic variations during the past 3100 years in southern India: evidence from pollen, magnetic susceptibility and particle size data. *Environ. Earth Sci.* 74, 3559–3572.
- Bisutti, I., Hilke, I., Raessler, M., 2004. Determination of total organic carbon - An overview of current methods. *TrAC - Trends Anal. Chem.* <https://doi.org/10.1016/j.trac.2004.09.003>
- Blaauw, M., Christen, J., 2011. Flexible paleoclimate age-depth models using an autoregressive gamma process. *Bayesian Anal.* 6, 457–474. <https://doi.org/10.1214/11-BA618>
- Böll, A., Lückge, A., Munz, P., Forke, S., Schulz, H., Ramaswamy, V., Rixen, T., Gaye, B., Emeis, K.-C., 2014. Late Holocene primary productivity and sea surface temperature variations in the northeastern Arabian Sea: Implications for winter monsoon variability. *Paleoceanography* 29, 778–794. <https://doi.org/10.1002/2013PA002579>
- Bond, G., Kromer, B., Beer, J., Muscheler, R., Evans, M.N., Showers, W., Hoffmann, S., Lotti-Bond, R., Hajdas, I., Bonani, G., 2001. Persistent solar influence on north atlantic climate during the Holocene. *Science (80-.)*. 294, 2130–2136. <https://doi.org/10.1126/science.1065680>
- Brown, E.T., Johnson, T.C., 2005. Coherence between tropical East African and South American records of the Little Ice Age. *Geochemistry, Geophys. Geosystems*. <https://doi.org/10.1029/2005GC000959>
- Bush, R.T., McInerney, F.A., 2013. Leaf wax n-alkane distributions in and across modern plants: Implications for paleoecology and chemotaxonomy. *Geochim. Cosmochim. Acta* 117, 161–179. <https://doi.org/10.1016/j.gca.2013.04.016>
- Chandrajith, R., Chaturangani, D., Abeykoon, S., Barth, J.A.C., van Geldern, R., Edirisinghe, E.A.N.V., Dissanayake, C.B., 2014. Quantification of groundwater-seawater interaction in a coastal sandy aquifer system: A study from Panama, Sri Lanka. *Environ. Earth Sci.*

- 72, 867–877. <https://doi.org/10.1007/s12665-013-3010-y>
- Chandrajith, R., Koralegedara, N., Ranawana, K.B., Tobschall, H.J., Dissanayake, C.B., 2009. Major and trace elements in plants and soils in Horton Plains National Park, Sri Lanka: an approach to explain forest die back. *Environ. Geol.* 57, 17–28. <https://doi.org/10.1007/s00254-008-1278-0>
- Chao, W.C., Chen, B., 2001. The origin of monsoons. *J. Atmos. Sci.* 58, 3497–3507. [https://doi.org/10.1175/1520-0469\(2001\)058<3497:TOOM>2.0.CO;2](https://doi.org/10.1175/1520-0469(2001)058<3497:TOOM>2.0.CO;2)
- Charney, J.G., 1968. Inter-tropical convergence zone and Hadley circulation of atmosphere, in: *Bulletin of the American Meteorological Society*. p. 1041.
- Chauhan, O.S., Dayal, A.M., Basavaiah, N., Kader, U.S.A., 2010. Indian summer monsoon and winter hydrographic variations over past millennia resolved by clay sedimentation. *Geochemistry, Geophys. Geosystems* 11.
- Chiang, J.C.H., 2009. The tropics in paleoclimate. *Annu. Rev. Earth Planet. Sci.* 37, 263–297. <https://doi.org/10.1146/annurev.earth.031208.100217>
- Chiang, J.C.H., Friedman, A.R., 2012. Extratropical Cooling, Interhemispheric Thermal Gradients, and Tropical Climate Change. *Annu. Rev. Earth Planet. Sci.* 40, 383–412. <https://doi.org/10.1146/annurev-earth-042711-105545>
- Clement, A.C., Seager, R., Cane, M.A., 2000. Suppression of El Niño during the mid-Holocene by changes in the Earth's orbit. *Paleoceanography*. <https://doi.org/10.1029/1999PA000466>
- Conroy, J.L., Overpeck, J.T., Cole, J.E., Shanahan, T.M., Steinitz-Kannan, M., 2008. Holocene changes in eastern tropical Pacific climate inferred from a Galápagos lake sediment record. *Quat. Sci. Rev.* 27, 1166–1180. <https://doi.org/10.1016/j.quascirev.2008.02.015>
- Cooray, P.G., 1978. Geology of Sri Lanka, in: *Regional Conference on Geology and Mineral Resources of Southeast Asia*. 3. pp. 701–710.
- Croudace, I.W., Rothwell, R.G., 2015. *Micro-XRF Studies of Sediment Cores: Applications of a non-destructive tool for the environmental sciences*. Springer.
- Dansgaard, W., 1964. Stable isotopes in precipitation. *Tellus* 16, 436–468.
- Davies, S.J., Lamb, H.F., Roberts, S.J., 2015. Micro-XRF core scanning in palaeolimnology: recent developments, in: *Micro-XRF Studies of Sediment Cores*. Springer, pp. 189–226.
- Davison, W., 1993. Iron and manganese in lakes. *Earth-Science Rev.* 34, 119–163. [https://doi.org/10.1016/0012-8252\(93\)90029-7](https://doi.org/10.1016/0012-8252(93)90029-7)
- Deraniyagala, S.U., 1989. *The prehistory of Sri Lanka: An ecological perspective*.
- Diefendorf, A.F., Freimuth, E.J., 2017. Extracting the most from terrestrial plant-derived n-alkyl lipids and their carbon isotopes from the sedimentary record: A review. *Org. Geochem.* 103, 1–21. <https://doi.org/10.1016/j.orggeochem.2016.10.016>
- Dixit, Y., Hodell, D. a., Sinha, R., Petrie, C. a., 2014. Abrupt weakening of the Indian summer monsoon at 8.2 kyrB.P. *Earth Planet. Sci. Lett.* 391, 16–23. <https://doi.org/10.1016/j.epsl.2014.01.026>
- Dixit, Y., Tandon, S.K., 2016. Hydroclimatic variability on the Indian subcontinent in the past millennium: Review and assessment. *Earth-Science Rev.* 161, 1–15.
- Donges, J.F., Donner, R., Marwan, N., Breitenbach, S.F.M., Rehfeld, K., Kurths, J., 2015. Non-linear regime shifts in Holocene Asian monsoon variability: potential impacts on cultural change and migratory patterns. *Clim. Past* 11, 709–741.
- Dutt, S., Gupta, A.K., Clemens, S.C., Cheng, H., Singh, R.K., Kathayat, G., Edwards, R.L., 2015. Abrupt changes in Indian summer monsoon strength during 33,800 to 5500 years B.P. *Geophys. Res. Lett.* 42, 5526–5532. <https://doi.org/10.1002/2015GL064015>
- Dutt, S., Gupta, A.K., Wünnemann, B., Yan, D., 2018. A long arid interlude in the Indian summer monsoon during ~4,350 to 3,450 cal. yr BP contemporaneous to displacement

- of the Indus valley civilization. *Quat. Int.* 482, 83–92.
<https://doi.org/10.1016/j.quaint.2018.04.005>
- DWC, 2007. Biodiversity Baseline Survey: Horton Plains National Park.
- Dykoski, C.A., Edwards, R.L., Cheng, H., Yuan, D., Cai, Y., Zhang, M., Lin, Y., Qing, J., An, Z., Revenaugh, J., 2005. A high-resolution, absolute-dated Holocene and deglacial Asian monsoon record from Dongge Cave, China. *Earth Planet. Sci. Lett.* 233, 71–86.
- Edirisinghe, E.A.N.V., Pitawala, H.M.T.G.A., Dharmagunawardhane, H.A., Wijayawardane, R.L., 2017. Spatial and temporal variation in the stable isotope composition ($\delta^{18}\text{O}$ and $\delta^2\text{H}$) of rain across the tropical island of Sri Lanka. *Isotopes Environ. Health Stud.* 53, 628–645. <https://doi.org/10.1080/10256016.2017.1304936>
- Eglinton, T.I., Eglinton, G., 2008. Molecular proxies for paleoclimatology. *Earth Planet. Sci. Lett.* 275, 1–16. <https://doi.org/10.1016/j.epsl.2008.07.012>
- Ekpo, B.O., Oyo-Ita, O.E., Wehner, H., 2005. Even-n-alkane/alkene predominances in surface sediments from the Calabar River, SE Niger Delta, Nigeria. *Naturwissenschaften* 92, 341–346. <https://doi.org/10.1007/s00114-005-0639-8>
- Elias, V.O., Simoneit, B.R.T., Cardoso, J.N., 1997. Even n-alkane predominances on the Amazon Shelf and a Northeast Pacific Hydrothermal System. *Naturwissenschaften* 84, 415–420. <https://doi.org/10.1007/s001140050421>
- Ellepola, G., Ranawana, K.B., 2015. Panama Lagoon : A unique mangrove ecosystem in the east coast of Sri Lanka. *Wetl. Sri Lanka* 2, 10–19.
- Englong, A., Punwong, P., Selby, K., Marchant, R., Traiperm, P., Pumijumnong, N., 2019. Mangrove dynamics and environmental changes on Koh Chang, Thailand during the last millennium. *Quat. Int.* 500, 128–138. <https://doi.org/10.1016/j.quaint.2019.05.011>
- Erdelen, W., 1988. Forest ecosystems and nature conservation in Sri Lanka. *Biol. Conserv.* 43, 115–135. [https://doi.org/10.1016/0006-3207\(88\)90086-9](https://doi.org/10.1016/0006-3207(88)90086-9)
- Fernando, C.H., 2012. Ecology and biogeography in Sri Lanka. Springer Science & Business Media.
- Ficken, K.J., Li, B., Swain, D.L., Eglinton, G., 2000. An n-alkane proxy for the sedimentary input of submerged/floating freshwater aquatic macrophytes. *Org. Geochem.* 31, 745–749. [https://doi.org/10.1016/S0146-6380\(00\)00081-4](https://doi.org/10.1016/S0146-6380(00)00081-4)
- Fleitmann, D., 2003. Holocene Forcing of the Indian Monsoon Recorded in a Stalagmite from Southern Oman. *Science (80-.)*. 300, 1737–1739.
<https://doi.org/10.1126/science.1083130>
- Fleitmann, D., Burns, S.J., Mangini, A., Mudelsee, M., Kramers, J., Villa, I., Neff, U., Al-Subbary, A.A., Buettner, A., Hippler, D., Matter, A., 2007. Holocene ITCZ and Indian monsoon dynamics recorded in stalagmites from Oman and Yemen (Socotra). *Quat. Sci. Rev.* 26, 170–188. <https://doi.org/10.1016/j.quascirev.2006.04.012>
- Fleitmann, D., Burns, S.J., Mudelsee, M., Neff, U., Kramers, J., Mangini, A., Matter, A., 2003. Holocene forcing of the Indian monsoon recorded in a stalagmite from southern Oman. *Science* 300, 1737–9. <https://doi.org/10.1126/science.1083130>
- Gadgil, S., 2018. The monsoon system: Land–sea breeze or the ITCZ? *J. Earth Syst. Sci.* 127, 1–29. <https://doi.org/10.1007/s12040-017-0916-x>
- Gadgil, S., 2003. The Indian monsoon and its variability. *Annu. Rev. Earth Planet. Sci.* 31, 429–467. <https://doi.org/10.1146/annurev.earth.31.100901.141251>
- Gadgil, Sulochana, Vinayachandran, P.N., Francis, P.A., Gadgil, Siddhartha, 2004. Extremes of the Indian summer monsoon rainfall, ENSO and equatorial Indian Ocean oscillation. *Geophys. Res. Lett.* 31.
- Gamarra, B., Sachse, D., Kahmen, A., 2016. Effects of leaf water evaporative ^2H -enrichment and biosynthetic fractionation on leaf wax n-alkane $\delta^2\text{H}$ values in C3 and C4 grasses. *Plant Cell Environ.* 39, 2390–2403. <https://doi.org/10.1111/pce.12789>

- Garcin, Y., Schefuß, E., Schwab, V.F., Garreta, V., Gleixner, G., Vincens, A., Todou, G., Sene, O., Onana, J.M., Achoundong, G., Sachse, D., 2014. Reconstructing C3 and C4 vegetation cover using n-alkane carbon isotope ratios in recent lake sediments from Cameroon, Western Central Africa. *Geochim. Cosmochim. Acta* 142, 482–500. <https://doi.org/10.1016/j.gca.2014.07.004>
- Gat, J., Mook, W., Meyer, H., 2000. Observed isotope effects in precipitation. *Environ. Isot. Hydrol. Cycle Princ. Appl. II Atmos. Water* 197–208.
- Gayantha, K., Routh, J., Anupama, K., Lazar, J., Prasad, S., Chandrajith, R., Roberts, P., Gleixner, G., 2020. Reconstruction of the Late Holocene climate and environmental history from North Bolgoda Lake, Sri Lanka, using lipid biomarkers and pollen records. *J. Quat. Sci.* 35, 514–525. <https://doi.org/10.1002/jqs.3196>
- Gayantha, K., Routh, J., Chandrajith, R., 2017. A multi-proxy reconstruction of the late Holocene climate evolution in Lake Bolgoda, Sri Lanka. *Palaeogeogr. Palaeoclimatol. Palaeoecol.* 473, 16–25. <https://doi.org/10.1016/j.palaeo.2017.01.049>
- Gilliland, K., Simpson, I.A., Adderley, W.P., Burbidge, C.I., Cresswell, A.J., Sanderson, D.C.W., Coningham, R.A.E., Manuel, M., Strickland, K., Gunawardhana, P., Adikari, G., 2013. The dry tank: development and disuse of water management infrastructure in the Anuradhapura hinterland, Sri Lanka. *J. Archaeol. Sci.* 40, 1012–1028. <https://doi.org/10.1016/J.JAS.2012.09.034>
- Goff, J., Chagué-Goff, C., Nichol, S., Jaffe, B., Dominey-Howes, D., 2012. Progress in palaeotsunami research. *Sediment. Geol.* 243–244, 70–88. <https://doi.org/10.1016/j.sedgeo.2011.11.002>
- Goldstein, G., Santiago, L.S., 2016. *Tropical Tree Physiology, Tree Physiology*. Springer International Publishing, Cham. <https://doi.org/10.1007/978-3-319-27422-5>
- GSMB, 1995. 1:100000 Geology Map, Sheet 17. Nuwara Eliya, Haputale.
- Günther, F., Thiele, A., Biskop, S., Mäusbacher, R., Haberzettl, T., Yao, T., Gleixner, G., 2016. Late quaternary hydrological changes at Tangra Yumco, Tibetan Plateau: a compound-specific isotope-based quantification of lake level changes. *J. Paleolimnol.* 55, 369–382. <https://doi.org/10.1007/s10933-016-9887-1>
- Gupta, A.A.K., Anderson, D.D.M., Overpeck, J.J.T., 2003. Abrupt changes in the Asian southwest monsoon during the Holocene and their links to the North Atlantic Ocean. *Nature* 421, 354–357. <https://doi.org/10.1038/nature01340>
- Gupta, A.K., Das, M., Anderson, D.M., 2005. Solar influence on the Indian summer monsoon during the Holocene. *Geophys. Res. Lett.* 32, 2–5. <https://doi.org/10.1029/2005GL022685>
- Gupta, A.K., Prakasam, M., Dutt, S., Clift, P.D., Yadav, R.R., 2020. Evolution and Development of the Indian Monsoon, in: *Geodynamics of the Indian Plate*. Springer, pp. 499–535.
- Halley, E., 1687. An historical account of the trade winds, and monsoons, observable in the seas between and near the Tropicks, with an attempt to assign the physical cause of the said winds. *Philos. Trans. R. Soc. London* 16, 153–168. <https://doi.org/10.1098/rstl.1686.0026>
- Hao, W., Kashiwabara, T., Jin, R., Takahashi, Y., Gingras, M., Alessi, D.S., Konhauser, K.O., 2020. Clay minerals as a source of cadmium to estuaries. *Sci. Rep.* 10, 10417. <https://doi.org/10.1038/s41598-020-67279-w>
- Hapuarachchi, H.A.S.U., Jayawardena, I.M.S.P., 2015. Modulation of Seasonal Rainfall in Sri Lanka by ENSO Extremes. *December Sri Lanka J. Meteorol.* 1, 3–11.
- Haug, G.H., 2001. Southward Migration of the Intertropical Convergence Zone Through the Holocene. *Science* (80-.). 293, 1304–1308. <https://doi.org/10.1126/science.1059725>
- Hoefs, J., 2009. *Stable Isotope Geochemistry*, 6th ed. Springer-Verlag Berlin Heidelberg.

- Holtvoeth, J., Whiteside, J.H., Engels, S., Freitas, F.S., Grice, K., Greenwood, P., Johnson, S., Kendall, I., Lengger, S.K., Lücke, A., Mayr, C., Naafs, B.D.A., Rohrsen, M., Sepúlveda, J., 2019. The paleolimnologist's guide to compound-specific stable isotope analysis – An introduction to principles and applications of CSIA for Quaternary lake sediments. *Quat. Sci. Rev.* 207, 101–133.
<https://doi.org/10.1016/j.quascirev.2019.01.001>
- Hrudya, P.H., Varikoden, H., Vishnu, R., 2020. A review on the Indian summer monsoon rainfall, variability and its association with ENSO and IOD. *Meteorol. Atmos. Phys.*
<https://doi.org/10.1007/s00703-020-00734-5>
- Hua, Q., Barbetti, M., Rakowski, A.Z., 2013. Atmospheric Radiocarbon for the Period 1950–2010. *Radiocarbon*. https://doi.org/10.2458/azu_js_rc.v55i2.16177
- Hurrell, J.W., 1995. Decadal trends in the North Atlantic Oscillation: regional temperatures and precipitation. *Science* (80-.). 269, 676–679.
- Jackson, K.L., 2008. Paleotsunami History Recorded in Holocene Coastal Lagoon Sediments, Southeastern Sri Lanka. Open Access Theses Paper 171.
- Jackson, K.L., Eberli, G.P., Amelung, F., Mcfadden, M.A., Moore, A.L., Rankey, E.C., Jayasena, H.A.H., 2014. Holocene Indian Ocean tsunami history in Sri Lanka. *Geol. Soc. Am.* 859–862.
- James, I.N., 1994. Introduction to Circulating Atmospheres, Introduction to Circulating Atmospheres. <https://doi.org/10.1017/cbo9780511622977>
- Jayakody, P.M., 2015. The Influence of La Nina on Sri Lanka Rainfall. *Sri Lanka J. Meteorol.* 1, 41–49.
- Jayasena, H.A.H., Chandrajith, R., Gangadhara, K.R., 2011. Water Management in Ancient Tank Cascade Systems (TCS) in Sri Lanka : Evidence for Systematic Tank Distribution. *J. Geol. Soc. Sri Lanka Prof. C . B . Dissanayake Felicitation* 14, 27–33.
- Jin, C., Günther, F., Li, S., Jia, G., Peng, P., Gleixner, G., 2015. Reduced early Holocene moisture availability inferred from δD values of sedimentary n-alkanes in Zigetang Co, Central Tibetan Plateau. *Holocene* 26, 556–566.
<https://doi.org/10.1177/0959683615612568>
- Kane, R.P., 1998. ENSO relationship to the rainfall of Sri Lanka. *Int. J. Climatol.* 18, 859–871. [https://doi.org/10.1002/\(SICI\)1097-0088\(19980630\)18:8<859::AID-JOC264>3.0.CO;2-W](https://doi.org/10.1002/(SICI)1097-0088(19980630)18:8<859::AID-JOC264>3.0.CO;2-W)
- Kassambara, A., Mundt, F., 2020. factoextra: Extract and Visualize the Results of Multivariate Data Analyses. R package version 1.0.7. <https://CRAN.R-project.org/package=factoextra>.
- Kathayat, G., Cheng, H., Sinha, A., Yi, L., Li, X., Zhang, H., Li, H., Ning, Y., Edwards, R.L., 2017. The Indian monsoon variability and civilization changes in the Indian subcontinent. *Sci. Adv.* 3, 1–9. <https://doi.org/10.1126/sciadv.1701296>
- Katupotha, J., 1995. Evolution and Geological Significance of Holocene Emerged Shell Beds on the Southern Coastal Zone of Sri Lanka. *J. Coast. Res.* 11, 1042–1061.
<https://doi.org/10.2307/4298410>
- Keefer, D.K., 1998. Early Maritime Economy and El Niño Events at Quebrada Tacahuay, Peru. *Science* (80-.). 281, 1833–1835. <https://doi.org/10.1126/science.281.5384.1833>
- Kilmer, V.J., Alexander, L.T., 1949. Methods of making mechanical analyses of soils. *Soil Sci.* 68, 15–24. <https://doi.org/10.1097/00010694-194907000-00003>
- Konecky, B.L., Russell, J.M., Rodysill, J.R., Vuille, M., Bijaksana, S., Huang, Y., 2013. Intensification of southwestern Indonesian rainfall over the past millennium. *Geophys. Res. Lett.* <https://doi.org/10.1029/2012GL054331>
- Kotlia, B.S., Singh, A.K., Joshi, L.M., Dhaila, B.S., 2015. Precipitation variability in the Indian Central Himalaya during last ca. 4,000 years inferred from a speleothem record:

- Impact of Indian Summer Monsoon (ISM) and Westerlies. *Quat. Int.*
<https://doi.org/10.1016/j.quaint.2014.10.066>
- Kripalani, R.H., Kumar, P., 2004. Northeast monsoon rainfall variability over south peninsular India vis-à-vis the Indian Ocean dipole mode. *Int. J. Climatol.* 24, 1267–1282. <https://doi.org/10.1002/joc.1071>
- Kumar, K.K., Rajagopalan, B., Hoerling, M., Bates, G., Cane, M., 2006. Unraveling the Mystery of Indian Monsoon Failure During El Niño. *Science* (80-). 314, 115–119. <https://doi.org/10.1126/science.1131152>
- Kylander, M.E., Ampel, L., Wohlfarth, B., Veres, D., 2011. High-resolution X-ray fluorescence core scanning analysis of Les Echets (France) sedimentary sequence: New insights from chemical proxies. *J. Quat. Sci.* 26, 109–117. <https://doi.org/10.1002/jqs.1438>
- Leipe, C., Demske, D., Tarasov, P.E., 2014. A Holocene pollen record from the northwestern Himalayan lake Tso Moriri: Implications for palaeoclimatic and archaeological research. *Quat. Int.* 348, 93–112. <https://doi.org/10.1016/j.quaint.2013.05.005>
- Lucero, L.J., Fletcher, R., Coningham, R., 2015. From ‘collapse’ to urban diaspora: the transformation of low-density, dispersed agrarian urbanism. *Antiquity* 89, 1139–1154. <https://doi.org/10.15184/aqy.2015.51>
- Lüning, S., Vahrenholt, F., 2016. The Sun’s Role in Climate, in: *Evidence-Based Climate Science*. Elsevier, pp. 283–305. <https://doi.org/10.1016/B978-0-12-804588-6.00016-1>
- Malmgren, B.A., Hulugalla, R., Hayashi, Y., Mikami, T., 2003. Precipitation trends in Sri Lanka since the 1870s and relationships to El Niño-southern oscillation. *Int. J. Climatol.* 23, 1235–1252. <https://doi.org/10.1002/joc.921>
- Martin-Puertas, C., Tjallingii, R., Bloemsmas, M., Brauer, A., 2017. Varved sediment responses to early Holocene climate and environmental changes in Lake Meerfelder Maar (Germany) obtained from multivariate analyses of micro X-ray fluorescence core scanning data. *J. Quat. Sci.* 32, 427–436. <https://doi.org/10.1002/jqs.2935>
- Mayle, F.E., Burbridge, R., Killeen, T.J., 2000. Millennial-scale dynamics of southern Amazonian rain forests. *Science* (80-). 290, 2291–2294.
- Meehl, G.A., 1992. Effect of tropical topography on global climate. *Annu. Rev. Earth Planet. Sci.* Vol. 20. <https://doi.org/10.1146/annurev.earth.20.1.85>
- Meyers, P. a., 1997. Organic geochemical proxies of paleoceanographic, paleolimnologic, and paleoclimatic processes. *Org. Geochem.* 27, 213–250. [https://doi.org/10.1016/S0146-6380\(97\)00049-1](https://doi.org/10.1016/S0146-6380(97)00049-1)
- Meyers, P.A., 2003. Application of organic geochemistry to paleolimnological reconstruction: a summary of examples from the Laurentian Great Lakes. *Org. Geochem.* 34, 261–289. [https://doi.org/10.1016/S0146-6380\(02\)00168-7](https://doi.org/10.1016/S0146-6380(02)00168-7)
- Meyers, P.A., Teranes, J.L., 2001. Sediment Organic Matter, in: *Tracking Environmental Change Using Lake Sediments. Volume 2: Physical and Geochemical Methods*. Kluwer Academic Publishers, pp. 240–243.
- Mirza, M.M.Q., 2011. Climate change, flooding in South Asia and implications. *Reg. Environ. Chang.* 11, 95–107. <https://doi.org/10.1007/s10113-010-0184-7>
- Mishra, P.K., Ankit, Y., Gautam, P.K., C.G., L., Singh, P., Anoop, A., 2019. Inverse relationship between south-west and north-east monsoon during the late Holocene: Geochemical and sedimentological record from Ennamangalam Lake, southern India. *Catena* 182, 104117. <https://doi.org/10.1016/j.catena.2019.104117>
- Misra, P., Tandon, S.K., Sinha, R., 2019. Holocene climate records from lake sediments in India: Assessment of coherence across climate zones. *Earth-Science Rev.* 190, 370–397. <https://doi.org/10.1016/j.earscirev.2018.12.017>
- Mohtadi, M., Prange, M., Steinke, S., 2016. Palaeoclimatic insights into forcing and response

- of monsoon rainfall. *Nature* 533, 191–199. <https://doi.org/10.1038/nature17450>
- Morton, R.A., Goff, J.R., Nichol, S.L., 2008. Hydrodynamic implications of textural trends in sand deposits of the 2004 tsunami in Sri Lanka. *Sediment. Geol.* 207, 56–64. <https://doi.org/10.1016/j.sedgeo.2008.03.008>
- Moy, C.M., Seltzer, G.O., Rodbell, D.T., Anderson, D.M., 2002. Variability of El Niño/Southern Oscillation activity at millennial timescales during the Holocene epoch. *Nature* 420, 162–165. <https://doi.org/10.1038/nature01194>
- Myrdal-Runebjer, E., 1996. Rice and millet: An archaeological case study of a Sri Lankan transbasin reservoir system. *Gotarc Ser. B. Gothenbg. Archaeol. These.*
- Naafs, B.D.A., Inglis, G.N., Blewett, J., McClymont, E.L., Laurentano, V., Xie, S., Evershed, R.P., Pancost, R.D., 2019. The potential of biomarker proxies to trace climate, vegetation, and biogeochemical processes in peat: A review. *Glob. Planet. Change* 179, 57–79. <https://doi.org/10.1016/j.gloplacha.2019.05.006>
- Nicholson, S.E., 2018. The ITCZ and the seasonal cycle over equatorial Africa. *Bull. Am. Meteorol. Soc.* 99, 337–348. <https://doi.org/10.1175/BAMS-D-16-0287.1>
- Nicholson, S.E., 2009. A revised picture of the structure of the “monsoon” and land ITCZ over West Africa. *Clim. Dyn.* 32, 1155–1171. <https://doi.org/10.1007/s00382-008-0514-3>
- Nishimura, M., Baker, E.W., 1986. Possible origin of n-alkanes with a remarkable even-to-odd predominance in recent marine sediments. *Geochim. Cosmochim. Acta* 50, 299–305. [https://doi.org/10.1016/0016-7037\(86\)90178-X](https://doi.org/10.1016/0016-7037(86)90178-X)
- Olsen, J., Anderson, N.J., Knudsen, M.F., 2012. Variability of the North Atlantic Oscillation over the past 5,200 years. *Nat. Geosci.* 5, 808–812. <https://doi.org/10.1038/ngeo1589>
- Ouyang, X., Guo, F., Bu, H., 2015. Lipid biomarkers and pertinent indices from aquatic environment record paleoclimate and paleoenvironment changes. *Quat. Sci. Rev.* 123, 180–192. <https://doi.org/10.1016/j.quascirev.2015.06.029>
- Panabokke, C.R., 1996. Soils and agro-ecological environments of Sri Lanka. NARESA.
- Peng, Y., Xiao, J., Nakamura, T., Liu, B., Inouchi, Y., 2005. Holocene East Asian monsoonal precipitation pattern revealed by grain-size distribution of core sediments of Daihai Lake in Inner Mongolia of north-central China. *Earth Planet. Sci. Lett.* 233, 467–479. <https://doi.org/10.1016/j.epsl.2005.02.022>
- Perera, N.P., 1975. A Physiognomic Vegetation Map of Sri Lanka (Ceylon). *J. Biogeogr.* 2, 185–203.
- Peters, K.E., Walters, C.C., Moldowan, J.M., 2007. The Biomarker Guide, in: *The Biomarker Guide: Biomarkers and Isotopes in the Environment and Human History.* <https://doi.org/http://dx.doi.org/10.1017/CBO9780511524868>
- Ponton, C., Giosan, L., Eglinton, T.I., Fuller, D.Q., Johnson, J.E., Kumar, P., Collett, T.S., 2012. Holocene aridification of India. *Geophys. Res. Lett.* 39, 1–6. <https://doi.org/10.1029/2011GL050722>
- Possehl, G.L., 1997. The transformation of the Indus civilization. *J. World Prehistory.* <https://doi.org/10.1007/BF02220556>
- Prasad, S., Anoop, A., Riedel, N., Sarkar, S., Menzel, P., Basavaiah, N., Krishnan, R., Fuller, D., Plessen, B., Gaye, B., Röhl, U., Wilkes, H., Sachse, D., Sawant, R., Wiesner, M.G., Stebich, M., 2014. Prolonged monsoon droughts and links to Indo-Pacific warm pool: A Holocene record from Lonar Lake, central India. *Earth Planet. Sci. Lett.* 391, 171–182. <https://doi.org/10.1016/j.epsl.2014.01.043>
- Prasad, S., Kusumgar, S., Gupta, S.K., 1997. A mid to late Holocene record of palaeoclimatic changes from Nal Sarovar: a palaeodesert margin lake in western India. *J. Quat. Sci.* 12, 153–159. [https://doi.org/10.1002/\(SICI\)1099-1417\(199703/04\)12:2<153::AID-JQS300>3.0.CO;2-X](https://doi.org/10.1002/(SICI)1099-1417(199703/04)12:2<153::AID-JQS300>3.0.CO;2-X)

- Premathilake, R., 2012. Human used upper montane ecosystem in the Horton Plains, central Sri Lanka - a link to Lateglacial and early Holocene climate and environmental changes. *Quat. Sci. Rev.* 50, 23–42. <https://doi.org/10.1016/j.quascirev.2012.07.002>
- Premathilake, R., 2006. Relationship of environmental changes in central Sri Lanka to possible prehistoric land-use and climate changes. *Palaeogeogr. Palaeoclimatol. Palaeoecol.* 240, 468–496. <https://doi.org/10.1016/j.palaeo.2006.03.001>
- Premathilake, R., Risberg, J., 2003. Late Quaternary climate history of the Horton Plains, central Sri Lanka. *Quat. Sci. Rev.* 22, 1525–1541. [https://doi.org/10.1016/S0277-3791\(03\)00128-8](https://doi.org/10.1016/S0277-3791(03)00128-8)
- R Core Team, 2020. R: A language and environment for statistical computing. R Foundation for Statistical Computing, Vienna, Austria. <https://www.r-project.org/>.
- Rach, O., Brauer, A., Wilkes, H., Sachse, D., 2014. Delayed hydrological response to Greenland cooling at the onset of the Younger Dryas in western Europe. *Nat. Geosci.* 7, 109–112. <https://doi.org/10.1038/ngeo2053>
- Rajmanickam, V., Achyuthan, H., Eastoe, C., Farooqui, A., 2017. Early-Holocene to present palaeoenvironmental shifts and short climate events from the tropical wetland and lake sediments, Kukkal Lake, Southern India: Geochemistry and palynology. *Holocene* 27, 404–417. <https://doi.org/10.1177/09596836166660162>
- Ranasinghe, P., Ortiz, J., Smith, A., Griffith, E., Siriwardana, C., De Silva, S., Wijesundara, D., 2013. Mid- to late-Holocene Indian winter monsoon variability from a terrestrial record in eastern and southeastern coastal environments of Sri Lanka. *The Holocene* 23, 945–960. <https://doi.org/10.1177/0959683612475141>
- Ranasinghe, P.N., Dissanayake, C.B., Samarasinghe, D.V.N., Galappatti, R., 2007. The relationship between soil geochemistry and die back of montane forests in Sri Lanka: A case study. *Environ. Geol.* <https://doi.org/10.1007/s00254-006-0399-6>
- Ranasinghe, P.N., Ortiz, J.D., Moore, A.L., McAdoo, B., Wells, N., Siriwardana, C.H.E.R., Wijesundara, D.T.D.S., 2013. Mid–Late Holocene coastal environmental changes in southeastern Sri Lanka: New evidence for sea level variations in southern Bay of Bengal. *Quat. Int.* 298, 20–36. <https://doi.org/10.1016/j.quaint.2013.02.030>
- Ranawana, K.B., 2017. Mangroves of Sri Lanka. *Publ. Seacology-Sudeesa Mangrove Museum* 1, 25–28.
- Ranjan, R.K., Routh, J., Val Klump, J., Ramanathan, A., 2015. Sediment biomarker profiles trace organic matter input in the Pichavaram mangrove complex, southeastern India. *Mar. Chem.* 171, 44–57. <https://doi.org/10.1016/j.marchem.2015.02.001>
- Ranwella, S.P., 1995. A checklist of Vertebrates of Bolgoda South Lake Area. Young Zoologists' Association.
- Rasmusson, E.M., Carpenter, T.H., 1983. The Relationship Between Eastern Equatorial Pacific Sea Surface Temperatures and Rainfall over India and Sri Lanka. *Mon. Weather Rev.* 111, 517–528. [https://doi.org/10.1175/1520-0493\(1983\)111<0517:TRBEEP>2.0.CO;2](https://doi.org/10.1175/1520-0493(1983)111<0517:TRBEEP>2.0.CO;2)
- Ratnayake, A.S., Sampei, Y., Ratnayake, N.P., Roser, B.P., 2017. Middle to late Holocene environmental changes in the depositional system of the tropical brackish Bolgoda Lake, coastal southwest Sri Lanka. *Palaeogeogr. Palaeoclimatol. Palaeoecol.* 465, 122–137. <https://doi.org/10.1016/j.palaeo.2016.10.024>
- Rawat, S., Gupta, A.K., Srivastava, P., Sangode, S.J., Nainwal, H.C., 2015. A 13,000 year record of environmental magnetic variations in the lake and peat deposits from the Chandra valley, Lahaul: implications to Holocene monsoonal variability in the NW Himalaya. *Palaeogeogr. Palaeoclimatol. Palaeoecol.* 440, 116–127.
- Reimer, P.J., Bard, E., Bayliss, A., Warren, B.J., Blackwell, P.G., Ramsey, C., Buck, C.E., Cheng, H., 2013. IntCal13 and Marine13 Radiocarbon Age Calibration Curves 0–50,000

- Years cal BP. Radiocarbon 55, 1869–1887. https://doi.org/10.2458/azu_js_rc.55.16947
- Rein, B., Lückge, A., Reinhardt, L., Sirocko, F., Wolf, A., Dullo, W.-C., 2005. El Niño variability off Peru during the last 20,000 years. *Paleoceanography* 20, n/a-n/a. <https://doi.org/10.1029/2004PA001099>
- Revelle, W., 2019. psych: Procedures for Personality and Psychological Research, Northwestern University, Evanston, Illinois, USA, <https://CRAN.R-project.org/package=psych> Version = 1.9.12.
- Roberts, P., Boivin, N., Petraglia, M., Masser, P., Meece, S., Weisskopf, A., Silva, F., Korisettar, R., Fuller, D.Q., 2016. Local diversity in settlement, demography and subsistence across the southern Indian Neolithic-Iron Age transition: site growth and abandonment at Sanganakallu-Kupgal. *Archaeol. Anthropol. Sci.* 8, 575–599. <https://doi.org/10.1007/s12520-015-0240-9>
- Roberts, P., Perera, N., Wedage, O., Deraniyagala, S., Perera, J., Eregama, S., Gledhill, A., Petraglia, M.D., Lee-Thorp, J.A., 2015. Direct evidence for human reliance on rainforest resources in late Pleistocene Sri Lanka. *Science* (80-.). 347, 1246–1249. <https://doi.org/10.1126/science.aaa1230>
- Rohli, R. V., Vega, A.J., 2017. *Climatology*, 4th ed. Jones & Bartlett Learning.
- Rommerskirchen, F., Plader, A., Eglinton, G., Chikaraishi, Y., Rullkötter, J., 2006. Chemotaxonomic significance of distribution and stable carbon isotopic composition of long-chain alkanes and alkan-1-ols in C4 grass waxes. *Org. Geochem.* 37, 1303–1332. <https://doi.org/10.1016/j.orggeochem.2005.12.013>
- Ronkainen, T., McClymont, E.L., Tuittila, E.S., Väiliranta, M., 2014. Plant macrofossil and biomarker evidence of fen-bog transition and associated changes in vegetation in two Finnish peatlands. *Holocene* 24, 828–841. <https://doi.org/10.1177/0959683614530442>
- Routh, J., Hugelius, G., Kuhry, P., Filley, T., Tillman, P.K., Becher, M., Crill, P., 2014. Multi-proxy study of soil organic matter dynamics in permafrost peat deposits reveal vulnerability to climate change in the European Russian Arctic. *Chem. Geol.* 368, 104–117.
- Rozanski, K., Araguás-Araguás, L., Gonfiantini, R., 1993. Isotopic patterns in modern global precipitation. *GMS* 78, 1–36.
- Ruddiman, W.F., 2006. Orbital changes and climate. *Quat. Sci. Rev.* 25, 3092–3112.
- Rühland, K., Phadtare, N.R., Pant, R.K., Sangode, S.J., Smol, J.P., 2006. Accelerated melting of Himalayan snow and ice triggers pronounced changes in a valley peatland from northern India. *Geophys. Res. Lett.* 33.
- Sachse, D., Billault, I., Bowen, G.J., Chikaraishi, Y., Dawson, T.E., Feakins, S.J., Freeman, K.H., Magill, C.R., McInerney, F.A., van der Meer, M.T.J., Polissar, P., Robins, R.J., Sachs, J.P., Schmidt, H.-L., Sessions, A.L., White, J.W.C., West, J.B., Kahmen, A., 2012. Molecular Paleohydrology: Interpreting the Hydrogen-Isotopic Composition of Lipid Biomarkers from Photosynthesizing Organisms. *Annu. Rev. Earth Planet. Sci.* 40, 221–249. <https://doi.org/10.1146/annurev-earth-042711-105535>
- Sachse, D., Radke, J., Gleixner, G., 2006. δD values of individual n-alkanes from terrestrial plants along a climatic gradient – Implications for the sedimentary biomarker record. *Org. Geochem.* 37, 469–483. <https://doi.org/10.1016/j.orggeochem.2005.12.003>
- Saji, N., Goswami, B., Vinayachandran, P., Yamagata, T., 1999. A dipole mode in the Tropical Ocean. *Nature* 401, 360–363.
- Sandeep, K., Shankar, R., Warriar, A.K., Yadava, M.G., Ramesh, R., Jani, R.A., Weijian, Z., Xuefeng, L., 2017. A multi-proxy lake sediment record of Indian summer monsoon variability during the Holocene in southern India. *Palaeogeogr. Palaeoclimatol. Palaeoecol.* 476, 1–14. <https://doi.org/10.1016/j.palaeo.2017.03.021>
- Sarkar, S., Prasad, S., Wilkes, H., Riedel, N., Stebich, M., Basavaiah, N., Sachse, D., 2015.

- Monsoon source shifts during the drying mid-Holocene: Biomarker isotope based evidence from the core “monsoon zone” (CMZ) of India. *Quat. Sci. Rev.* 123, 144–157. <https://doi.org/10.1016/j.quascirev.2015.06.020>
- Schneider, T., Bischoff, T., Haug, G.H., 2014. Migrations and dynamics of the intertropical convergence zone. *Nature* 513, 45–53. <https://doi.org/10.1038/nature13636>
- Sessions, A.L., 2016. Factors controlling the deuterium contents of sedimentary hydrocarbons. *Org. Geochem.* 96, 43–64. <https://doi.org/10.1016/j.orggeochem.2016.02.012>
- Sessions, A.L., Burgoyne, T.W., Schimmelmann, A., Hayes, J.M., 1999. Fractionation of hydrogen isotopes in lipid biosynthesis. *Org. Geochem.* 30, 1193–1200.
- Sikka, D.R., Gadgil, S., 1980. On the maximum cloud zone and the ITCZ over Indian, longitudes during the southwest monsoon. *Mon. Weather Rev.* 108, 1840–1853.
- Silva, E.I.L., Katupotha, J., Amarasinghe, O., Manthrilake, H., Ariyaratna, R., 2013. Lagoons of Sri Lanka: from the origins to the present, Lagoons of Sri Lanka: from the origins to the present. International Water Management Institute (IWMI). <https://doi.org/10.5337/2013.215>
- Sinha, A., Kathayat, G., Cheng, H., Breitenbach, S.F.M., Berkelhammer, M., Mudelsee, M., Biswas, J., Edwards, R.L., 2015. Trends and oscillations in the Indian summer monsoon rainfall over the last two millennia. *Nat. Commun.* <https://doi.org/10.1038/ncomms7309>
- Sinha, A., Kathayat, G., Weiss, H., Li, H., Cheng, H., Reuter, J., Schneider, A.W., Berkelhammer, M., Adali, S.F., Stott, L.D., Lawrence Edwards, R., 2019. Role of climate in the rise and fall of the neo-assyrian empire. *Sci. Adv.* 5, 1–11. <https://doi.org/10.1126/sciadv.aax6656>
- Sinha, A., Stott, L., Berkelhammer, M., Cheng, H., Edwards, R.L., Buckley, B., Aldenderfer, M., Mudelsee, M., 2011. A global context for megadroughts in monsoon Asia during the past millennium. *Quat. Sci. Rev.* <https://doi.org/10.1016/j.quascirev.2010.10.005>
- Sreekala, P.P., Rao, S.V.B., Rajeevan, M., 2012. Northeast monsoon rainfall variability over south peninsular India and its teleconnections. *Theor. Appl. Climatol.* 108, 73–83. <https://doi.org/10.1007/s00704-011-0513-x>
- Sridhar, A., Laskar, A., Prasad, V., Sharma, A., Tripathi, J.K., Balaji, D., Maurya, D.M., Chamyal, L.S., 2015. Late Holocene flooding history of a tropical river in western India in response to southwest monsoon fluctuations: A multi proxy study from lower Narmada valley. *Quat. Int.* <https://doi.org/10.1016/j.quaint.2014.10.052>
- Srivastava, R., Ramesh, R., Rao, T.N., 2014. Stable isotopic differences between summer and winter monsoon rains over southern India. *J. Atmos. Chem.* 71, 321–331. <https://doi.org/10.1007/s10874-015-9297-1>
- Staubwasser, M., Sirocko, F., Grootes, P.M.M., Segl, M., 2003. Climate change at the 4.2 ka BP termination of the Indus valley civilization and Holocene south Asian monsoon variability. *Geophys. Res. Lett.* 30, 1425. <https://doi.org/10.1029/2002GL016822>
- Staubwasser, M., Weiss, H., 2006. Holocene Climate and Cultural Evolution in Late Prehistoric–Early Historic West Asia. *Quat. Res.* 66, 372–387. <https://doi.org/10.1016/j.yqres.2006.09.001>
- Steinhilber, F., Beer, J., Fröhlich, C., 2009. Total solar irradiance during the Holocene. *Geophys. Res. Lett.* 36.
- Steinhof, A., Altenburg, M., Machts, H., 2017. Sample Preparation at the Jena 14C Laboratory. *Radiocarbon* 59, 815–830. <https://doi.org/10.1017/RDC.2017.50>
- Still, C.J., Berry, J.A., Collatz, G.J., DeFries, R.S., 2003. Global distribution of C3 and C4 vegetation: Carbon cycle implications. *Global Biogeochem. Cycles* 17. <https://doi.org/10.1029/2001gb001807>
- Strobel, P., Kasper, T., Frenzel, P., Schitteck, K., Quick, L.J., Meadows, M.E., Mäusbacher,

- R., Haberzettl, T., 2019. Late Quaternary palaeoenvironmental change in the year-round rainfall zone of South Africa derived from peat sediments from Vankervelsvlei. *Quat. Sci. Rev.* 218, 200–214. <https://doi.org/10.1016/j.quascirev.2019.06.014>
- Thamban, M., Kawahata, H., Rao, V.P., 2007. Indian summer monsoon variability during the Holocene as recorded in sediments of the Arabian Sea: timing and implications. *J. Oceanogr.* 63, 1009–1020.
- Tipple, B.J., Pagani, M., 2013. Environmental control on eastern broadleaf forest species' leaf wax distributions and d/h ratios. *Geochim. Cosmochim. Acta* 111, 64–77. <https://doi.org/10.1016/j.gca.2012.10.042>
- Veena, M., Achyuthan, H., Eastoe, C., Farooqui, A., 2014. A multi-proxy reconstruction of monsoon variability in the late Holocene, South India. *Quat. Int.* 325, 63–73. <https://doi.org/10.1016/j.quaint.2013.10.026>
- Vitanage, P.W., 1970. A study of the geomorphology and the morphotectonics of Ceylon. *Proc. Second Semin. Geochemical Prospect. Methods Tech. United Nations, New York, N.Y* 391–405.
- Wang, P., 2009. Global monsoon in a geological perspective. *Chinese Sci. Bull.* 54, 1113–1136. <https://doi.org/10.1007/s11434-009-0169-4>
- Wang, Y. V., Larsen, T., Leduc, G., Andersen, N., Blanz, T., Schneider, R.R., 2013. What does leaf wax δD from a mixed C3/C4 vegetation region tell us? *Geochim. Cosmochim. Acta* 111, 128–139. <https://doi.org/10.1016/j.gca.2012.10.016>
- Wanner, H., Beer, J., Bütikofer, J., Crowley, T.J., Cubasch, U., Flückiger, J., Goosse, H., Grosjean, M., Joos, F., Kaplan, J.O., Küttel, M., Müller, S.A., Prentice, I.C., Solomina, O., Stocker, T.F., Tarasov, P., Wagner, M., Widmann, M., 2008. Mid- to Late Holocene climate change: an overview. *Quat. Sci. Rev.* 27, 1791–1828. <https://doi.org/10.1016/j.quascirev.2008.06.013>
- Wedage, O., Picin, A., Blinkhorn, J., Douka, K., Deraniyagala, S., Kourampas, N., Perera, N., Simpson, I., Boivin, N., Petraglia, M., Roberts, P., 2019. Microliths in the South Asian rainforest ~45-4 ka: New insights from Fa-Hien Lena Cave, Sri Lanka, *PLoS ONE*. <https://doi.org/10.1371/journal.pone.0222606>
- Weerakkody, U., 1992. The Holocene Coasts of Sri Lanka. *Geogr. J.* 158, 300–306.
- Weltje, G.J., Tjallingii, R., 2008. Calibration of XRF core scanners for quantitative geochemical logging of sediment cores: Theory and application. *Earth Planet. Sci. Lett.* 274, 423–438. <https://doi.org/10.1016/j.epsl.2008.07.054>
- Weninger, B., Alram-Stern, E., Bauer, E., Clare, L., Danzeglocke, U., Jöris, O., Kubatzki, C., Rollefson, G., Todorova, H., van Andel, T., 2006. Climate forcing due to the 8200 cal yr BP event observed at Early Neolithic sites in the eastern Mediterranean. *Quat. Res.* <https://doi.org/10.1016/j.yqres.2006.06.009>
- Werner, R.A., Brand, W.A., 2001. Referencing strategies and techniques in stable isotope ratio analysis. *Rapid Commun. Mass Spectrom.* 15, 501–519. <https://doi.org/10.1002/rcm.258>
- Werner, R.A., Bruch, B.A., Brand, W.A., 1999. ConFlo III—an interface for high precision $\delta^{13}C$ and $\delta^{15}N$ analysis with an extended dynamic range. *Rapid Commun. Mass Spectrom.* 13, 1237–1241.
- Wijetunge, J.J., 2006. Tsunami on 26 December 2004: Spatial Distribution of Tsunami Height and the Extent of Inundation in Sri Lanka. *Sci. Tsunami Hazards* 24, 225–239.
- Yadav, R.K., 2012. Why is ENSO influencing Indian northeast monsoon in the recent decades? *Int. J. Climatol.* 32, 2163–2180. <https://doi.org/10.1002/joc.2430>
- Yamoah, K.A., Chabangborn, A., Chawchai, S., Schenk, F., Wohlfarth, B., Smittenberg, R.H., 2016. A 2000-year leaf wax-based hydrogen isotope record from Southeast Asia suggests low frequency ENSO-like teleconnections on a centennial timescale. *Quat. Sci.*

- Rev. 148, 44–53. <https://doi.org/10.1016/j.quascirev.2016.07.002>
- Zubair, L., Ropelewski, C.F., 2006. The strengthening relationship between ENSO and northeast monsoon rainfall over Sri Lanka and southern India. *J. Clim.* 19, 1567–1575. <https://doi.org/10.1175/JCLI3670.1>
- Zubair, L., Siriwardhana, M., Chandimala, J., Yahiya, Z., 2007. Predictability of Sri Lankan rainfall based on ENSO. *Int. J. Climatol.* 28, 91–101. <https://doi.org/10.1002/joc.1514>

Appendix

Appendix Tables:

Table A-1. Results of ^{14}C dating in Bolgoda South Lake

P-Nr.	Depth (cm)	F ^{14}C	Error	$\Delta^{14}\text{C}$ (‰)	error (‰)	^{14}C Age (conventional; yr BP)	Material dated
17916	0-1	0.9281	0.0019	-79.5	1.9	599 ± 19	Bulk sediment
16515	3-4	1.0098	0.0017	1.6	1.7	-78 ± 14	Shell (fragments)
21605	5-6	0.7676	0.0018	-238.8	1.8	2125 ± 19	Bulk sediment
21606	10-11	0.7256	0.0017	-280.4	1.7	2577 ± 19	Bulk sediment
21607	17-18	0.6823	0.0017	-323.4	1.7	3071 ± 20	Bulk sediment
16289	20-21	0.6532	0.0037	-352.1	3.7	3421 ± 19	Bulk sediment
16288	29-30	0.6104	0.0035	-394.5	3.5	3965 ± 19	Bulk sediment
16278	39-41	0.5791	0.0026	-425.6	2.7	4388 ± 20	Shell (Gastropods)
16287	40-41	0.5766	0.0040	-428	4	4423 ± 46	Bulk sediment
16285	50-51	0.5594	0.0036	-445.1	3.6	4666 ± 46	Bulk sediment
16286	60-61	0.5555	0.0037	-449	3.7	4722 ± 36	Bulk sediment
21608	63-64	0.5185	0.0016	-485.8	1.6	5276 ± 25	Bulk sediment
21609	67-68	0.5056	0.0012	-498.6	1.2	5479 ± 19	Bulk sediment
16509	68-69	0.5162	0.0013	-488	1.3	5312 ± 20	Bulk sediment
16303	68-69	0.4404	0.0026	-563.1	2.6	6588 ± 52	Wood fragment

Table A-2 Results of ^{14}C dating in Panama Lagoon

P-Nr.	Depth (cm)	F ^{14}C	Error	$\Delta^{14}\text{C}$ (‰)	error (‰)	^{14}C Age (conventional; yr BP)	Material dated
22608	3-4	0.6546	0.0014	-350.8	1.4	3404 ± 17	Shells (Gastropods)
16516	6-7	1.2211	0.0019	211.1	1.9	-1605 ± 13	Shell (Bivalve)
22609	11-12	1.2421	0.0021	231.8	2.1	-1742 ± 14	Shell (Bivalve)
22610	23-24	0.7030	0.0015	-302.9	1.5	2831 ± 17	Shells (Gastropods)
22612	34-35	0.9281	0.0018	-79.6	1.8	599 ± 16	Shells (Gastropods)
16284	36-37	0.6929	0.0047	-312.7	4.7	2947 ± 55	Shells (Gastropods)
16283	51-52	0.6711	0.0036	-334.3	3.6	3204 ± 43	Shells (Gastropods)
22613	54-55	0.6009	0.0015	-404.1	1.5	4091 ± 20	Shells (Gastropods)
16578	67-68	0.5795	0.0012	-425.2	1.2	4383 ± 17	Shells (Gastropods)
16282	82-83	0.4968	0.0029	-507.2	2.9	5620 ± 47	Shells (Gastropods)
16579	82-83	0.5645	0.0012	-440.1	1.2	4593 ± 17	Shells (Gastropods)
22614	84-85	0.5899	0.0014	-415	1.4	4240 ± 19	Shells (Gastropods)
22615	93-94	0.5330	0.0013	-471.4	1.3	5055 ± 20	Shells (Gastropods)
22616	96-97	0.4886	0.0012	-515.5	1.2	5753 ± 20	Shells (Gastropods)
16281	101-102	0.4744	0.0028	-529.4	2.8	5990 ± 48	Shells (Gastropods)

Table A-3 Results of ^{14}C dating in Horton Plains

P-Nr.	Depth (cm)	F ^{14}C	Error	$\Delta^{14}\text{C}$ (‰)	error (‰)	^{14}C Age (conventional; yr BP)	Material dated
15366	12-13	1.0312	0.0039	22.8	3.9	-247 ± 30	Peat
21590	20-21	1.0151	0.0020	6.6	2	-120 ± 16	Peat
21591	29-30	0.9936	0.0019	-14.7	1.9	52 ± 15	Peat
15367	42-43	0.9612	0.0035	-46.6	3.5	318 ± 29	Peat
21592	50-51	0.9341	0.0019	-73.7	1.9	548 ± 16	Peat
15368	65-66	0.9476	0.0036	-60.1	3.6	432 ± 31	Peat
21593	75-76	0.9266	0.0018	-81.2	1.8	612 ± 16	Peat
21594	87-88	0.8801	0.0019	-127.2	1.9	1026 ± 17	Peat
15369	98-99	0.8277	0.0035	-179.0	3.5	1519 ± 34	Peat
21595	110-111	0.7541	0.0016	-252.2	1.6	2267 ± 17	Peat
21596	117-118	0.7119	0.0016	-294	1.6	2730 ± 18	Peat
21597	124-125	0.6553	0.0014	-350.1	1.4	3395 ± 17	Peat
15370	129-130	0.6394	0.0029	-365.8	2.9	3593 ± 37	Peat
21598	136-137	0.5934	0.0013	-411.6	1.3	4192 ± 18	Peat
15371	139-140	0.5836	0.0027	-421.1	2.7	4326 ± 37	Peat
15372	147-148	0.5621	0.0030	-442.4	3.0	4628 ± 43	Peat

Table A-4 Contents of sterols (ng/g) identified in Bolgoda South Lake. Units of Depth in 'cm' and Age in 'cal yr BP'.

Sample	Depth	Age	Coprostanol	Cholesterol	Cholestanol	Stigmasterol	Stigmastanol	b-Sitosterol	Taraxerol	b-Amyrine	Germinicol	Freidelene
BGSL_1	1.5	0	19	60	47	72	84	9	1773	648	69	8
BGSL_2	2.5	0	0	16	15	36	47	7	2002	550	61	29
BGSL_4	7.5	1684	0	9	9	22	24	0	5881	1077	125	61
BGSL_5	11.5	2049	0	10	0	24	0	3	6890	714	122	70
BGSL_6	14.5	2320	0	13	0	24	24	-5	6578	850	112	61
BGSL_7	17.5	2661	0	8	0	21	13	0	6449	654	108	68
BGSL_8	19.5	2880	0	17	0	26	14	0	8033	1034	140	75
BGSL_26	23.5	3239	0	3	0	0	9	5	3651	937	93	44
BGSL_27	24.5	3319	0	11	0	14	12	2	5257	644	93	24
BGSL_28	26.5	3476	0	11	10	24	21	0	9899	911	149	105
BGSL_29	30.5	3762	0	23	0	16	11	0	5343	1197	112	71
BGSL_12	33.5	3936	0	7	0	12	7	3	6668	709	99	66
BGSL_13	36.5	4095	0	0	0	12	0	5	5232	613	51	60
BGSL_14	39.5	4244	0	15	0	13	0	1	5048	904	78	56
BGSL_15	41.5	4323	0	0	0	0	0	2	5226	707	105	56
BGSL_16	44.5	4444	0	0	0	0	0	2	4476	553	35	42
BGSL_17	47.5	4530	0	0	0	10	6	0	4726	742	47	42
BGSL_18	51.5	4656	0	0	0	8	0	3	3631	764	77	36
BGSL_19	54.5	4735	0	0	0	12	8	0	4626	392	47	46
BGSL_20	57.5	4784	0	6	0	8	0	2	3687	184	25	37
BGSL_21	62.5	5131	0	0	0	6	4	4	2347	134	28	28
BGSL_22	66.5	5521	0	0	0	7	0	1	2854	244	17	36
BGSL_23	68.5	5619	0	0	0	0	0	0	1642	194	0	27
BGSL_24	69.5	5674	0	18	0	0	0	0	1168	301	21	4

Table A-5 Contents of sterols (ng/g) identified in Panama Lagoon. Units of Depth in 'cm' and Age in 'cal yr BP'.

Sample	Depth	Age	Coprostanol	Cholesterol	Cholestanol	Stigmasterol	Stigmastanol	b-Sitosterol	Taraxerol	b-Amyrine	Germinicol	Freidelene
PN17_1	0.5	0	21	65	37	46	16	0	3042	956	154	9
PN17_2	3.5	0	8	16	8	26	8	0	2075	536	84	17
PN17_3	7.5	210	0	14	0	0	0	0	1226	287	-7	0
PN17_4	11.5	568	0	5	0	0	0	0	1849	349	57	16
PN17_5	16.5	1275	0	5	0	3	0	1	1355	245	40	10
PN17_6	21.5	1959	0	5	0	0	0	0	1114	211	38	9
PN17_7	26.5	2244	0	0	0	0	0	1	1173	216	32	11
PN17_8	32.5	2455	0	0	0	0	0	0	1025	217	20	9
PN17_9	39	2704	0	4	0	3	0	0	945	144	32	10
PN17_10	45	2957	0	0	0	0	0	0	679	115	12	6
PN17_11	50.5	3252	0	0	0	0	0	0	782	142	22	0
PN17_12	54.5	3584	0	3	0	0	0	1	906	123	23	6
PN17_13	63	4090	3	6	0	0	0	2	1216	192	29	9
PN17_14	69	4312	0	0	0	0	0	0	661	72	12	0
PN17_15	79	4588	0	3	0	0	0	1	614	69	11	0
PN17_16	85	4768	0	0	0	0	0	0	568	72	12	0
PN17_17	93.5	5323	0	6	0	0	0	2	943	136	19	16
PN17_18	97.5	5970	0	6	0	0	0	0	481	59	0	0

Table A-6 Contents of sterols (ng/g) identified in Horton Plains. Units of Depth in 'cm' and Age in 'cal yr BP'.

Sample	Depth	Age (cal yr BP)	Cholestanol	Campesterol	Campestanol	Stigmasterol	Stigmastanol	Sitosterol	Sitostanol
HP14_1	4	-40	57	314	63	693	0	895	159
HP14_2	8.5	-33	45	152	116	280	0	481	146
HP14_4	22.5	1	38	135	56	239	0	476	170
HP14_5	32.5	127	-1	121	81	185	0	496	301
HP14_6	44.5	344	46	104	101	146	0	518	457
HP14_7	55.5	430	40	110	96	161	0	504	396
HP14_8	64.5	497	74	137	175	166	0	712	810
HP14_9	75.5	626	20	37	52	45	0	221	271
HP14_10	83.5	832	39	97	112	84	0	581	624
HP14_11	88.5	976	16	36	36	1	0	204	195
HP14_12	94.5	1247	0	45	12	43	0	289	139
HP14_13	103.5	1733	33	64	101	63	0	369	576
HP14_14	109.5	2225	51	100	167	95	0	625	933
HP14_15	116.5	2736	30	67	81	66	0	399	478
HP14_16	122.5	3424	40	90	138	86	0	530	786
HP14_17	128.5	3874	63	114	197	110	0	500	1123
HP14_18	133.5	4429	43	92	143	104	0	553	796
HP14_19	142.5	5085	32	53	84	62	0	331	558
HP14_20	146.5	5312	25	46	29	49	0	297	386
HP14_21	149.5	5460	43	58	76	62	0	323	483

Appendix Figures:

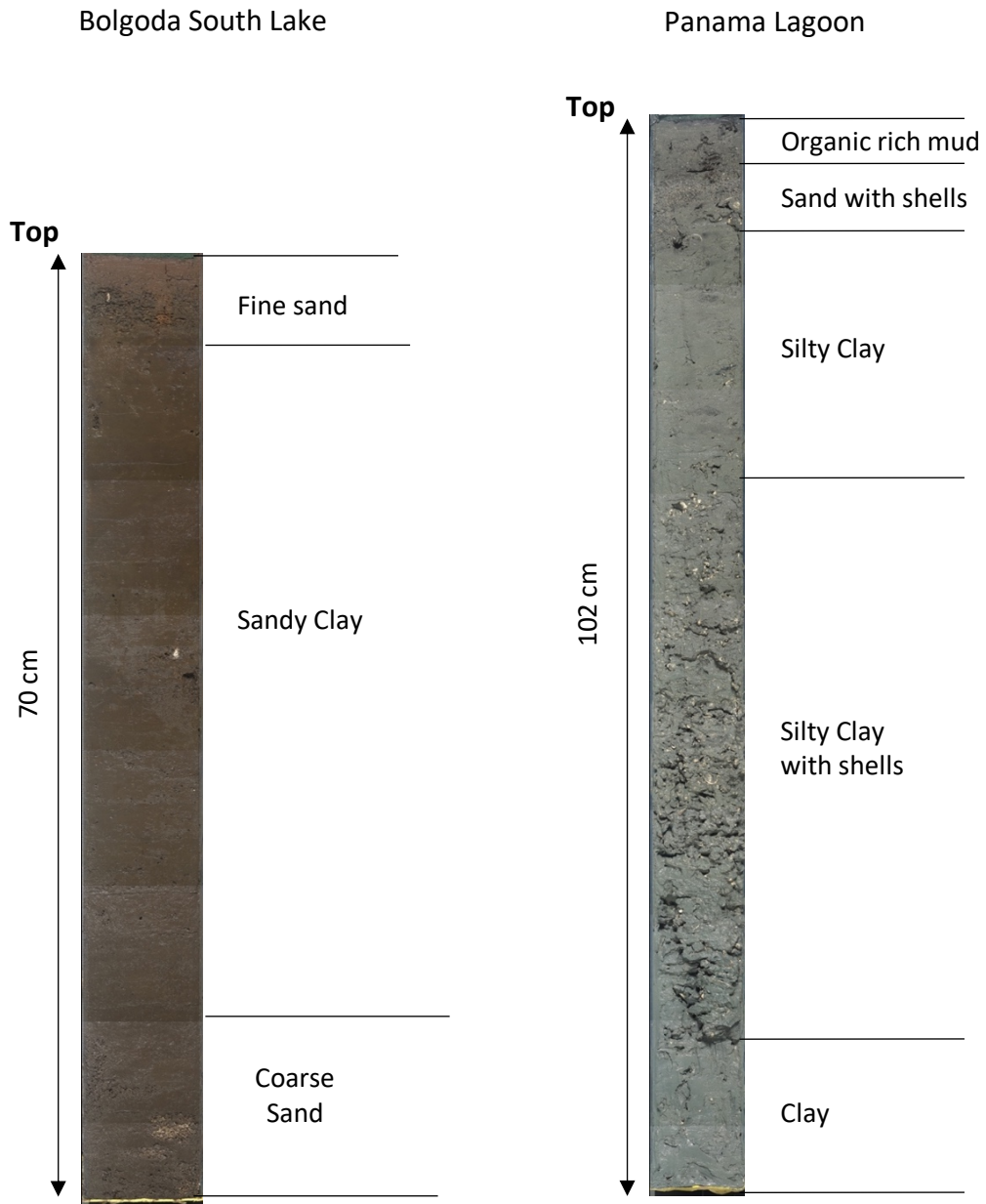


Fig.A-1 Sediment core images of Bolgoda South Lake (Left) and Panama Lagoon (right)

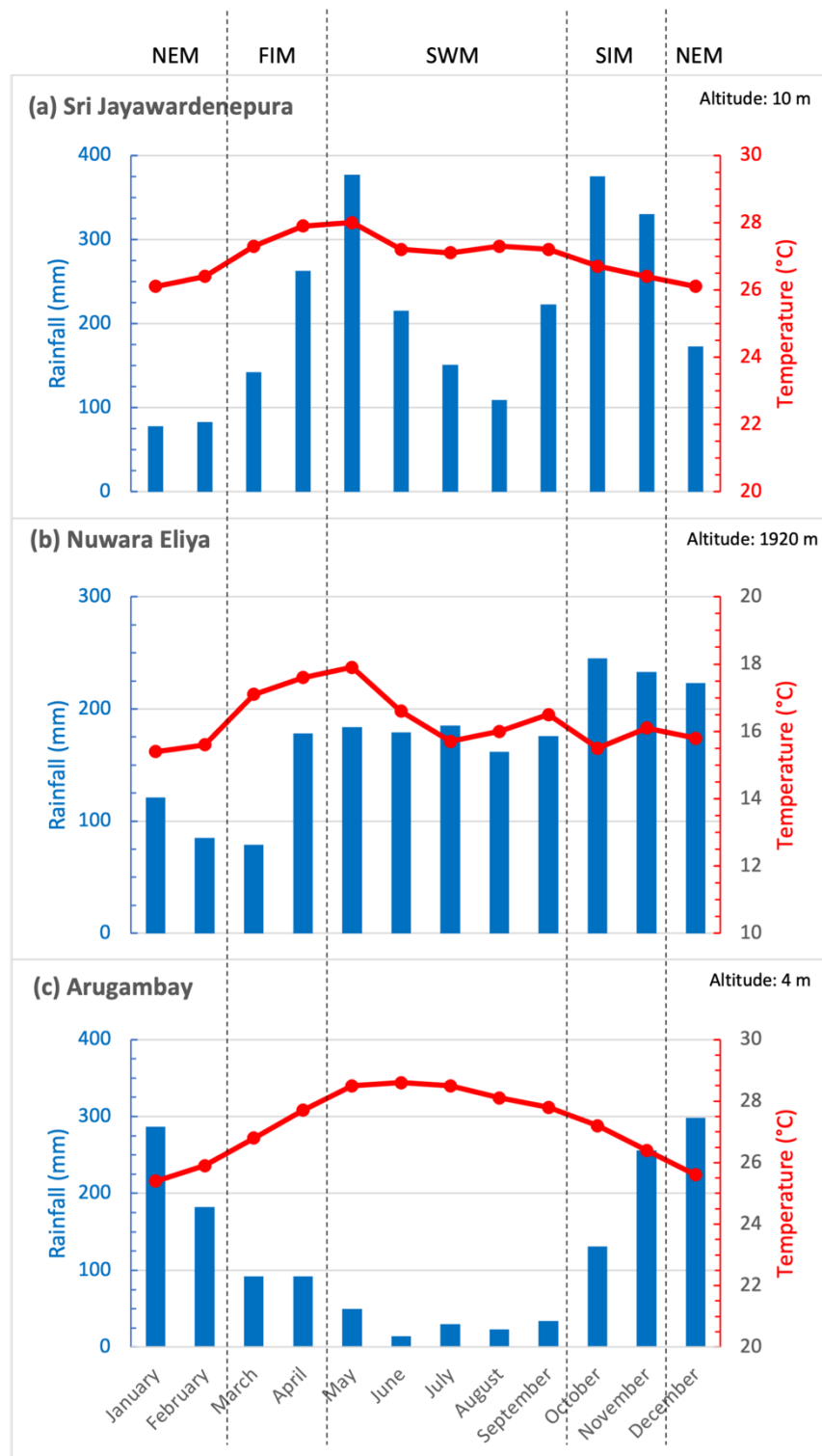


Fig.A-2 Monthly average rainfall and temperature variations in three cities of Sri Lanka. (a) Sri Jayawardanepura-Colombo (Western province; lowland-wet zone), (b) Nuwara Eliya (Central province; central highlands-wet zone), (c) Arugambay (Eastern province; lowland-dry zone). (data source: <https://en.climate-data.org/>)

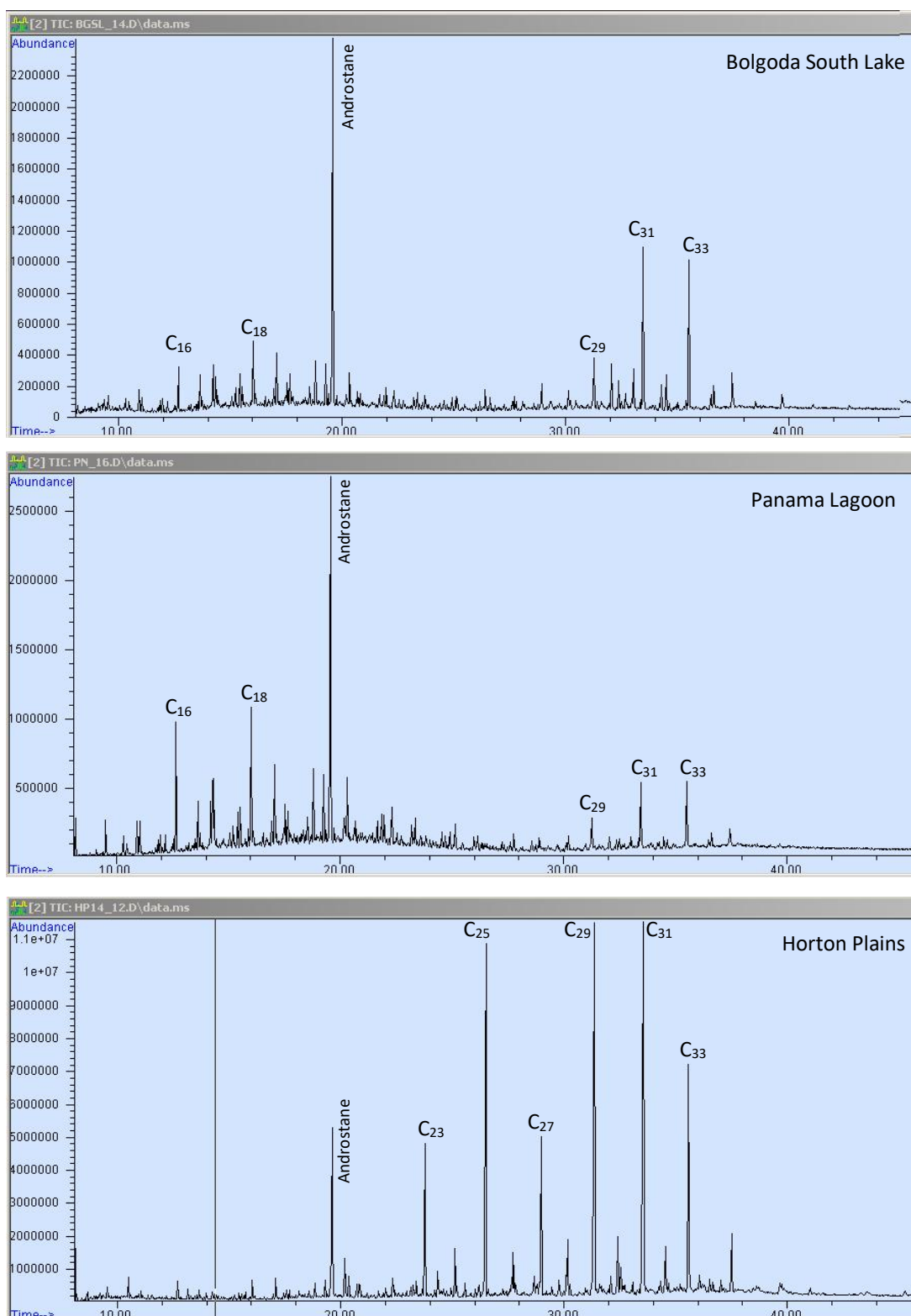


Fig.A-3 Representative *n*-alkane chromatograms of Bolgoda South Lake, Panama Lagoon and Horton Plains

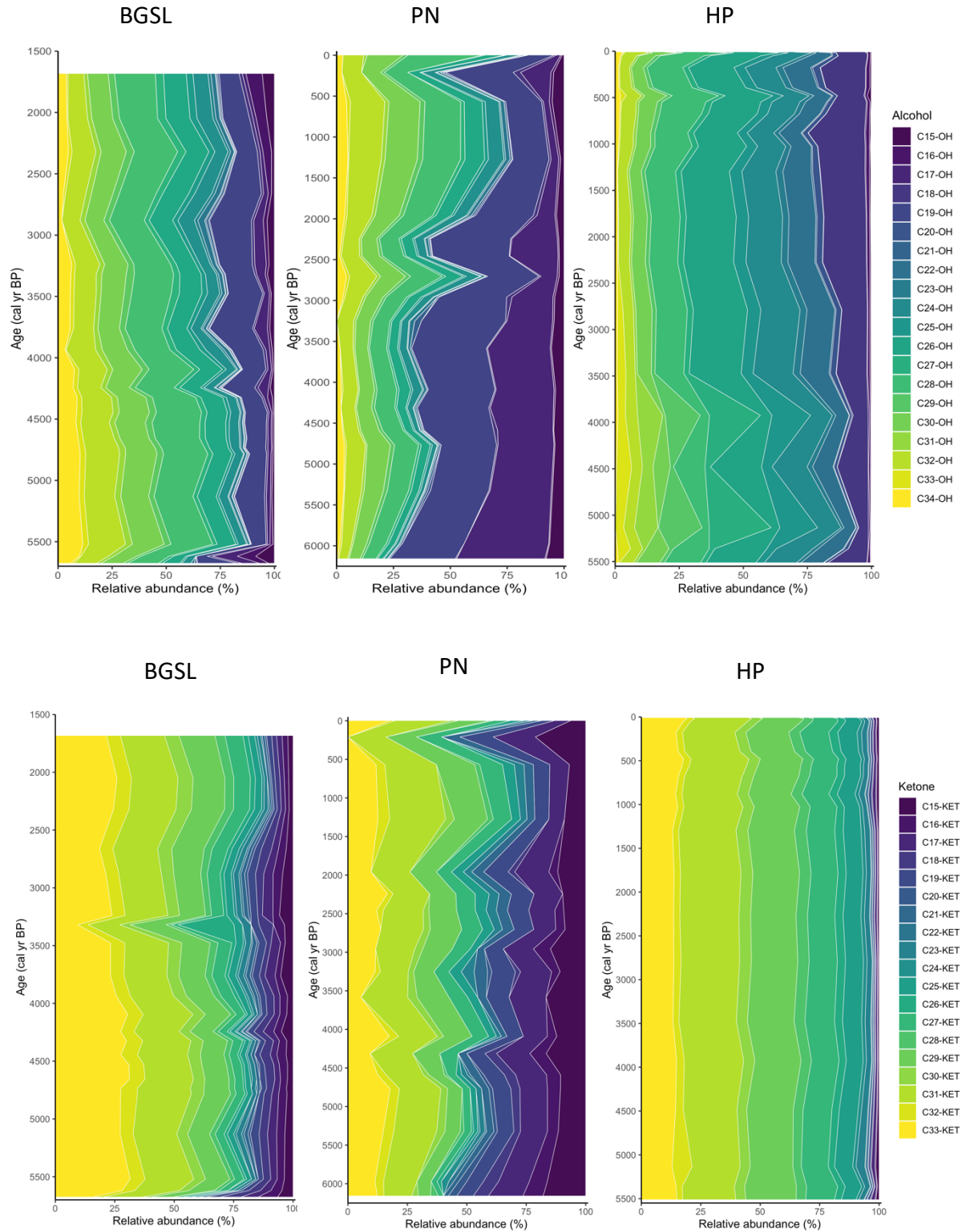


Fig.A-4 Relative distribution of n-alkanol (top) and n-alkenone (bottom) in Bolgoda South Lake, Panama Lagoon and Horton Plains

Selbständigkeitserklärung

Ich erkläre, dass ich die vorliegende Arbeit selbständig und unter Verwendung der angegebenen Hilfsmittel, persönlichen Mitteilungen und Quellen angefertigt habe.

Jena, 20.08.2021

Ort, Datum

.....

Unterschrift des Verfassers